NASA Contractor Report 189052

NASA-CR-189052
19920010472

Development of an Integrated BEM Approach for Hot Fluid Structure Interaction

Gary F. Dargush, Prasanta K. Banerjee,
and Keith A. Honkala
State University of New York at Buffalo
Buffalo, New York

November 1991

Prepared for
Lewis Research Center
Under Grant NAG3–712

National Aeronautics and
Space Administration

LIST OF CONTENTS

1. INTRODUCTION 1

2. LITERATURE REVIEW 3

3. INTEGRAL FORMULATION FOR SOLIDS 4
3.1 Introduction 4
3.2 Governing Equations 4
3.3 Integral Representations 5
3.4 Numerical Implementation 7
3.4.1 Introduction 7
3.4.2 Temporal Discretization 7
3.4.3 Spatial Discretization 8
3.4.4 Numerical Integration 12
3.4.5 Assembly 13
3.4.6 Solution 16
3.4.7 Interior Quantities 17
3.4.8 Advanced Features 20
3.5 Examples 22
3.5.1 Sudden Heating of an Aluminum Block . . . 22
3.5.2 Circular Disc 23
3.5.3 Turbine Blade 24

4. INTEGRAL FORMULATIONS FOR FLUIDS 32
4.1 Introduction 32
4.2 Governing Equations 32
4.2.1 Compressible Thermoviscous Flow 32
4.2.2 Incompressible Thermoviscous Flow 39
4.2.3 Incompressible Viscous Flow 39
4.2.4 Convective Heat Transfer 40
4.3 Fundamental Solutions 40
4.3.1 Compressible Thermoviscous FLow 40
4.3.2 Incompressible Thermoviscous Flow 51
4.3.3 Incompressible Viscous Flow 52
4.3.4 Convective Heat Transfer 52
4.4 Integral Representations 55
4.4.1 Compressible Thermoviscous Flow 55
4.4.2 Incompressible Viscous Flow 60
4.4.3 Convective Heat Transfer 61
4.5 Numerical Implementation 61
4.6 Coupling of Solid and Fluid 64
4.7 Examples 64
4.7.1 Parallel Flow 64
4.7.2 Driven Cavity 65
4.7.3 Converging Channel 66
4.7.4 Flow Over a Cylinder 67
4.7.5 Flow Over an Airfoil 64

5. SUMMARY 95

6. WORKPLAN FOR THE NEXT YEAR 97

APPENDICES

APPENDIX A - REFERENCES 98
APPENDIX B - KERNELS FOR THERMOELASTICTY 101
APPENDIX C - FUNDAMENTAL SOLUTION FOR CONVECTIVE COMPRESSIBLE THERMOVICOUS FLOW 105
APPENDIX D - FUNDAMENTAL SOLUTION FOR CONVECTIVE INCOMPRESSIBLE THERMOVISCOUS FLOW 107
APPENDIX E - KERNELS FOR STATIONARY INCOMPRESSIBLE THERMOVISCOUS FLOW 108

1. INTRODUCTION

Accurate determination of the thermal stresses induced in hot section components remains one of the most difficult problems facing engine design/analysts. There currently exists no rational analytical nor numerical techniques which can effectively deal with this problem. Analysts involved in hot fluid dynamics using the finite difference method have little interaction with those engaged in thermal stress analysis where the finite element method is dominant. However, the temperature distribution in many structural components is strongly influenced by the external hot gas flow, the internal cooling system of the component, and the structural deformation. As a result, the only effective way to deal with this problem is to develop an integrated solid mechanics, fluid mechanics, and heat transfer approach.

In the present work, the boundary element method (BEM) is chosen as the basic analysis tool principally because the definition of temperature, flux, displacement and traction are very precise on a boundary-based discretization scheme. One fundamental difficulty is, of course, that a BEM formulation requires a considerable amount of analytical work, which is not needed in the other numerical methods.

This report details progress made, during the period November 1987 - November 1988 in a multi-year program commencing in March 1986, toward the development of a boundary element formulation for the study of hot fluid-structure interaction in Earth-to-Orbit engine hot section components. The primary thrust of the program to date has been directed quite naturally toward the examination of fluid flow, since boundary element methods for fluids are at a much less developed state.

During the first year, work focused on the completion of a comprehensive literature review of integral methods in fluids, the

development of integral formulations for both the solid and fluid, and some preliminary infrastructural enhancements to a boundary element code to permit incorporation of the fluid-structure problem. In the second year, emphasis shifted to the implementation and validation phases. Boundary element formulations were implemented in two-dimensions for both the solid and the fluid. The solid was modeled as an uncoupled thermoelastic medium under plane strain conditions, while several formulations were investigated for the fluid. For example, both vorticity and primative variable approaches were implemented for viscous, incompressible flow, and a compressible version was developed. All of the above boundary element implementations were incorporated in a general purpose two-dimensional code. Thus, problems involving intricate geometry, multiple generic modeling regions, and arbitrary boundary conditions are all supported. Further details can be found in Dargush et al (1986, 1987).

In the early portion of this past year, a number of significant advances were made. First, two-dimensional integration schemes were enhanced to obtain more accurate coefficients with somewhat less computing effort. This improvement was found to be particularly beneficial for incompressible flow, where the precise determination of the coefficients is imperative. Secondly, both full and modified Newton-Raphson algorithms were developed. This greatly improved the convergence characteristics of the set of nonlinear equations governing viscous flow. Additionally, a region-by-region reference velocity was introduced into the formulation to shift the highly nonlinear portion away from the free stream and toward obstacles and walls, where a more refined model is appropriate.

The combination of these advances permits the solution of a wide variety of thermoviscous flow problems in the low to moderate Reynolds number range. Several examples are included in this report. However, at

higher Reynolds numbers, there is a need to get more of the physics of the problem into the boundary element fundamental solution. Consequently, the development of new convective fundamental solutions and integral formulations has been the primary focus of our most recent efforts.

In the next section, a brief review of the applicable boundary element literature is presented. This is followed by the development of integral formulations for the solid in Section 3 and for the fluid in Section 4. Several detailed numerical examples are presented at the end of each of those two sections. In the fluids portion, development of the new convective formulations is emphasized. The remaining sections then summarize the progress achieved to date, and outline the work plan for the next year. Tables and figures appear at the end of the corresponding section, while references are provided in Appendix A.

2. LITERATURE REVIEW

Virtually nothing has appeared in the literature on the analysis of coupled thermoviscous fluid/structure problems via the boundary element method, although some work has been done on the fluid and solid separately. In general, the solid portion of the problem has been addressed to a much greater degree. For example, a boundary-only steady-state thermoelastic formulation was initially presented by Cruse et al (1977) and Rizzo and Shippy (1977). Recently, the present authors developed and implemented the quasistatic counterpart (Dargush, 1987; Dargush and Banerjee, 1988a,b), which is presented in detail in Section 3. Others, notably Sharp and Crouch (1986) and Chaudouet (1987), introduce volume integrals, to represent the equivalent thermal body forces. A similar domain based approach was taken earlier by Banerjee and Butterfield (1981) in the context of the analogous geomechanical problem.

An extensive review of the applications of integral formulations to

viscous flow problems was included in the previous annual report (Dargush, et al, 1987), and will not be repeated here. Interestingly, only a few groups of researchers are actively pursuing the further development of boundary elements for the analysis of viscous fluids. The work reported in Piva and Morino (1987) and Piva et al (1987) focuses heavily on the development of fundamental solutions and integral formulations with little emphasis on implementation. On the other hand, Tosaka and Kakuda (1986, 1987), Tosaka and Onishi (1986) have implemented single region boundary element formulations using approximate incompressible fundamental solutions. This latter group has developed sophisticated non-linear solution algorithms, and consequently, are able to demonstrate moderately high Reynolds number solutions. Meanwhile, as will be seen in Section 4, the present work represents a significant advancement in the state-of-the-art from both a formulation and implementation standpoint.

3. INTEGRAL FORMULATION FOR SOLIDS

3.1 Introduction

In the current section, a surface only time domain boundary element method will be described for a thermoelastic body under quasistatic loading. Thus, transient heat conduction is included, but inertial effects are ignored. Formulations have been developed for three-dimensional, two-dimensional and axisymmetric problems (Dargush, 1987; Dargush and Banerjee, 1988a,b), however, only the 2D plane strain case is detailed below. Separate subsections present the governing differential equations, the integral equations, and an overview of the numerical implementation.

3.2 Governing Equations

With the solid assumed to be a linear thermoelastic medium, the governing differential equations for transient thermoelasticity can be

written:

$$(\lambda+\mu)\,\frac{\partial^2 u_j}{\partial x_i \partial x_j} + \mu\,\frac{\partial^2 u_i}{\partial x_j \partial x_j} - (3\lambda+2\mu)\,\alpha\,\frac{\partial \theta}{\partial x_i} = 0 \tag{3.1a}$$

$$\rho c_\varepsilon\,\frac{\partial \theta}{\partial t} = k\,\frac{\partial^2 \theta}{\partial x_j \partial x_j} \tag{3.1b}$$

where

u_i	displacement vector
θ	temperature
t	time
x_i	Lagrangian coordinate
k	thermal conductivity
ρ	mass density
c_ε	specific heat at constant deformation
λ, μ	Lame's constants
α	coefficient of thermal expansion

Standard indicial notation has been employed with summations indicated by repeated indices. For two-dimensional problems considered herein, the Latin indices i and j vary from one to two.

Note that (3.1b) is the energy equation and that (3.1a) represents the momentum balance in terms of displacements and temperature. The theory portrayed by the above set of equations, formally labeled uncoupled quasistatic thermoelasticity, can be derived from thermodynamic principles. (See Boley and Weiner (1960) for details.)

3.3 Integral Representations

Utilizing equation (3.1) for the solid along with a generalized form of the reciprocal theorem, permits one to develop the following boundary

integral equation:

$$c_{\beta\alpha}(\xi)u_\beta(\xi,t) = \int_S [\dot{G}_{\beta\alpha} * t_\beta(X,t) - \dot{F}_{\beta\alpha} * u_\beta(X,t)]dS(X) \ . \qquad (3.2)$$

where

α,β indices varying from 1 to 3

s surface of solid

u_α, t_α generalized displacement and traction

$u_\alpha = [u_1 \ u_2 \ \Theta]^T$

$t_\alpha = [t_1 \ t_2 \ q]^T$

Θ, q temperature, heat flux

$G_{\alpha\beta}, F_{\alpha\beta}$ generalized displacement and traction kernels (Dargush, 1987,1988a)

$c_{\alpha\beta}$ constants determined by the relative smoothness of s at ξ

and, for example,

$$\dot{G}_{\alpha\beta} * t_\alpha = \int_0^t \dot{G}_{\alpha\beta}(x,t;\ \xi,\tau)\ t_\alpha(x,\tau)\ d\tau$$

denotes a Riemann convolution integral.

In principle, at each instant of time progressing from time zero, this equation can be written at every point on the boundary. The collection of the resulting equations could then be solved simultaneously, producing exact values for all the unknown boundary quantities. In reality, of course, discretization is needed to limit this process to a finite number of equations and unknowns. Techniques useful for the discretization of (3.2) are the subject of the following section.

3.4 Numerical Implementation

3.4.1 Introduction

The boundary integral equation (3.2), developed in the last section, is an exact statement. No approximations have been introduced other than those used to formulate the boundary value problem. However, in order to apply (3.2) for the solution of practical engineering problems, approximations are required in both time and space. In this section, an overview of a general-purpose, state-of-the-art numerical implementation is presented. Many of the features and techniques to be discussed, in this section, were developed previously for elastostatics (e.g., Banerjee et al, 1985,1988), and elastodynamics (e.g., Banerjee et al, 1986; Ahmad and Banerjee, 1988), but are here adapted for thermoelastic analysis.

3.4.2 Temporal Discretization

Consider, first, the time integrals represented in (3.2) as convolutions. Clearly, without any loss of precision, the time interval from zero to t can be divided into N equal increments of duration Δt.

By assuming that the primary field variables, t_β and u_β, are constant within each Δt time increment, these quantities can be brought outside of the time integral. That is,

$$\dot{G}_{\beta\alpha} * t_\beta(X,t) = \sum_{n=1}^{N} t_\beta^n(X) \int_{(n-1)\Delta t}^{n\Delta t} \dot{G}_{\beta\alpha}(X-\xi, t-\tau)\, d\tau \qquad (3.3a)$$

$$\dot{F}_{\beta\alpha} * u_\beta(X,t) = \sum_{n=1}^{N} u_\beta^n(X) \int_{(n-1)\Delta t}^{n\Delta t} \dot{F}_{\beta\alpha}(X-\xi, t-\tau)\, d\tau \,, \qquad (3.3b)$$

where the superscript on the generalized tractions and displacements, obviously, represents the time increment number. Notice, also, that, within an increment, these primary field variables are now functions of

position only. Next, since the integrands remaining in (3.3) are known in explicit form from the fundamental solutions, the required temporal integration can be performed analytically, and written as

$$G_{\beta\alpha}^{N+1-n}(X-\xi) = \int_{(n-1)\Delta t}^{n\Delta t} \dot{G}_{\beta\alpha}(X-\xi, t-\tau)\,d\tau \qquad (3.4a)$$

$$F_{\beta\alpha}^{N+1-n}(X-\xi) = \int_{(n-1)\Delta t}^{n\Delta t} \dot{F}_{\beta\alpha}(X-\xi, t-\tau)\,d\tau \; . \qquad (3.4b)$$

These kernel functions, $G_{\beta\alpha}^{n}(X-\xi)$ and $F_{\beta\alpha}^{n}(X-\xi)$, are detailed in Appendix B. Combining (3.3) and (3.4) with (3.2) produces

$$c_{\beta\alpha}(\xi)u_{\beta}^{N}(\xi) = \sum_{n=1}^{N} \int_{S} \left[G_{\beta\alpha}^{N+1-n}(X-\xi)t_{\beta}^{n}(X) - F_{\beta\alpha}^{N+1-n}(X-\xi)u_{\beta}^{n}(X) \right] dS(X) \quad , \qquad (3.5)$$

which is the boundary integral statement after the application of the temporal discretization.

3.4.3 Spatial Discretization

With the use of generalized primary variables and the incorporation of a piecewise constant time stepping algorithm, the boundary integral equation (3.5) begins to show a strong resemblance to that of elastostatics, particularly for the initial time step (i.e., N=1). In this subsection, those similarities will be exploited to develop the spatial discretization for the coupled quasistatic problem with two-dimensional geometry. This approximate spatial representation will, subsequently, permit numerical evaluation of the surface integrals appearing in (3.5). The techniques described here, actually, originated in the finite element literature, but were later applied to boundary elements by Lachat and

Watson (1976).

The process begins by subdividing the entire surface of the body into individual elements of relatively simple shape. The geometry of each element is, then, completely defined by the coordinates of the nodal points and associated interpolation functions. That is,

$$X(\zeta) = x_i(\zeta) = N_w(\zeta)x_{iw} \tag{3.6}$$

with

ζ	intrinsic coordinates
N_w	shape functions
x_{iw}	nodal coordinates

and where w is an integer varying from one to W, the number of geometric nodes in the element. Next, the same type of representation is used, within the element, to describe the primary variables. Thus,

$$u^n_\alpha(\zeta) = N_\omega(\zeta)u^n_{\alpha\omega} \tag{3.7a}$$

$$t^n_\alpha(\zeta) = N_\omega(\zeta)t^n_{\alpha\omega} \tag{3.7b}$$

in which $u^n_{\alpha\omega}$ and $t^n_{\alpha\omega}$ are the nodal values of the generalized displacement and tractions, respectively, for time step n. Also, in (3.7), the integer ω varies from one to Ω, the total number of functional nodes in the element. From the above, note that the same number of nodes, and consequently shape functions, are not necessarily used to describe both the geometric and functional variations. Specifically, in the present work, the geometry is exclusively defined by quadratic shape functions. In two-dimensions, this requires the use of three-noded line elements. On the other hand, the variation of the primary quantities can be described, within an element, by either quadratic or linear shape functions. (The

introduction of linear variations proves computationally advantageous in some instances.)

Once this spatial discretization has been accomplished and the body has been subdivided into M elements, the boundary integral equation can be rewritten as

$$c_{\beta\alpha}(\xi)u^N_\beta(\xi) = \sum_{n=1}^{N}\{\sum_{m=1}^{M}\int_{S_m}[\,G_{\beta\alpha}(X(\zeta)-\xi)N_\omega(\zeta)t^n_{\beta\omega}^{N+1-n} - F_{\beta\alpha}(X(\zeta)-\xi)N_\omega(\zeta)u^n_{\beta\omega}^{N+1-n}\,]dS(X(\zeta))\,\}\,, \tag{3.8}$$

where

$$S = \sum_{m=1}^{M}\int S_m\,.$$

In the above equation, $t^n_{\beta\omega}$ and $u^n_{\beta\omega}$ are nodal quantities which can be brought outside the surface integrals. Thus,

$$c_{\beta\alpha}(\xi)u^N_\beta(\xi) = \sum_{n=1}^{N}\{\sum_{m=1}^{M} t^n_{\beta\omega}\int_{S_m} G_{\beta\alpha}(X(\zeta)-\xi)N_\omega(\zeta)dS(X(\zeta))^{N+1-n} - u^n_{\beta\omega}\int_{S_m} F_{\beta\alpha}(X(\zeta)-\xi)N_\omega(\zeta)dS(X(\zeta))^{N+1-n}\,\}\,. \tag{3.9}$$

The positioning of the nodal primary variables outside the integrals is, of course, a key step, since now the integrands contain only known functions. However, before discussing the techniques used to numerically evaluate these integrals, a brief discussion of the singularities present in the kernels $G^n_{\beta\alpha}$ and $F^n_{\beta\alpha}$ is in order.

The fundamental solutions to the uncoupled quasistatic problem contain singularities when the load point and field point coincide, that is, when r=0. The same is true of $G^n_{\beta\alpha}$ and $F^n_{\beta\alpha}$, since these kernels are derived

directly from the fundamental solutions. Series expansions of terms present in the evolution functions can be used to deduce the level of singularities existing in the kernels.

A number of observations concerning the results of these expansions should be mentioned. First, as would be expected, $F^1_{\alpha\beta}$ has a stronger level of singularity than does the corresponding $G^1_{\alpha\beta}$, since an additional derivative is involved in obtaining $F^1_{\alpha\beta}$ from $G^1_{\alpha\beta}$. Second, the coupling terms do not have as a high degree of singularity as do the corresponding non-coupling terms. Third, all of the kernel functions for the first time step could actually be rewritten as a sum of steady-state and transient components. That is,

$$G^1_{\alpha\beta} = {}^{ss}G_{\alpha\beta} + {}^{tr}G^1_{\alpha\beta}$$

$$F^1_{\alpha\beta} = {}^{ss}F_{\alpha\beta} + {}^{tr}F^1_{\alpha\beta} \ .$$

Then, the singularity is completely contained in the steady-state portion. Furthermore, the singularity in G^1_{ij} and F^1_{ij} is precisely equal to that for elastostatics, while the $G^1_{\theta\theta}$ and $F^1_{\theta\theta}$ singularities are identical to those for potential flow. (For two-dimensions, the subscript θ equals three.) This observation is critical in the numerical integration of the $F_{\alpha\beta}$ kernel to be discussed in the next subsection. However, from a physical standpoint, this means simply that, at any time t, the nearer one moves toward the load point, the closer the quasistatic response field corresponds with a steady-state field. Eventually, when the sampling and load points coincide, the quasistatic and steady-state responses are indistinguishable. As a final item, after careful examination of Appendix B, it is evident that the steady-state components in the kernels $G^n_{\alpha\beta}$ and $F^n_{\alpha\beta}$, with $n>1$, vanish. In that case, all that remains is a transient portion that contains no singularities. Thus, all singularities reside in

the ${}^{ss}G_{\alpha\beta}$ and ${}^{ss}F_{\alpha\beta}$ components of $G^1_{\alpha\beta}$ and $F^1_{\alpha\beta}$, respectively.

3.4.4 Numerical Integration

Having clarified the potential singularities present in the coupled kernels, it is now possible to consider the evaluation of the integrals in equation (3.9). That is, for any element m, the integrals

$$\int_{S_m} G^{N+1-n}_{\beta\alpha}(X(\zeta)-\xi)N_\omega(\zeta)dS(X(\zeta)) \tag{3.10a}$$

$$\int_{S_m} F^{N+1-n}_{\beta\alpha}(X(\zeta)-\xi)N_\omega(\zeta)dS(X(\zeta)) \tag{3.10b}$$

will be examined. To assist in this endeavor, the following three distinct categories can be identified:

(1) The point ξ does not lie on the element m

(2) The point ξ lies on the element m, but only non-singular or weakly singular integrals are involved

(3) The point ξ lies on the element m, and the integral is strongly singular.

In practical problems involving many elements, it is evident that most of the integration occurring in equation (3.9) will be of the Category (1) variety. In this case, the integrand is always non-singular, and standard Gaussian quadrature formulas can be employed. Sophisticated error control routines are needed, however, to minimize the computational effort for a certain level of accuracy. This non-singular integration is the most expensive part of a boundary element analysis, and, consequently, must be optimized to achieve an efficient solution. In the present implementation, error estimates, based upon the work of Stroud and Secrest (1966), are employed to automatically select the proper order of the quadrature rule.

Additionally, to improve accuracy in a cost-effective manner, a graded subdivision of the element is incorporated, especially when ξ is nearby. For two-dimensional problems, the integration order varies from two to twelve, within each of up to four element subdivisions.

Turning next to Category (2), one finds that again Gaussian quadrature is applicable, however, a somewhat modified scheme must be utilized to evaluate the weakly singular integrals. This is accomplished in two-dimensional elements via suitable subsegmentation along the length of the element so that the product of shape function, Jacobian and kernel remains well behaved.

Unfortunately, the remaining strongly singular integrals of Category (3) exist only in the Cauchy principal value sense and cannot, in general, be evaluated numerically, with sufficient precision. It should be noted that this apparent stumbling block is limited to the strongly singular portions, ${}^{ss}F_{ij}$ and ${}^{ss}F_{\theta\theta}$, of the $F^1_{\alpha\beta}$ kernel. The remainder of $F^1_{\alpha\beta}$, including ${}^{tr}F^1_{ij}$ and ${}^{tr}F^1_{\theta\theta}$, can be computed using the procedures outlined for Category (2). However, as will be discussed in the next subsection, even the Category (3) ${}^{ss}F_{ij}$ and ${}^{ss}F_{\theta\theta}$ kernels can be accurately determined by employing an indirect 'rigid body' method originally developed by Cruse (1974).

3.4.5 Assembly

The complete discretization of the boundary integral equation, in both time and space, has been described, along with the techniques required for numerical integration of the kernels. Now, a system of algebraic equations can be developed to permit the approximate solution of the original quasistatic problem. This is accomplished by systematically writing (3.9) at each global boundary node. The ensuing nodal collocation process, then,

produces a global set of equations of the form

$$\sum_{n=1}^{N} \left([G^{N+1-n}]\{t^n\} - [\bar{F}^{N+1-n}]\{u^n\} \right) = \{0\} , \qquad (3.11)$$

where

$[G^{N+1-n}]$ unassembled matrix of size (d+1)P x (d+1)Q, with coefficients determined from (3.10a)

$[\bar{F}^{N+1-n}]$ assembled matrix of size (d+1)P x (d+1)P, with coefficients determined from (3.10b) and $c_{\beta\alpha}$ included in the diagonal blocks

$\{t^n\}$ global generalized nodal traction vector with (d+1)Q components

$\{u^n\}$ global generalized nodal displacement vector with (d+1)P components

$\{0\}$ null vector with (d+1)P components

P total number of global functional nodes

$$Q = \sum_{m=1}^{M} A_m$$

A_m number of functional nodes in element m

d dimensionality of the problem.

In the above, recall that the terms generalized displacement and traction refer to the inclusion of the temperature and flux, respectively, as the (d+1) component at any point.

Consider, now, the first time step. Thus, for N=1, equation (3.11)

becomes

$$[G^1]\{t^1\} - [\bar{F}^1]\{u^1\} = \{0\} \ . \tag{3.12}$$

However, at this point, the diagonal block of $[\bar{F}^1]$ has not been completely determined due to the strongly singular nature of ${}^{SS}F_{ij}$ and ${}^{SS}F_{\theta\theta}$. Following Cruse (1974) and, later, Banerjee et al (1986) in elastodynamics, these diagonal contributions can be calculated indirectly by imposing a uniform 'rigid body' generalized displacement field on the same body, but under steady-state conditions. Then, obviously, the generalized tractions must be zero, and

$$[{}^{SS}F]\{1\} = \{0\} \ , \tag{3.13}$$

where $\{1\}$ is a vector having all $(d+1)P$ components equal to one. Using (3.13), the desired diagonal blocks, ${}^{SS}F_{ij}$ and ${}^{SS}F_{\theta\theta}$, can be obtained from the summation of the off-diagonal terms of $[{}^{SS}F]$. The remaining transient portion of the diagonal block is non-singular, and hence can be evaluated to any desired precision. With that step completed, (3.12) is rewritten as

$$[G^1]\{t^1\} - [F^1]\{u^1\} = \{0\} \ . \tag{3.14}$$

In a well-posed problem, at time Δt, the set of global generalized nodal displacements and tractions will contain exactly $(d+1)P$ unknown components. Then, as the final stage in the assembly process, equation (3.14) can be rearranged to form

$$[A^1]\{x^1\} = [B^1]\{y^1\} \ , \tag{3.15}$$

in which

$\{x^1\}$ unknown components of $\{u^1\}$ and $\{t^1\}$

$\{y^1\}$ known components of $\{u^1\}$ and $\{t^1\}$

$[A^1]$, $[B^1]$ associated coefficient matrices.

3.4.6 Solution

To obtain a solution of (3.15) for the unknown nodal quantities, a decomposition of matrix $[A^1]$ is required. In general, $[A^1]$ is a densely populated, unsymmetric matrix. The out-of-core solver, utilized here, was developed originally for elastostatics from the LINPACK software package (Dongarra et al, 1979) and operates on a submatrix level. Within each submatrix, Gaussian elimination with single pivoting reduces the block to upper triangular form. The final decomposed form of $[A^1]$ is stored in a direct-access file for reuse in subsequent time steps. Backsubstitution then completes the determination of $\{x^1\}$. Additional information on this solver is available in Banerjee et al (1985).

After returning from the solver routines, the entire nodal response vectors, $\{u^1\}$ and $\{t^1\}$, at time Δt are known. For solutions at later times, a simple marching algorithm is employed. Thus, from (3.11) with N=2,

$$[G^2]\{t^1\} - [F^2]\{u^1\} + [G^1]\{t^2\} - [F^1]\{u^2\} = \{0\} \ . \qquad (3.16)$$

Assuming that the same set of nodal components are unknown as in (3.14) for the first time step, equation (3.16) is reformulated as

$$[A^1]\{x^2\} = [B^1]\{y^2\} - [G^2]\{t^1\} + [F^2]\{u^1\} \ . \qquad (3.17)$$

Since, at this point, the right-hand side contains only known quantities, (3.17) can be solved for $\{x^2\}$. However, the decomposed form of $[A^1]$ already exists on a direct-access file, so only the relatively inexpensive backsubstitution phase is required for the solution.

The generalization of (3.17) to any time step N is simply

$$[A^1]\{x^N\} = [B^1]\{y^N\} - \sum_{n=1}^{N-1} \left([G^{N+1-n}]\{t^n\} - [F^{N+1-n}]\{u^n\} \right) \qquad (3.18)$$

in which the summation represents the effect of past events. By systematically storing all of the matrices and nodal response vectors computed during the marching process, surprisingly little computing time is required at each new time step. In fact, for any time step beyond the first, the only major computational task is the integration needed to form $[G^N]$ and $[F^N]$. Even this process is somewhat simplified, since now the kernels are non-singular. Also, as time marches on, the effect of events that occurred during the first time step diminishes. Consequently, the terms containing $[G^N]$ and $[F^N]$ will eventually become insignificant compared to those associated with recent events. Once that point is reached, further integration is unnecessary, and a significant reduction in the computing effort per time step can be achieved.

It should be emphasized that the entire boundary element method developed, in this section, has involved surface quantities exclusively. A complete solution to the well-posed linear uncoupled quasistatic problem, with homogeneous properties, can be obtained in terms of the nodal response vectors, without the need for any volume discretization. In many practical situations, however, additional information, such as, the temperature at interior locations or the stress at points on the boundary, is required. The next subsection discusses the calculation of these quantities.

3.4.7 Interior Quantities

Once equation (3.18) is solved, at any time step, the complete set of primary nodal quantities, $\{u^N\}$ and $\{t^N\}$, is known. Subsequently, the response at points within the body can be calculated in a straightforward

manner. For any point ξ in the interior, the generalized displacement can be determined from (3.9) with $c_{\beta\alpha} = \delta_{\beta\alpha}$. That is,

$$u^N_\alpha(\xi) = \sum_{n=1}^{N} \{ \sum_{m=1}^{M} [t^n_{\beta\omega} \int_{S_m} G^{N+1-n}_{\beta\alpha}(X(\zeta)-\xi) N_\omega(\zeta) dS(X(\zeta)) - u^n_{\beta\omega} \int_{S_m} F^{N+1-n}_{\beta\alpha}(X(\zeta)-\xi) N_\omega(\zeta) dS(X(\zeta))] \} . \tag{3.19}$$

Now, all the nodal variables on the right-hand side are known, and, as long as, ξ is not on the boundary, the kernel functions in (3.19) remain non-singular. However, when ξ is on the boundary, the strong singularity in ${}^{ss}F_{\beta\alpha}$ prohibits accurate evaluation of the generalized displacement via (3.19), and an alternate approach is required. The apparent dilemma is easily resolved by recalling that the variation of surface quantities is completely defined by the elemental shape functions. Thus, for boundary points, the desired relationship is simply

$$u^N_\alpha(\xi) = N_\omega(\zeta)\, u^N_{\alpha\omega} \tag{3.20}$$

where $N_\omega(\zeta)$ are the shape functions for the appropriate element and ζ are the intrinsic coordinates corresponding to ξ within that element. Obviously, from (3.20), neither integration nor the explicit contribution of past events are needed to evaluate generalized boundary displacements.

In many problems, additional quantities, such as heat flux and stress, are also important. The boundary integral equation for heat flux, can be written

$$q^N_i(\xi) = \sum_{n=1}^{N} \{ \sum_{m=1}^{M} [t^n_{\beta\omega} \int_{S_m} E^{N+1-n}_{\beta\theta i}(X(\zeta)-\xi) N_\omega(\zeta) dS(X(\zeta)) - u^n_{\beta\omega} \int_{S_m} D^{N+1-n}_{\beta\theta i}(X(\zeta)-\xi) N_\omega(\zeta) dS(X(\zeta))] \} \tag{3.21}$$

where

$$E^n_{\beta\theta i}(X(\zeta)-\xi) = - k \frac{\partial G^n_{\beta\theta}(X(\zeta)-\xi)}{\partial \xi_i} \tag{3.21a}$$

$$D^n_{\beta\theta i}(X(\zeta)-\xi) = - k \frac{\partial F^n_{\beta\theta}(X(\zeta)-\xi)}{\partial \xi_i} \, . \tag{3.21b}$$

This is valid for interior points, whereas, when ξ is on the boundary, the shape functions can again be used. In this latter case,

$$N_\omega(\zeta) q^N_\omega = n_i(\xi) q^N_i(\xi) \tag{3.22a}$$

$$\frac{\partial N_\omega(\zeta)}{\partial \zeta} \theta^N_\omega = - \frac{1}{k} \frac{\partial x_i}{\partial \zeta} q^N_i(\xi) \, , \tag{3.22b}$$

which can be solved for boundary flux. Meanwhile, interior stresses can be evaluated from

$$\sigma^N_{ij}(\xi) = \sum_{n=1}^{N} \{ \sum_{m=1}^{M} [t^n_{\beta\omega} \int_{S_m} E^{N+1-n}_{\beta ij}(X(\zeta)-\xi) N_\omega(\zeta) dS(X(\zeta)) - u^n_{\beta\omega} \int_{S_m} D^{N+1-n}_{\beta ij}(X(\zeta)-\xi) N_\omega(\zeta) dS(X(\zeta))] \} \tag{3.23}$$

in which

$$E^n_{\beta ij}(X(\zeta)-\xi) = \frac{2\mu\nu}{1-2\nu} \delta_{ij} \frac{\partial G^n_{\beta l}}{\partial \xi_l} + \mu \left(\frac{\partial G^n_{\beta i}}{\partial \xi_j} + \frac{\partial G^n_{\beta j}}{\partial \xi_i} \right) - \beta \delta_{ij} G^n_{\beta\theta} \tag{3.23a}$$

$$D^n_{\beta ij}(X(\zeta)-\xi) = \frac{2\mu\nu}{1-2\nu} \delta_{ij} \frac{\partial F^n_{\beta l}}{\partial \xi_l} + \mu \left(\frac{\partial F^n_{\beta i}}{\partial \xi_j} + \frac{\partial F^n_{\beta j}}{\partial \xi_i} \right) - \beta \delta_{ij} F^n_{\beta\theta} \, . \tag{3.23b}$$

Equation (3.23) is, of course, developed from (3.19). Since strong kernel singularities appear when (3.23) is written for boundary points, an

alternate procedure is needed to determine surface stress. This alternate scheme exploits the interrelationships between generalized displacement, traction, and stress and is the straightforward extension of the technique typically used in elastostatic implementations (Cruse and Van Buren, 1971). Specifically, the following can be obtained

$$n_j(\xi)\sigma^N_{ij}(\xi) = N_\omega(\zeta)t^N_{i\omega} \tag{3.24a}$$

$$\sigma^N_{ij}(\xi) - \frac{D^e_{ijkl}}{2}\left(u^N_{k,l}(\xi)+u^N_{l,k}(\xi)\right) = -\beta\delta_{ij}N_\omega(\zeta)u^N_{\theta\omega} \tag{3.24b}$$

$$\frac{\partial x_j}{\partial \zeta}\, u^N_{i,j}(\xi) = \frac{\partial N_\omega}{\partial \zeta}\, u^N_{i\omega} \tag{3.24c}$$

in which $u^N_{\theta\omega}$ is obviously the nodal temperatures, and,

$$D^e_{ijkl} = \lambda\delta_{ij}\delta_{kl} + 2\mu\delta_{ik}\delta_{jl}\ .$$

Equations (3.24) form an independent set that can be solved numerically for $\sigma^N_{ij}(\xi)$ and $u^N_{i,j}(\xi)$ completely in terms of known nodal quantities $u^N_{\alpha\omega}$ and $t^N_{\alpha\omega}$, without the need for kernel integration nor convolution. Notice, however, that shape function derivatives appear in (3.24c), thus constraining the representation of stress on the surface element to something less than full quadratic variation. The interior stress kernel functions, defined by (3.23), are also detailed in Appendix B.

3.4.8 Advanced Features

The thermoelastic formulation has been implemented as a segment of the state-of-the-art, general purpose boundary element computer program, GP-BEST. Consequently, many additional features, beyond those detailed above, are available for the analysis of complex engineering problems. Perhaps,

the most significant of these items, is the capability to analyze substructured problems. This, not only extends the analysis to bodies composed of several different materials, but also often provides computational efficiencies. An individual substructure or generic modeling region (GMR) must contain a single material. During the integration process, each GMR remains a separate entity. The GMR's are then brought together at the assembly stage, where compatibility relationships are enforced on common boundaries between regions. Typically, compatibility ensures continuous displacement and temperature fields across an interface, however, recent enhancements to the code permit sliding between regions, spring contacts and interfacial thermal resistance to model air gaps or coating resistances. In the latter instances, discontinuities appear at the interface. In any case, the multi-GMR assembly process produces block-banded system matrices that are solved in an efficient manner.

As another feature, a high degree of flexibility is provided for the specification of boundary conditions. In general, time-dependent values can be defined in either global or local coordinates. Not only can generalized displacements and tractions be specified, but also spring and convection boundary conditions area available. Another recent addition permits time-dependent ambient temperatures. A final item, worthy of note, is the availability of a comprehensive symmetry capability which includes provisions for both planar and cyclic symmetry.

These advanced features greatly extend the range of applicability of the present formulation. In the next section, several examples are presented to demonstrate the validity and applicability of this boundary-only formulation.

3.5 Examples

3.5.1 Sudden Heating of an Aluminum Block

As a first example, transient heating of an aluminum block is examined under plane strain conditions. The block, shown in Figure 3.1, initially rests in thermodynamic equilibrium at zero temperature. Then, suddenly, the face at Y = 1.0 in. is elevated to 100°F, while the remaining three faces are insulated and restrained against normal displacements. Thus, only axial deformation in the Y-direction is permitted. Naturally, as the diffusive process progresses, temperature builds along with the lateral stresses σ_{xx} and σ_{zz}. To complete the specification of the problem, the following standard set of material properties are used to characterize the aluminum:

$E = 10 \times 10^6$ psi , $\quad \nu = 0.33$,

$\alpha = 13 \times 10^{-6}/^{o}F$,

$k = 25$ in.-lb./sec. in.^{o}F , $\quad \rho c_g = 200$ in.-lb./in.^{3o}F .

The two-dimensional boundary element idealization consists of the simple four element, eight node model included in Figure 3.1. A time step of 0.4 sec. is selected, corresponding to a non-dimensional time step of 0.05. Additionally, a finite element analysis of this same problem was conducted using a modified thermal version of the computer code CRISP (Gunn and Britto, 1984). The finite element model is also a two-dimensional plane strain representation, however sixteen linear strain quadralaterals are placed along the diffusion length. In the FE run, a time step of 0.2 sec. is employed.

Temperatures, displacements, and stresses are compared in Table 3.1. Notice that the boundary element analysis, with only one element in the flow direction, produces a better time-temperature history than does a

sixteen element FE analysis with a smaller time step. Both methods exhibit greatest error during the initial stages of the process. This is the result of the imposition of a sudden temperature change. Meanwhile, the comparison of the overall axial displacement indicates agreement to within 3% for the BE analysis and 5% for the FE run. A steady-state analysis via both methods produces the exact answer to three digit accuracy. The last comparison, in the table, involves lateral stresses at an integration point in the FE model. The boundary element results are quite good throughout the range, however, the FE stresses exhibit considerable error, particularly during the initial four seconds. Actually, these finite element stress variations are not unexpected in light of the errors present in the temperature and displacement response. Recall that in the standard finite element process, stresses are computed on the basis of numerical differentiation of the displacements, whereas in boundary elements, the stresses at interior points are obtained directly from a discretized version of an exact integral equation. Consequently, the BE interior stress solution more nearly coincides with the actual response.

3.5.2 Circular Disc

Next, transient thermal stresses in a circular disc are investigated. The disc of radius 'a' initially rests at zero uniform temperature. The top and bottom surfaces are thermally insulated, and all boundaries are completely free of mechanical constraint. Then, suddenly, at time zero, the temperature of the entire outer edge (i.e., r=a) is elevated to unity and, subsequently, maintained at that level.

The boundary element model of the disc with unit radius is shown in Figure 3.2. Only four quadratic elements are employed, along with quarter symmetry. Ten interior points are also included strictly to monitor response. In addition, the following non-dimensionalized material

properties are arbitrarily selected for the plane stress analysis:

$E = 1.333$ $\qquad$ $\rho c_g = 1.0$

$\nu = 0.333$ $\qquad$ $k = 1.0$

$\alpha = 0.75$

Results obtained under quasistatic conditions for a time step of 0.005 are compared, in Figures 3.3, 3.4 and 3.5, to the analytical solution presented in Timoshenko and Goodier (1970). Notice that temperatures, as well as radial and tangential stresses are accurately determined via the boundary element analysis. In particular from Figure 3.5, even the tangential stress on the outer edge is faithfully reproduced.

3.5.3 Turbine Blade

For the final application, the plane strain response of an internally cooled turbine blade is examined under startup thermal transients. The boundary element model of the blade is illustrated in Figure 3.6. In this problem, the two GMR approach is chosen solely to enhance computational efficiency. This is accomplished by reducing the aspect ratio of individual GMR's and by creating a block banded system matrix. The leading (lefthand) GMR consists of 26 quadratic elements, while 24 elements are used to model the trailing (righthand) region.

The blade is manufactured of stainless steel with the following thermomechanical properties:

$E = 29.0 \times 10^6$ psi $\qquad$ $\rho c_g = 368$ in.-lb./in.^{3} $^\circ$F

$\nu = 0.30$ $\qquad$ $k = 1.65$ in.-lb./sec.in.$^\circ$F

$\alpha = 9.6 \times 10^{-6}$ in./in.$^\circ$F

During operation a hot gas flows outside the blade, while a relatively cool

gas passes through the internal holes. The gas temperature transients are plotted in Figure 3.7 for a typical startup. Convection film coefficients are specified as follows:

Outer surface at leading edge	$h = 50$ in.-lb./sec.in.^{2}°F
Remainder of outer surface	$h = 20$ in.-lb./sec.in.^{2}°F
Inner cooling hole surfaces	$h = 10$ in.-lb./sec.in.^{2}°F

A time step of 0.2 sec. is employed for the boundary element analysis.

The response at two points, A, on the leading edge and, B, at midspan are displayed in Figures 3.8 and 3.9. Notice that temperatures and stresses are consistently higher on the leading edge, reaching peak values of approximately 1500°F and -60 ksi, respectively. Also, as is evident from Figure 3.9, significant stress reversals occur during this startup. As a next step, these numerical results could be used as input for a fatigue analysis to assess the durability of the design. In that regard, it should be emphasized that the stresses presented for points A and B are surface stresses, calculated by satisfying the constitutive laws, strain-displacement and equilibrium directly at the boundary point. This can be expected to produce much more accurate results than the standard practice utilized in finite element approaches of extrapolating interior Gauss point stress values to the boundary.

TABLE 3.1

SUDDEN HEATING OF A CUBE

Time (sec)	Temperature (^{O}F) at Y = 0			Axial Displacement (μin.) at Y = 1.0			Lateral Stress (ksi) at Y = 0.5312		
	Exact	FE	GP-BEST	Exact	FE	GP-BEST	Exact	FE	GP-BEST
0.8	4.7	3.4	3.8	910	860	920	-5.6	-3.9	-5.4
1.6	22.0	19.8	20.7	1290	1250	1320	-9.1	-7.7	-9.2
2.4	38.3	36.4	37.7	1570	1540	1610	-11.3	-10.3	-11.7
3.2	51.5	50.0	51.5	1780	1760	1840	-13.1	-12.2	-13.5
4.0	61.9	60.7	62.2	1950	1930	2000	-14.4	-13.8	-14.8
4.8	70.1	69.1	70.5	2090	2070	2130	-15.5	-15.0	-15.9
5.6	76.5	75.7	76.9	2200	2180	2230	-16.3	-15.9	-16.7
6.4	81.5	80.9	81.9	2280	2270	2310	-17.0	-16.7	-17.3
7.2	85.5	84.9	85.8	2340	2330	2370	-17.5	-17.2	-17.8
8.0	88.6	88.2	88.8	2400	2390	2410	-17.9	-17.7	-18.1

FIGURE 3.1

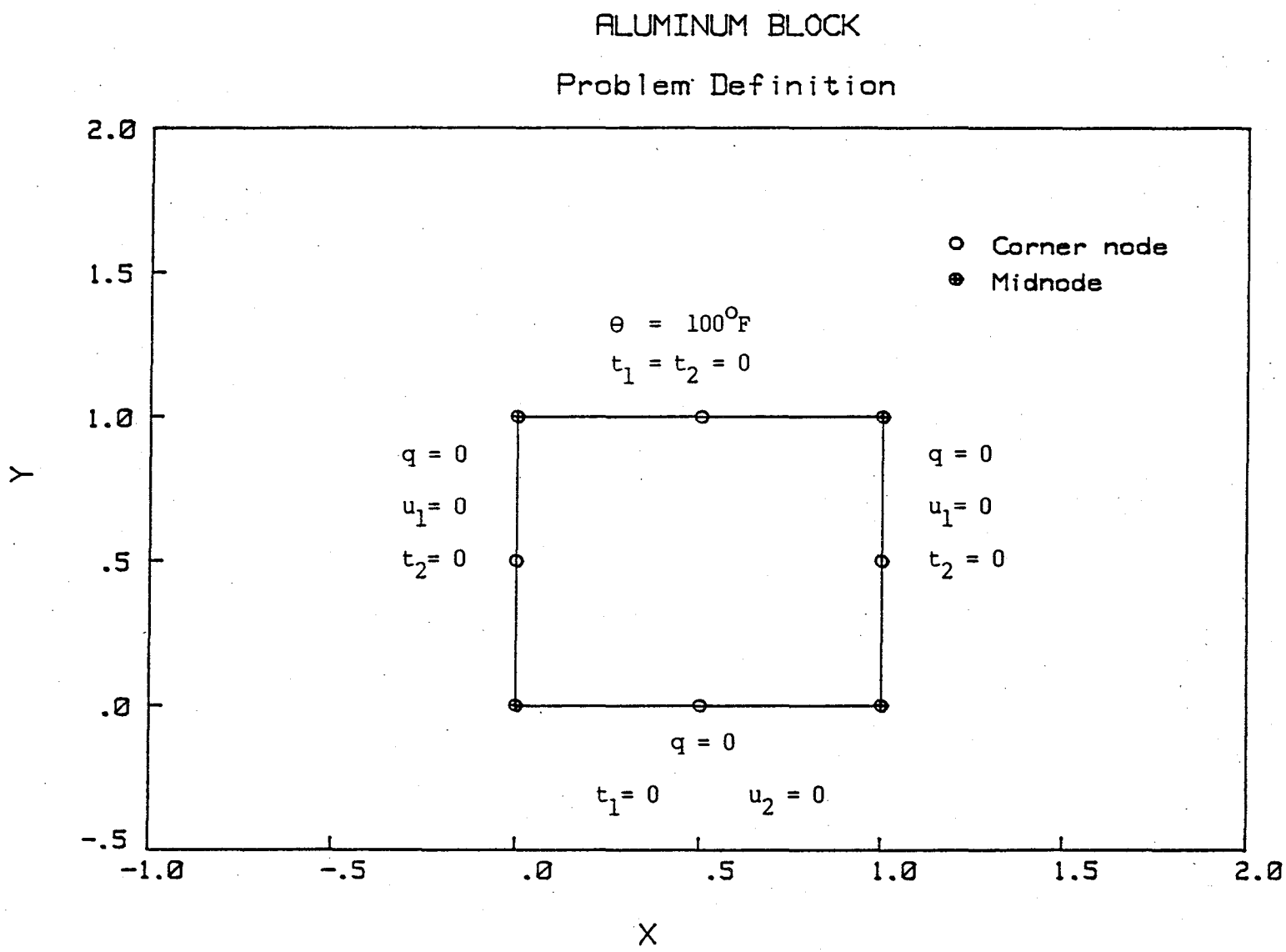
ALUMINUM BLOCK
Problem Definition
Corner node
Midnode
θ = 100°F
t1 = t2 = 0
q = 0
u1 = 0
t2 = 0
q = 0
u1 = 0
t2 = 0
q = 0
t1 = 0
u2 = 0
2.0
1.5
1.0
.5
.0
-.5
-1.0
-.5
.0
.5
1.0
1.5
2.0
Y
X

FIGURE 3.2

CIRCULAR DISC

Boundary Element Model

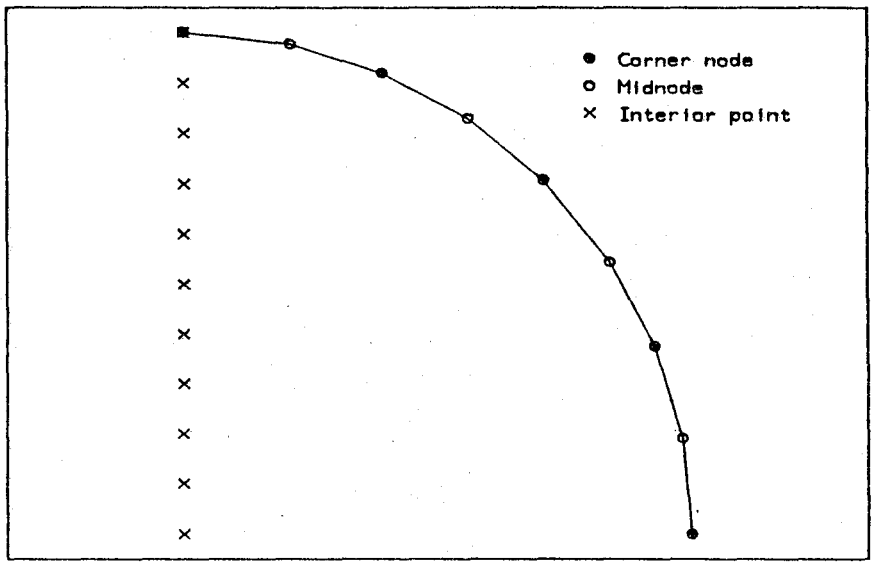

FIGURE 3.3

CIRCULAR DISC

GP-BEST Results

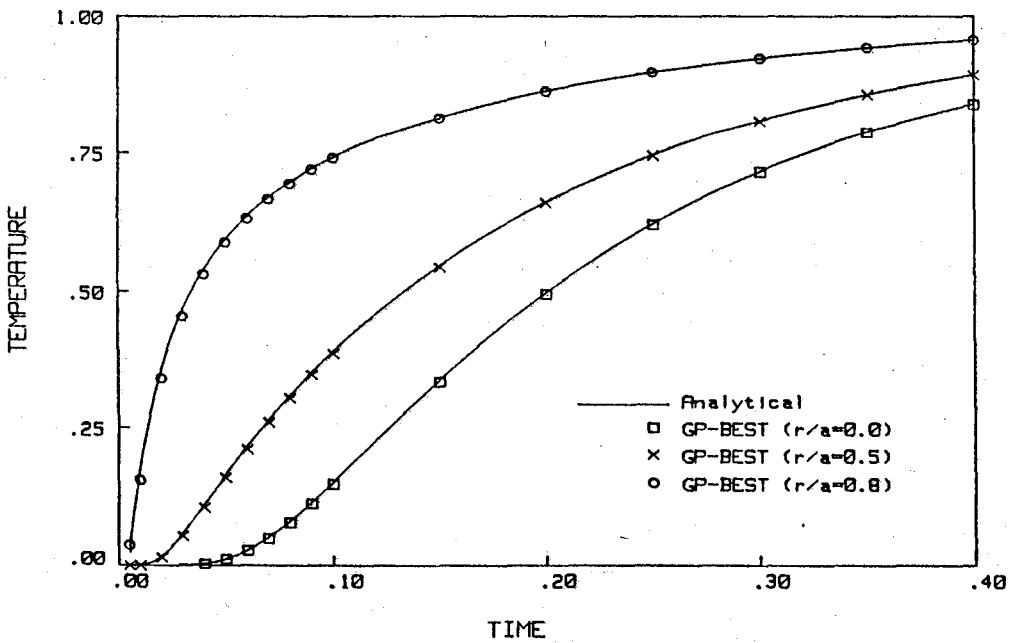

FIGURE 3.4

CIRCULAR DISC

GP-BEST Results

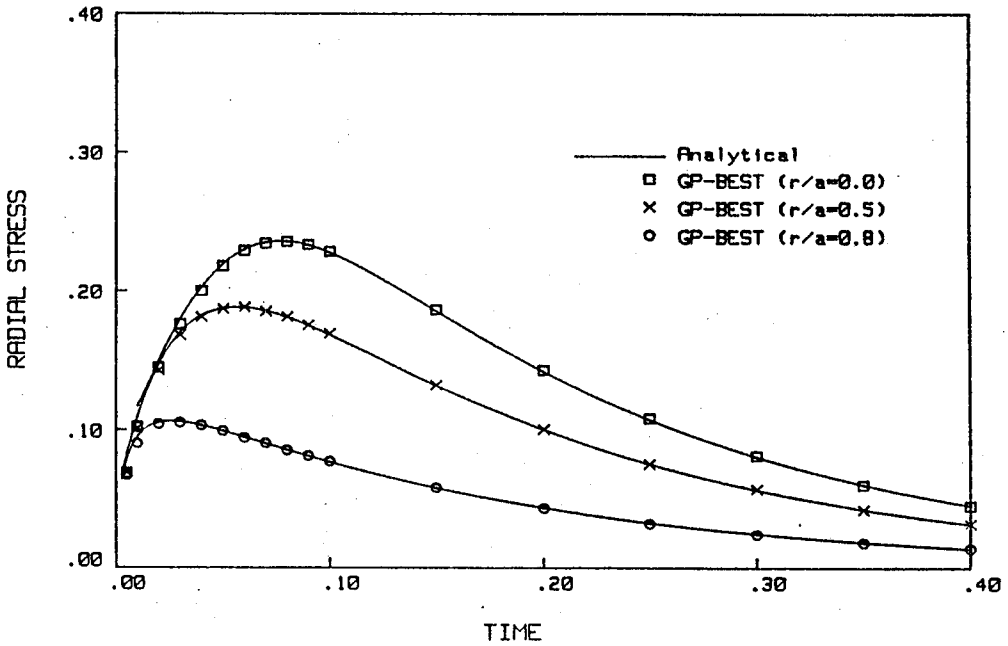

FIGURE 3.5

CIRCULAR DISC

GP-BEST Results

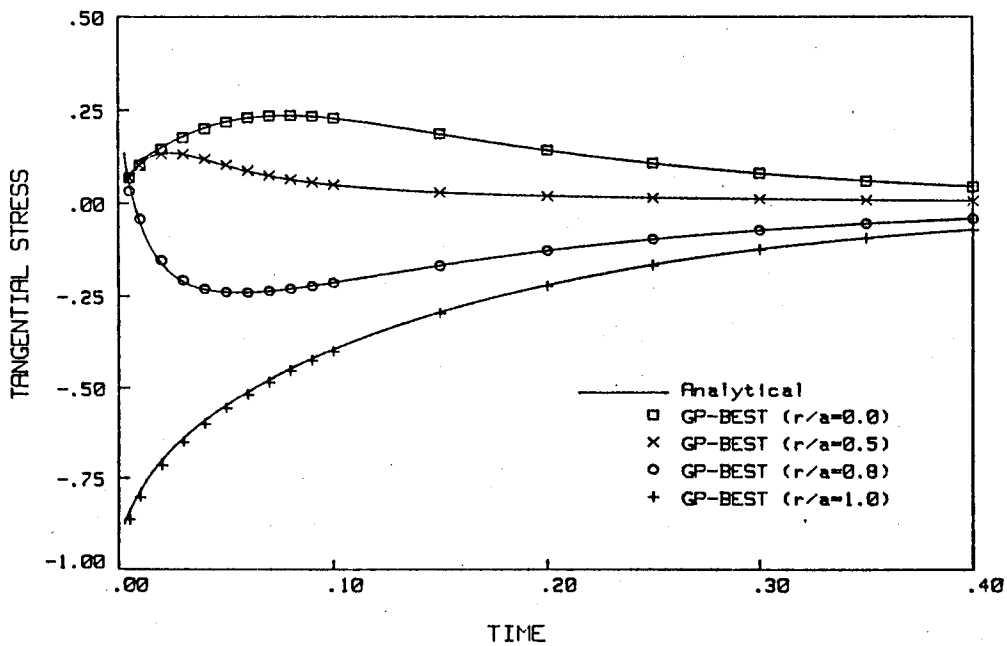

FIGURE 3.6

TURBINE BLADE

Boundary Element Model

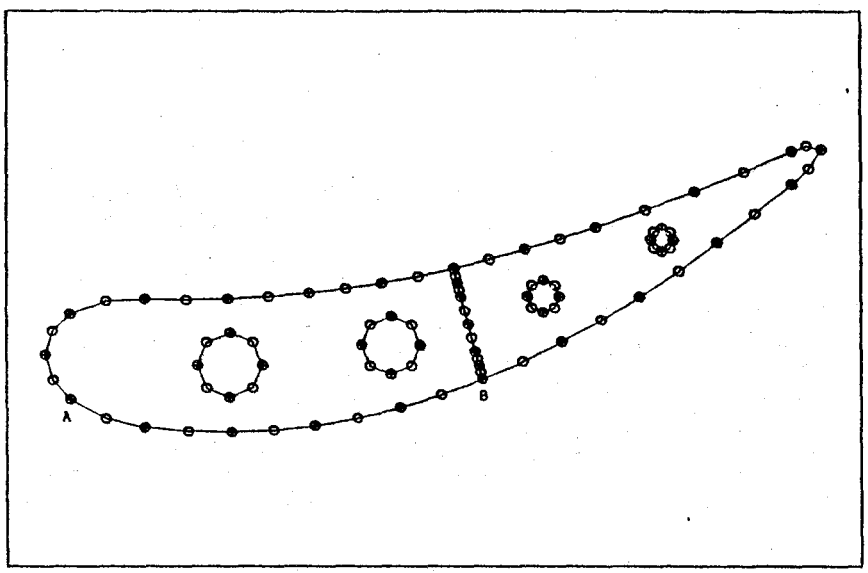

FIGURE 3.7

TURBINE BLADE

Startup Transient

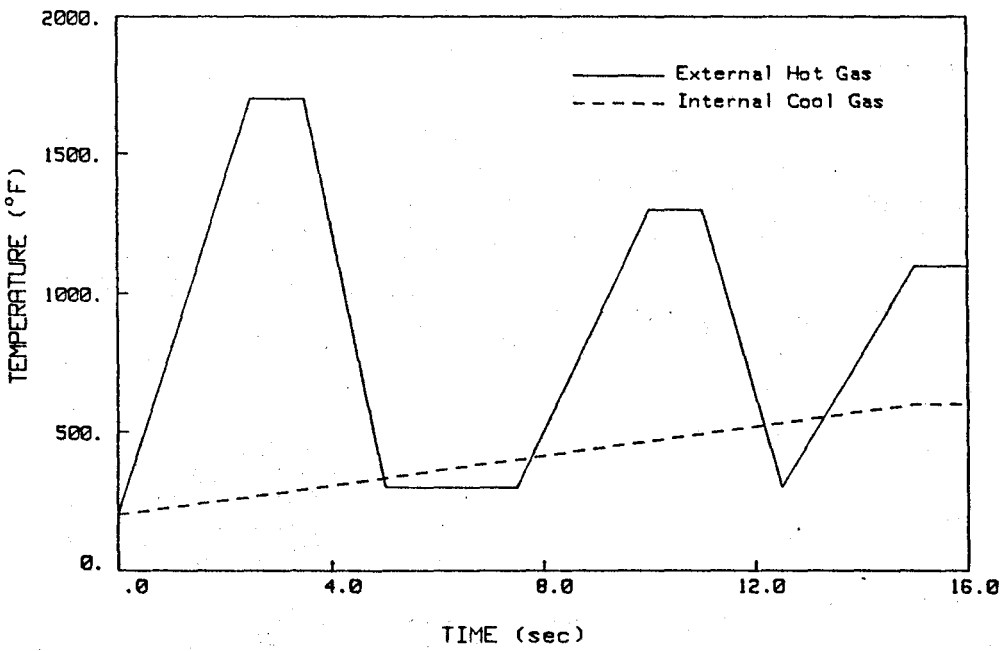

FIGURE 3.8
TURBINE BLADE
GP-BEST Results

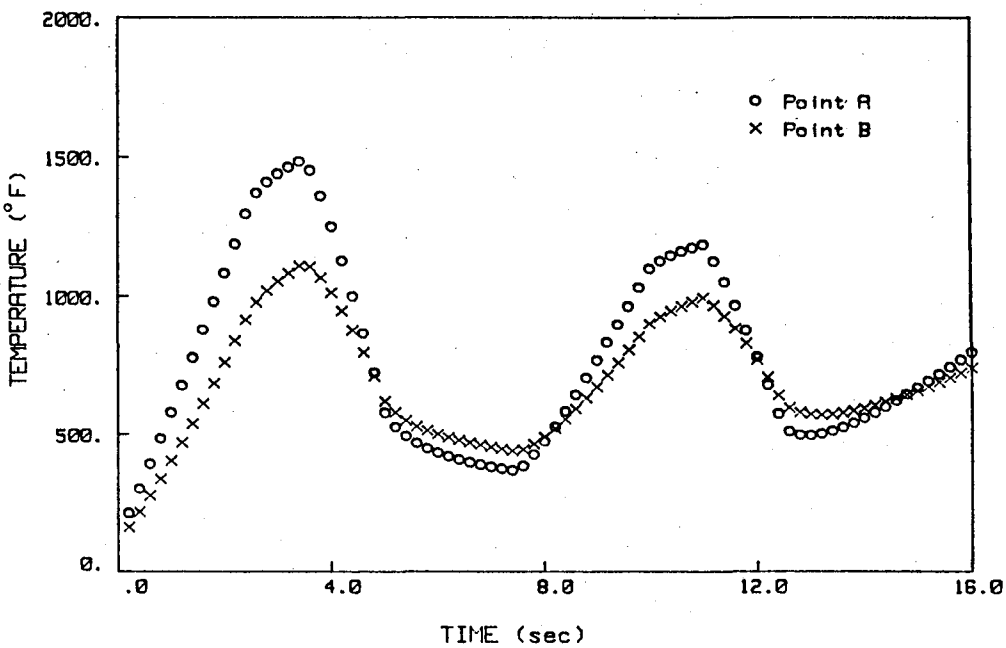

FIGURE 3.9
TURBINE BLADE
GP-BEST Results

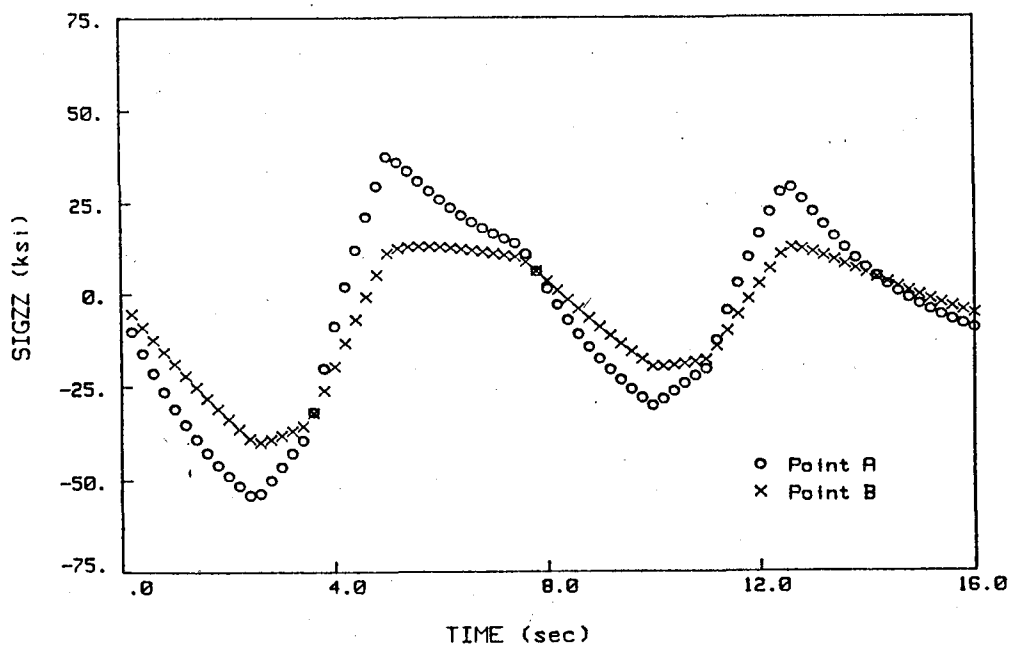

4 INTEGRAL FORMULATIONS FOR FLUIDS

4.1 Introduction

Next, attention turns to the hot fluid. In the following, a number of integral formulations are developed for compressible and incompressible thermoviscous flow and, additionally, for the simpler theory of convective heat transfer. Subsections present the governing equations, fundamental solutions, integral representations, an overview of the numerical implementation, a brief description of the approach for coupling the fluid with the solid, and, finally, a number of detailed numerical examples.

4.2 Governing Equations

4.2.1 Compressible Thermoviscous Flow

The governing equations for a thermally-sensitive, compressible, viscous fluid can be developed from the consideration of the conservation laws of mass, momentum, and energy. In each case, the law is first written for a continuum which is, in general, moving non-uniformly with respect to the observer. The local (differential) form of the law is then derived. Although a derivation of the governing equations of fluid dynamics, similar to the following, can be found in a number of texts, it is a useful means for establishing the underlying assumptions and limitations.

The Principle of the Conservation of Mass asserts that the time rate of change of mass must equal the rate of mass increase due to internal sources. That is,

$$\frac{D}{Dt}\int_{V(t)} \rho dV = \int_{V(t)} \psi dV \ , \tag{4.1}$$

where ρ is the mass density, ψ is the mass source rate per unit volume, and the operator D/Dt represents a material time derivative. Notice that in (4.1) the mass of interest occupies V(t), a region of space which may vary

with time. Applying a generalized version of Leibnitz's Rule to the left-hand side of (4.1) produces

$$\frac{D}{Dt}\int_{V(t)} \rho dV = \int_{V(t)} \frac{\partial \rho}{\partial t}\, dV + \int_{S(t)} \rho v_j n_j dS \ , \tag{4.2}$$

where S(t) is the surface enclosing V(t), and v_j and n_j are the local velocities and outward normals on that surface, respectively. However, via the Divergence Theorem, the surface integral can be rewritten as

$$\int_{S(t)} \rho v_j n_j dS = \int_{V(t)} \frac{\partial}{\partial x_j}(\rho v_j) dV \ . \tag{4.3}$$

Therefore, from (4.1), (4.2), and (4.3)

$$\int_{V(t)} \left[\frac{\partial \rho}{\partial t} + \frac{\partial}{\partial x_j}(\rho v_j) - \psi \right] dV = 0 \ . \tag{4.4}$$

Since this integral must vanish for all regions V(t), the integrand must be identically zero. Thus,

$$\frac{\partial \rho}{\partial t} + \frac{\partial}{\partial x_j}(\rho v_j) - \psi = 0 \ , \tag{4.5}$$

which is the desired local form of continuity or Conservation of Mass. This can also be written

$$\frac{D\rho}{Dt} + \rho \frac{\partial v_j}{\partial x_j} - \psi = 0 \ , \tag{4.6}$$

where

$$\frac{D}{Dt} = \frac{\partial}{\partial t} + v_j \frac{\partial}{\partial x_j} \tag{4.7}$$

is again the material time derivative.

Next, consideration is given to the Conservation of Linear Momentum. In this case, according to Newton's Second Law, it is postulated that the time rate of change of momentum is equal to the resultant of the applied forces. Alternatively, these applied forces can be visualized as the rate of momentum entering the region through the surface plus the rate of momentum increase due to internal generation. With either interpretation,

$$\frac{D}{Dt}\int_{V(t)} \rho v_i dV = \int_{S(t)} \sigma_{ij} n_j dS + \int_{V(t)} (f_i + v_i \psi) dV \ , \tag{4.8}$$

where σ_{ij} is the total stress tensor and f_i is the body force vector. Notice that the term $v_i\psi$ is included in the last volume integral to account for the internal momentum generation due to mass sources. Applying the generalized Leibnitz's Rule and the Divergence Theorem to the left-hand integral of (4.8) yields

$$\frac{D}{Dt}\int_{V(t)} \rho v_i dV = \int_{V(t)} \left[\frac{\partial}{\partial t}(\rho v_i) + \frac{\partial}{\partial x_j}(\rho v_i v_j) \right] dV \ . \tag{4.9}$$

The Divergence Theorem can also be invoked to convert the surface integral in (4.8) into a volume integral. Thus,

$$\int_{S(t)} \sigma_{ij} n_j dS = \int_{V(t)} \frac{\partial \sigma_{ij}}{\partial x_j} dV \ . \tag{4.10}$$

Utilizing (4.9) and (4.10), Newton's Second Law becomes

$$\int_{V(t)} \left[\frac{\partial}{\partial t}(\rho v_i) + \frac{\partial}{\partial x_j}(\rho v_i v_j) - \frac{\partial \sigma_{ij}}{\partial x_j} - f_i - v_i \psi \right] dV = 0 \ . \tag{4.11}$$

Again, since this integral must vanish for arbitrary regions, the integrand must be zero. That is,

$$\frac{\partial}{\partial t}(\rho v_i) + \frac{\partial}{\partial x_j}(\rho v_i v_j) - \frac{\partial \sigma_{ij}}{\partial x_j} - f_i - v_i \psi = 0 . \qquad (4.12)$$

However, equation (4.12) can be rewritten as

$$\rho \frac{\partial v_i}{\partial t} + \rho v_j \frac{\partial v_i}{\partial x_j} - \frac{\partial \sigma_{ij}}{\partial x_j} - f_i + v_i \left[\frac{\partial \rho}{\partial t} + \frac{\partial}{\partial x_j}(\rho v_j) - \psi \right] = 0 . \qquad (4.13)$$

But since the bracketed term multiplying v_i in (4.13) equals zero from the continuity equation (4.5), the local form of the Conservation of Linear Momentum becomes

$$\rho \frac{\partial v_i}{\partial t} + \rho v_j \frac{\partial v_i}{\partial x_j} - \frac{\partial \sigma_{ij}}{\partial x_j} - f_i = 0 , \qquad (4.14)$$

or simply

$$\rho \frac{Dv_i}{Dt} - \frac{\partial \sigma_{ij}}{\partial x_j} - f_i = 0 . \qquad (4.15)$$

Note that although continuity is invoked above, a flow field that conserves linear momentum does not automatically conserve mass. In addition, the moment of momentum must also be conserved as a consequence of Newton's Second Law. However, satisfaction of this law only necessitates that the stress tensor σ_{ij} be symmetric.

Finally, the Conservation of Energy is examined. For energy balance, the time rate of change of kinetic plus internal energy must equate the rate of work done by the body forces and surface tractions, along with the rate of energy entering via heat transfer across the surface, the rate of kinetic and internal energy increase due to mass sources, and the rate of energy input due to heat sources. In equation form,

$$\frac{D}{Dt}\int_{V(t)} \rho\left(\frac{v_i v_i}{2} + E\right)dV = \int_{V(t)} f_i v_i dV + \int_{S(t)} \sigma_{ij} n_j v_i dS - \int_{S(t)} q_i n_i dS$$

$$+ \int_{V(t)} \psi \left(\frac{v_i v_i}{2} + E\right) dV + \int_{V(t)} \phi \, dV \tag{4.16}$$

where E is the internal energy per unit mass, q_i is the heat flux vector and ϕ is the heat source rate per unit volume. By first applying the generalized Leibnitz's Rule to the left-hand side of (4.16), and then invoking the Divergence Theorem for all of the remaining surface integrals, equation (4.16) is transformed into

$$\int_{V(t)} \Bigg[\rho \frac{D}{Dt} \left(\frac{v_i v_i}{2} + E\right) - \rho v_i f_i - \frac{\partial}{\partial x_j} (\sigma_{ij} v_i) + \frac{\partial q_i}{\partial x_i} - \phi$$

$$+ \left(\frac{v_i v_i}{2} + E\right)\left(\frac{\partial \rho}{\partial t} + \frac{\partial}{\partial x_i}(\rho v_i) - \psi\right) \Bigg] dV = 0 \, . \tag{4.17}$$

Since this is valid for any region V(t),

$$\rho \frac{D}{Dt} \left(\frac{v_i v_i}{2} + E\right) - \rho v_i f_i - \frac{\partial}{\partial x_j} (\sigma_{ij} v_i) + \frac{\partial q_i}{\partial x_i} - \phi$$

$$+ \left(\frac{v_i v_i}{2} + E\right)\left(\frac{\partial \rho}{\partial t} + \frac{\partial}{\partial x_i}(\rho v_i) - \psi\right) = 0 \, . \tag{4.18}$$

After further rearrangement this becomes,

$$\rho \frac{DE}{Dt} + \frac{\partial q_i}{\partial x_i} - \sigma_{ij} \frac{\partial v_i}{\partial x_j} - \phi + v_i \left[\rho \frac{Dv_i}{Dt} - \frac{\partial \sigma_{ij}}{\partial x_j} - f_i \right]$$

$$+ \left(\frac{v_i v_i}{2} + E\right) \left[\frac{\partial \rho}{\partial t} + \frac{\partial}{\partial x_i} (\rho v_i) - \psi \right] = 0. \tag{4.19}$$

Now, the first bracketed expression in (4.19) vanishes via the Conservation of Linear Momentum, while the second bracketed expression is zero from the Conservation of Mass. Thus, equation (4.19) reduces to

$$\rho \frac{DE}{Dt} + \frac{\partial q_i}{\partial x_i} - \sigma_{ij} \frac{\partial v_i}{\partial x_j} - \Phi = 0 \qquad (4.20)$$

as the expression for the Conservation of Energy.

To recapitulate, the conservation laws for a thermoviscous fluid can be written collectively as

$$\frac{D\rho}{Dt} + \rho \frac{\partial v_j}{\partial x_j} - \psi = 0 \qquad \text{Mass} \qquad (4.21a)$$

$$\rho \frac{Dv_i}{Dt} - \frac{\partial \sigma_{ij}}{\partial x_j} - f_i = 0 \qquad \text{Momentum} \qquad (4.21b)$$

$$\rho \frac{DE}{Dt} + \frac{\partial q_i}{\partial x_i} - \sigma_{ij} \frac{\partial v_i}{\partial x_j} - \Phi = 0 \; . \qquad \text{Energy} \qquad (4.21c)$$

Next, constitutive relationships are introduced. In particular, a homogeneous isotropic Newtonian fluid is assumed such that

$$\sigma_{ij} = 2\mu \left(\frac{\partial v_i}{\partial x_j} + \frac{\partial v_j}{\partial x_i}\right) + \lambda \delta_{ij} \frac{\partial v_k}{\partial x_k} - \delta_{ij} p \; , \qquad (4.22)$$

where p is the thermodynamic pressure, while μ and λ are coefficients of viscosity. Fourier's law of heat conduction is also envoked, which for an isotropic medium becomes

$$q_i = -k \frac{\partial \theta}{\partial x_i} \qquad (4.23)$$

where θ is the thermodynamic temperature and k is the thermal conductivity. Additionally, the fluid is modeled as a perfect gas. Thus, the kinetic equation of state is simply

$$p = \rho R \theta \; , \qquad (4.24)$$

in which R is the gas constant. Finally, a relationship is needed for the internal energy E. From thermodynamic considerations for a perfect gas,

$$h = E + \frac{p}{\rho} = E + R\theta \tag{4.25a}$$

where h is the enthalpy. In addition, if the specific heat at constant pressure, c_p, does not vary with temperature, then

$$h = c_p\theta \ , \tag{4.25b}$$

and, hence,

$$E = (c_p - R)\theta = c_v\theta \ , \tag{4.26}$$

where c_v is the specific heat at constant volume. Equations (4.22), (4.23), (4.24), and (4.26) lead to the following form of the governing equations for the idealized thermoviscous fluid:

$$\frac{D\rho}{Dt} + \rho \frac{\partial v_i}{\partial x_i} - \psi = 0 \tag{4.27a}$$

$$\rho \frac{Dv_i}{Dt} - (\lambda+\mu) \frac{\partial^2 v_j}{\partial x_j \partial x_i} - \mu \frac{\partial^2 v_i}{\partial x_j \partial x_j} + \frac{\partial p}{\partial x_i} - f_i = 0 \tag{4.27b}$$

$$\rho c_v \frac{D\theta}{Dt} - k \frac{\partial^2 \theta}{\partial x_i \partial x_i} + p \frac{\partial v_i}{\partial x_i} - \Phi - \dot{\Phi} = 0 \ , \tag{4.27c}$$

where Φ is the viscous dissipation defined by

$$\Phi = \tau_{ij} \frac{\partial v_i}{\partial x_j} \ , \tag{4.28}$$

and the fluid stresses

$$\tau_{ij} = 2\mu \left(\frac{\partial v_i}{\partial x_j} + \frac{\partial v_j}{\partial x_i}\right) + \lambda \delta_{ij} \frac{\partial v_k}{\partial x_k} . \qquad (4.29)$$

Equations (4.27), along with (4.24), define a highly non-linear set of six equations in the six variables: velocity (v_i), pressure (p), temperature (θ), and density (ρ).

4.2.2 Incompressible Thermoviscous Flow

For incompressible flow, a number of simplifications are in order. In particular, the divergence of the velocity is zero, which from continuity requires that the density remain constant. As a result, the governing equations reduce to the following:

$$\rho \frac{Dv_i}{Dt} - \mu \frac{\partial^2 v_i}{\partial x_j \partial x_j} + \frac{\partial p}{\partial x_i} - f_i = 0 \qquad (4.30a)$$

$$\rho c_v \frac{D\theta}{Dt} - k \frac{\partial^2 \theta}{\partial x_i \partial x_i} - \mathfrak{G} - \phi = 0 \qquad (4.30b)$$

where

$$\tau_{ij} = 2\mu \left(\frac{\partial v_i}{\partial x_j} + \frac{\partial v_j}{\partial x_i}\right) , \qquad (4.31)$$

and the viscous dissiptation $\mathfrak{G}$ is again defined by (4.28). It should be noted that now the quantity p, appearing in (4.30a), is no longer the thermodynamic pressure determined from (4.24), but rather the mean fluid pressure.

4.2.3 Incompressible Viscous Flow

With the assumption of isothermal conditions, the energy equation (4.30b) is no longer required. All that remains is the familiar Navier-Stokes equation

$$\rho \frac{Dv_i}{Dt} - \mu \frac{\partial^2 v_i}{\partial x_j \partial x_j} + \frac{\partial p}{\partial x_i} - f_i = 0 . \qquad (4.32)$$

4.2.4 Convective Heat Transfer

On the other hand, if the flow field is known or can be approximated, then equation (4.30a) is superfluous. Consequently, fluid temperatures can be determined directly from the scalar convective-diffusion equation

$$\rho c_v \frac{D\theta}{Dt} - k \frac{\partial^2 \theta}{\partial x_i \partial x_i} - \phi = 0 \ . \tag{4.33}$$

In (4.33), the effects of viscous dissipation are included as body heat sources.

4.3 Fundamental Solutions

4.3.1 Compressible Thermoviscous Flow

One of the primary requirements for developing a boundary element formulation is that the fundamental solution of the governing differential equations must exist. These fundamental solutions can be viewed in same sense as the shape functions in the finite element method. For solid mechanics these have been very well explored. Starting with Kelvin's solution (1846), investigators such as Stokes, Poisson, Boussinesq, Mindlin, and Nowacki have provided both static and transient solutions which form the basis of the boundary element formulations in solid mechanics. It is unfortunate that workers in fluid mechanics have not found much use for these fundamental solutions in the infinite space and therefore have not derived the corresponding fluid solutions. The exception is the time-dependent fundamental solution for viscous, incompressible Stokes flow presented in Ladyzhenskaya (1969). Since the boundary element formulations could not be developed without these solutions, a substantial amount of effort has been devoted in the present work to successively derive more complete solutions of the differential equations. In essence, each advancement brings more of the physics of the

problem into the fundamental solution. Below is an overview of the derivation for compressible, thermoviscous flow.

As a starting point, reference values for each of the primary variables are introduced in an effort to produce a linearized differential operator. Thus, let

$$v_i = U_i + u_i \tag{4.34a}$$

$$p = p_o + p_\Delta \tag{4.34b}$$

$$\theta = \theta_o + \theta_\Delta \tag{4.34c}$$

$$\rho = \rho_o + \rho_\Delta \ , \tag{4.34d}$$

in which U_i, p_o, θ_o, and ρ_o are constant reference values, and u_i, p_Δ, θ_Δ, and ρ_Δ are the perturbations. Plugging (4.34) into (4.27) yields, after some manipulation,

$$\frac{D_o p_\Delta}{Dt} + p_o \frac{\partial u_i}{\partial x_i} = -u_i \frac{\partial p_\Delta}{\partial x_i} + \rho R \frac{D\theta_\Delta}{Dt} - p_\Delta \frac{\partial u_i}{\partial x_i} + R\theta\psi \tag{4.35a}$$

$$\rho_o \frac{D_o u_i}{Dt} - (\lambda+\mu) \frac{\partial^2 u_j}{\partial x_i \partial x_j} - \mu \frac{\partial^2 u_i}{\partial x_j \partial x_j} + \frac{\partial p_\Delta}{\partial x_i} = - \rho u_j \frac{\partial u_i}{\partial x_j} - \rho_\Delta \frac{D_o u_i}{Dt} + f_i \tag{4.35b}$$

$$\rho_o c_v \frac{D_o \theta_\Delta}{Dt} - k \frac{\partial^2 \theta_\Delta}{\partial x_i \partial x_i} = - \rho c_v u_i \frac{\partial \theta_\Delta}{\partial x_i} - \rho_\Delta c_v \frac{D_o \theta_\Delta}{Dt}$$

$$- p \frac{\partial u_i}{\partial x_i} + \Phi + \dot{\Phi} \ , \tag{4.35c}$$

where

$$\frac{D_Q}{Dt} = \frac{\partial}{\partial t} + U_i \frac{\partial}{\partial x_i} \ . \tag{4.36}$$

Now, in (4.35), the entire left-hand side involves a linear differential operator with constant coefficients. Notice that in the above form, the

operator for the energy equation involves only temperature (θ_Δ), while the mass and momentum balance operators are coupled by the inclusion of both velocity (u_i) and pressure (p_Δ). Terms on the right-hand side of (4.35) are, in general, non-linear, and can for the present be considered as body sources and forces of unknown magnitude. Then, the governing equations become

$$\frac{D_o p_\Delta}{Dt} + \rho_o \frac{\partial u_i}{\partial x_i} = \bar{\psi} \tag{4.37a}$$

$$\rho_o \frac{D_o u_i}{Dt} - (\lambda+\mu) \frac{\partial^2 u_j}{\partial x_i \partial x_j} - \mu \frac{\partial^2 u_i}{\partial x_j \partial x_j} + \frac{\partial p_\Delta}{\partial x_i} = \bar{f}_i \tag{4.37b}$$

$$\rho_o c_v \frac{D_o \theta_\Delta}{Dt} - k \frac{\partial^2 \theta_\Delta}{\partial x_i \partial x_i} = \bar{\Phi} \tag{4.37c}$$

A fundamental solution of (4.37) is required for the boundary element formulation. This will be obtained subsequently, and referred to as the convective fundamental solution for compressible, thermoviscous flow, since a linearized portion of the convective derivatives are included in the differential operator. Interestingly, it may also be viewed as the fundamental solution due to stationary point forces and sources in a uniformly moving medium or, equivalently, as a uniformly moving point force and source solution in a stationary medium. The concept of moving media fundamental solutions is clearly developed in the excellent monograph on aeroacoustics by Goldstein (1976).

Consider, first, the coupled set of equations (4.37a) and (4.37b), and introduce the Hemholtz decomposition of the velocity and body force, such that

$$u_i = \frac{\partial w}{\partial x_i} + e_{ijk} \frac{\partial W_k}{\partial x_j} \qquad \text{with } \frac{\partial W_i}{\partial x_i} = 0 \ , \tag{4.38a}$$

$$\bar{f}_i = \frac{\partial f}{\partial x_i} + e_{ijk} \frac{\partial F_k}{\partial x_j} \qquad \text{with } \frac{\partial F_i}{\partial x_i} = 0 \ . \tag{4.38b}$$

Then, (4.37b) becomes

$$\frac{\partial}{\partial x_i} \left[\rho_o \frac{D_o w}{Dt} - (\lambda+2\mu) \frac{\partial^2 w}{\partial x_j \partial x_j} + p_\Delta - f \right]$$

$$+ e_{ikl} \frac{\partial}{\partial x_k} \left[\rho_o \frac{D_o W_l}{Dt} - \mu \frac{\partial^2 W_l}{\partial x_j \partial x_j} - F_l \right] = 0 \ . \tag{4.39}$$

For generality, the bracketed terms must vanish independently. Thus,

$$\rho_o \frac{D_o w}{Dt} - (\lambda+2\mu) \frac{\partial^2 w}{\partial x_j \partial x_j} + p_\Delta - f = 0 \tag{4.40a}$$

$$\rho_o \frac{D_o W_l}{Dt} - \mu \frac{\partial^2 W_l}{\partial x_j \partial x_j} - F_l = 0 \ . \tag{4.40b}$$

Notice that equation (4.40b) is completely independent of w and p_Δ, and, consequently can be solved separately. In fact, this is the vortical component of the flow, which behaves in an identical manner for both compressible and incompressible flows. The fundamental solution of (4.40b) in the non-convective form was originally developed by Ladyzhenskaya (1969). This provides the basis for the development of the convective solution to (4.40b), as will be seen subsequently. However, next attention turns to the dilatational component of the flow.

The velocity appearing in the linearized continuity equation (4.37a) can also be decomposed. As a result,

$$\frac{D_o p_\Delta}{Dt} + p_o \frac{\partial^2 w}{\partial x_i \partial x_i} = \bar{\psi} \ , \tag{4.41}$$

since the divergence of the vortical component is zero. Combining appropriate derivatives of (4.40a) and (4.41), to eliminate the variable w, yields the following third order differential equation for pressure:

$$\frac{\partial^2 p_\Delta}{\partial x_i \partial x_i} + \frac{\gamma(\lambda+2\mu)}{\rho_o c_o^2} \frac{D_o}{Dt} \frac{\partial^2 p_\Delta}{\partial x_i \partial x_i} - \frac{\gamma}{c_o^2} \frac{D_o^2 p_\Delta}{Dt^2} - \Omega = 0 \ , \tag{4.42}$$

where

$$\Omega = \left(\frac{\gamma(\lambda+2\mu)}{\rho_o c_o^2} \frac{\partial^2 \bar{\psi}}{\partial x_i \partial x_i} - \frac{\gamma}{c_o^2} \frac{D_o \bar{\psi}}{Dt}\right) + \frac{\partial^2 f}{\partial x_i \partial x_i} \ . \tag{4.43}$$

with c_o representing the speed of sound in the perfect gas at the reference state and

$$\gamma \equiv \frac{c_p}{c_v} > 1 \tag{4.44}$$

$$c_o^2 = \frac{\gamma p_o}{\rho_o} \ . \tag{4.45}$$

The fundamental solution of (4.42), even in the non-convective form, does not appear to exist in the literature, although an attempt was made recently to obtain the nonconvective form by Piva and Morino (1987).

Actually, the solutions of (4.42) that are required for the boundary element formulation are those due to instantaneous point mass sources and point forces. Furthermore, in addition to the pressure response, the velocity field corresponding to these sources and force must be determined. In all cases, the results can be determined directly from the solution of the equation

$$\frac{\partial^2\beta_U}{\partial x_i\partial x_i} + \frac{\gamma(\lambda+2\mu)}{\rho_o c_o^2}\frac{D_o}{Dt}\left(\frac{\partial^2\beta_U}{\partial x_i\partial x_i}\right) - \frac{\gamma}{c_o^2}\frac{D_o^2\beta_U}{Dt^2} - \delta(x-\xi)\delta(t-\tau) = 0 \ , \qquad (4.46)$$

where the scalar variable β_U is introduced along with the usual generalized function δ. The subscript, U, is merely a reminder that β_U is a uniformly moving medium solution. Equation (4.46) is a scalar damped wave equation, which has an approximate fundamental solution of the form

$$\beta_U = \frac{c_o}{2\pi\bar{R}}\left[\ (1 + \frac{\eta t'}{\bar{R}^2})\ H(c_o t'-R_U) - \frac{\eta}{c_o^2}\,\delta(c_o t'-R_U)\ \right] \qquad (4.47)$$

where

$$\eta = \frac{\lambda+2\mu}{\rho_o} \qquad (4.48a)$$

$$t' = t-\tau \qquad (4.48b)$$

$$R_U^2 = (y_i-U_i t')(y_i-U_i t') \qquad (4.48c)$$

$$y_i = x_i-\xi_i \qquad (4.48d)$$

$$\bar{R} = (c_o^2 t'^2-R_U^2)^{1/2} \ . \qquad (4.48e)$$

The presence of the Heaviside and delta functions in (4.47) establishes the hyperbolic nature of the dilatational response. Thus, β_U portrays the propagation of a scalar wave in a moving medium. Furthermore, the appearance of the convective radial distance R_U in the arguments of H and δ leads directly to shock phenomena. As a result, equation (4.47) is appropriate for supersonic, as well as, subsonic flow.

Consider, initially, the medium subjected to a unit pulse body force. In two-dimensions, let

$$\bar{f}_i = \delta(x-\xi)\delta(t-\tau)e_i \qquad (4.49a)$$

$$\bar{\psi} = 0 \ . \tag{4.49b}$$

From Gel'fand and and Shilov (1964), equation (4.49a) can be written alternatively as

$$\bar{f}_i = \frac{\delta(t-\tau)}{2\pi} \frac{\partial^2}{\partial x_j \partial x_j} (\ln r) e_i . \tag{4.49c}$$

which, in light of (4.38b), yields

$$f = \frac{\delta(t-\tau)}{2\pi} \frac{\partial}{\partial x_j} (\ln r) e_j \tag{4.49d}$$

$$F_l = - e_{lij} \frac{\delta(t-\tau)}{2\pi} \frac{\partial}{\partial x_i} (\ln r) e_j \ . \tag{4.49e}$$

Then, the pressure field can be determined by using (4.49d) in (4.43) and, subsequently, (4.42). From the result,

$$\frac{\partial^2 p_\Delta}{\partial x_i \partial x_i} + \frac{\gamma(\lambda+2\mu)}{\rho_o c_o^2} \frac{D_o}{Dt} \frac{\partial^2 p_\Delta}{\partial x_i \partial x_i} - \frac{\gamma}{c_o^2} \frac{D_o^2 p_\Delta}{Dt^2} + \frac{\partial}{\partial x_i} \left[\delta(x-\xi)\delta(t-\tau) \right] e_i = 0 \ , \tag{4.50}$$

and (4.46), it is evident that

$$p_\Delta = - \frac{\partial \beta_U}{\partial x_i} e_i \ . \tag{4.51}$$

Additionally, eliminating the Laplacian operator in (4.40a), by employing (4.41), produces

$$\rho_o \frac{D_o w}{Dt} + \frac{(\lambda+2\mu)}{p_o} \frac{D_o p_\Delta}{Dt} + p_\Delta - f = 0 \tag{4.52}$$

or

$$\frac{D_o w}{Dt} = - \frac{\gamma(\lambda+2\mu)}{\rho_o^2 c_o^2} \frac{D_o p_\Delta}{Dt} - \frac{p_\Delta}{\rho_o} + \frac{\delta(t-\tau)}{2\pi\rho_o} \frac{\partial}{\partial x_j} (\ln r) e_j \ . \tag{4.53}$$

The solution, w, of equation (4.53) can be found by integrating over time within a uniformly moving media. Finally, the dilatational component of the velocity is determined via (4.38a) as

$$u_i^{(dil)} = \frac{\partial w}{\partial x_i} , \tag{4.54}$$

which from (4.53) can be written

$$u_i^{(dil)} = \left[\frac{\gamma(\lambda+2\mu)}{\rho_o^2 c_o^2} \frac{\partial^2 \beta_U}{\partial x_i \partial x_j} + \frac{1}{\rho_o} \int_0^t \frac{\partial^2}{\partial x_i \partial x_j} (\beta_U - \alpha_U) d\tau \right] e_j , \tag{4.55}$$

with

$$\alpha_U = - \frac{\delta(t-\tau)}{2\pi} \ln r, \tag{4.56}$$

and β_U defined in Appendix C. Again, the subscripts, U, signify that the solutions β and α should be expressed in convective coordinates.

To complete the unit force solution, the vortical component of the velocity must be added to (4.55). In this case, the equation of interest is (4.40b) with F_1 specified by (4.49e). Thus,

$$\rho_o \frac{D_o W_1}{Dt} - \mu \frac{\partial^2 W_1}{\partial x_j \partial x_j} + e_{lij} \frac{\delta(t-\tau)}{2\pi} \frac{\partial}{\partial x_i} (\ln r) e_j = 0 . \tag{4.57}$$

The solution to (4.57) can be determined in terms of a scalar ω_U, which is the fundamental solution of the convective heat equation

$$- \rho_o \frac{D_o \omega_U}{Dt} + \mu \frac{\rho^2 \omega_U}{\partial x_j \partial x_j} - \delta(x-\xi)\delta(t-\tau) = 0 , \tag{4.58}$$

detailed in Appendix C. In particular, from (4.57) and (4.58),

$$\frac{\partial^2 W_1}{\partial x_i \partial x_i} = - e_{lij} \frac{\partial \omega_U}{\partial x_i} e_j . \tag{4.59}$$

Substituting (4.59) into (4.57), and then taking the curl of the result, produces

$$\rho_o \frac{D_o}{Dt} \left(e_{mkl} \frac{\partial W_l}{\partial x_k}\right) = - e_{mkl} e_{lij} \left[\mu \frac{\partial^2 \omega_U}{\partial x_k \partial x_i} - \frac{\partial^2}{\partial x_k \partial x_i} \left(\frac{\delta(t-\tau)}{4\pi r}\right) \right] e_j \, , \tag{4.60}$$

which from (4.38a) leads to the following form of the vortical component of the velocity

$$u_m^{(vort)} = \left[- \frac{e_{mkl} e_{lij}}{\rho_o} \int_0^t \frac{\partial^2}{\partial x_i \partial x_k} (\mu \omega_U - \alpha_U) d\tau \right] e_j . \tag{4.61}$$

Again, the subscript U is a reminder that the time integration should be performed for a uniformly moving media.

To summarize, the unit instantaneous point force solution can be written, from (4.51), (4.55), and (4.61), in the following form

$$u_i = \{ \frac{\gamma(\lambda+2\mu)}{\rho_o^2 c_o^2} \frac{\partial^2 \beta_U}{\partial x_i \partial x_j} + \frac{1}{\rho_o} \int_0^t \left[\frac{\partial^2}{\partial x_i \partial x_j} (\beta_U - \alpha_U) \right.$$

$$\left. - e_{ikl} e_{lmj} \frac{\partial^2}{\partial x_k \partial x_m} (\mu \omega_U - \alpha_U) \right] d\tau \} e_j \, , \tag{4.62a}$$

$$p_\Delta = - \frac{\partial \beta_U}{\partial x_j} e_j \, , \tag{4.62b}$$

$$\theta_\Delta = 0 \, . \tag{4.62c}$$

This completely defines the fundamental solutions pertaining to point forces, however, instantaneous point mass source solutions are also required. Returning to (4.43) and letting

$$\bar{\psi} = \delta(x-\xi)\delta(t-\tau) \tag{4.63a}$$

$$f = 0 \, , \tag{4.63b}$$

leads to the simple result that

$$p_\Delta = \frac{\gamma(\lambda+2\mu)}{\rho_o c_o^2} \frac{\partial^2 \beta_U}{\partial x_i \partial x_i} - \frac{\gamma}{c_o^2} \frac{D_o \beta_U}{Dt} \ . \tag{4.64}$$

The corresponding velocity can be determined most easily by returning to equations (4.40a) and (4.41), and eliminating the pressure. This produces

$$\frac{\partial^2 w}{\partial x_i \partial x_i} + \frac{\gamma(\lambda+2\mu)}{\rho_o c_o^2} \frac{D_o}{Dt} \left(\frac{\partial^2 w}{\partial x_i \partial x_i}\right) - \frac{\gamma}{c_o^2} \frac{D_o^2 w}{Dt^2} - \frac{\gamma}{c_o^2} \delta(x-\xi)\delta(t-\tau) = 0 \ , \tag{4.65}$$

which when compared with (4.46), establishes

$$w = \frac{\gamma}{c_o^2} \beta_U \tag{4.66}$$

Additionally, since (4.40b) is independent of p_Δ, w, and $\bar{\psi}$, the vortical component of velocity

$$e_{ijk} \frac{\partial w_k}{\partial x_j} = 0 \ , \tag{4.67}$$

and the velocity field becomes becomes

$$u_i = \frac{\gamma}{c_o^2} \frac{\partial \beta_U}{\partial x_i} \ . \tag{4.68}$$

Equations (4.64) and (4.68), along with

$$\theta_\Delta = 0 \ , \tag{4.69}$$

comprise the instantaneous unit mass source fundamental solution.

The final item that is required involves the response to an instantaneous unit heat source. In this case,

$$\bar{\psi} = 0 \tag{4.70a}$$

$$\bar{f}_i = 0 \tag{4.70b}$$

$$\bar{\phi} = \delta(x-\xi)\delta(t-\tau) \ . \tag{4.70c}$$

Then, from (4.37),

$$p_\Delta = 0 \tag{4.71a}$$

$$u_i = 0 \ , \tag{4.71b}$$

and θ_Δ is simply the solution to the convective heat equation.

It is convenient, at this point to collect the fundamental point force, mass source, and heat source solutions into a tensor $g^U_{\alpha\beta}$, where for the Dirac delta functions in the infinite space,

$$u_\alpha = g^U_{\alpha\beta}\bar{f}_\beta \tag{4.72}$$

and

$$u_\alpha = \{u_1 \ \ u_2 \ \ p \ \ \theta\}^T \tag{4.73a}$$

$$\bar{f}_\beta = \{\bar{f}_1 \ \ \bar{f}_2 \ \ \bar{\psi} \ \ \bar{\phi}\}^T \ . \tag{4.73b}$$

The superscript U denotes that $g^U_{\alpha\beta}$ is a moving medium solution. Furthermore, the subscripts α and β vary from one to four, while in the following i and j vary from one to two. Additionally, the subscript p always takes the value three and the subscript θ is four. Then,

$$g^U_{\alpha\beta} = \begin{bmatrix} g^U_{ij} & g^U_{ip} & g^U_{i\theta} \\ g^U_{pj} & g^U_{pp} & g^U_{p\theta} \\ g^U_{\theta j} & g^U_{\theta p} & g^U_{\theta\theta} \end{bmatrix} \ . \tag{4.74}$$

The individual components of $g^U_{\alpha\beta}$ are detailed in Appendix C. It should be emphasized that these are moving force and source fundamental solutions

and, as such, are quite involved. The explicit form of these kernels have recently been obtained, however the accurate numerical evaluation of the functions involved at high reference velocities (U_i) still requires some additional effort.

It may be recalled that in previous work (e.g., Dargush et al, 1987; Dargush and Banerjee, 1988c,1989), all of the convective terms were brought to the right-hand side and included as body forces and sources. The corresponding fundamental solutions then involve instantaneous stationary point forces and sources acting in a stationary medium. These solutions remain time-dependent, but take a much simpler form than the convective Green's functions presented in Appendix C. Unfortunately, except in the low to medium Reynolds number range, the stationary fundamental solutions do not contain enough of the physics of the problem to produce numerical solutions. (This will be evident in a number of examples in Section 4.7.) On the other hand, the convective fundamental solutions do capture the nature of high velocity flows, although this is not at all obvious due to the complicated form of the convective kernels. However, the simplified fundamental solution highlighted in Section 4.3.4 for convective heat transfer will provide some additional insight.

4.3.2 Incompressible Thermoviscous Flow

In the incompressible case, the pressure becomes superfluous and is no longer needed as a primary variable. Additionally, the dilational component of the velocity vanishes. As a result, the convective fundamental solution for incompressible thermoviscous flow can be written

$$u_\alpha = g^U_{\alpha\beta} \bar{f}_\beta \tag{4.75}$$

where

$$u_\alpha = \{u_1 \quad u_2 \quad \theta\}^T \tag{4.76a}$$

$$\bar{f}_\beta = (\bar{f}_1 \quad \bar{f}_2 \quad \bar{0})^T , \tag{4.76b}$$

with α and β varying from one to three, and the subscript θ set to three. The kernel $g^U_{\alpha\beta}$ is detailed in Appendix D. Once again, the development of techniques for the numerical evaluation of these kernels is still underway. Meanwhile, the stationary medium fundamental solutions, pertaining to continuous point forces and sources, are defined in Appendix E.

4.3.3 Incompressible Viscous Flow

Under isothermal conditions, the temperature is not required as an independent variable and the corresponding degree of freedom can be eliminated. The convective incompressible viscous flow fundamental solution is then equivalent to g^U_{ij} from Appendix D.

4.3.4 Convective Heat Transfer

The final case of convective heat transfer will be examined in some detail. As will be seen, the fundamental solutions are manageable, yet still reflect several aspects of compressible thermoviscous flow. To begin, the reference velocity U_i is introduced to (4.33) to modify the convective derivatives. Thus, (4.33) becomes

$$\rho c_v \frac{D_Q \theta}{Dt} - k \frac{\partial^2 \theta}{\partial x_i \partial x_i} = \bar{0} \tag{4.75}$$

where, again,

$$\frac{D_Q}{Dt} = \frac{\partial}{\partial t} + U_i \frac{\partial}{\partial x_i} . \tag{4.76}$$

The fundamental solution, g^U, due to an instantaneous point source, obtained from

$$\rho c_v \frac{D_o g^U}{Dt} - k \frac{\partial^2 g^U}{\partial x_i \partial x_i} = \delta(x-\xi)\delta(t-\tau) \ , \tag{4.77}$$

is a well-known result. A slight generalization of the solution presented in Carslaw and Jaeger (1947) produces, in two-dimensions,

$$g^U(x_i,t;\xi_i,\tau) = \frac{1}{4\pi k} \frac{e^{-R_U/4ct'}}{t'} \tag{4.78}$$

where

$$c = \frac{k}{\rho c_v} \tag{4.79a}$$

$$t' = t-\tau \tag{4.79b}$$

$$R_U^2 = (y_i - U_i t')(y_i - U_i t') \tag{4.79c}$$

$$y_i = x_i - \xi_i \ . \tag{4.79d}$$

The steady-state response can be obtained from (4.78) by integrating over τ. Thus,

$$G^U(x_i,\xi_i) = \frac{1}{4\pi k} \int_0^\infty \frac{e^{-R_U/4ct'}}{t'} d\tau \ , \tag{4.80}$$

which simplifies to

$$G^U(x_i,\xi_i) = \frac{e^{U_i y_i/2c}}{2\pi k} K_o(UR/2c) \ , \tag{4.81}$$

where

$$R = (y_i y_i)^{1/2} \tag{4.82a}$$

$$U = (U_i U_i)^{1/2} \tag{4.82b}$$

and K_o is the modified Bessel function of the second kind of order zero. It is of interest to compare (4.81) with its stationary counterpart. Of course, for a heat source in a stationary medium, the fundamental solution

is just the potential flow kernel

$$G(x_i,\xi_i) = \frac{\ln R}{2\pi k} \quad . \tag{4.83}$$

Figure 4.1 provides a comparison of the two kernels, G^U and G, for a source point at the origin. The kernel values are plotted for field points along the x_1-axis, and in the convective case for a medium moving uniformly in the x_1-direction with a velocity of ten. Notice, in particular, that the static response is symmetric about the source point, however the convective response is magnified ahead of the source point, but greatly reduced behind it. This latter phenomenon is just the Doppler effect applied to moving heat sources. Thus, as illustrated for points on the positive x_1-axis in Figure 4.1, the strength of an oncoming source appears to be intensified. On the other hand, the source has already passed the points on the negative x_1-axis, and a quick silencing is apparent.

Interestingly, from another vantage point, the convective Green's function G^U can be viewed as the boundary element counterpart of the so-called 'upwinding' techniques that are required in finite difference and finite element approaches to convective problems. The distinguishing feature is that G^U embodies an analytical form of upwinding, while the other two methods use ad hoc representations. As a result, a boundary element formulation based upon G^U will have a significant advantage for convection-dominated problems.

The transient convective diffusion kernel can also be formed by integrating (4.78), but this time from zero to t. The result is a two-dimensional fundamental solution, which can be written in series form as,

$$G^U(x_i,t;\ \xi_i,0) = \frac{e^{U_i y_i/2c}}{4\pi k} \sum_{n=0}^{\infty} \frac{(-U_i U_i t/4c)^n}{n!} E_{n+1}\left(\frac{R^2}{4ct}\right) \tag{4.84}$$

where E_{n+1} is the exponential integral of order n+1. Figure 4.2 compares the steady-state kernel (4.81) with this transient kernel for several values of t. Note that the Doppler effect is still quite pronounced.

Before closing this section on fundamental solutions, it should be emphasized that behavior similar to that displayed in (4.81) and (4.84) will be included in the convective thermoviscous kernels, since the scalar Green's function G^U provides the basis for the development of the more complicated fundamental solutions. In fact, for the incompressible theories, G^U is the only scalar Green's function that is needed. (More precisely, a change in material constants is required to produce ω_U of equation (4.58) from G^U.) However, for compressible flow a second scalar fundamental solution, β_U, comes into play for the dilatational component of the flow. As mentioned previously, this latter solution involves the propagation of a damped wave, which at high velocities produces shock phenomena.

4.4 Integral Representations

4.4.1 Compressible Thermoviscous Flow

The desired integral representation for general compressible thermoviscous flow can be derived directly from the set of governing differential equations. First, however, a convenient differential operator notation is introduced. As a result, equations (4.37) are rewritten as

$$L^U_{\alpha\beta} u_\beta + \bar{f}_\alpha = 0 \ , \tag{4.85}$$

where, again

$$u_\beta = \{u_1 \quad u_2 \quad p \quad \theta\}^T \tag{4.73a}$$

$$\bar{f}_\alpha = \{\bar{f}_1 \quad \bar{f}_2 \quad \bar{\psi} \quad \bar{\phi}\}^T \tag{4.73b}$$

and

$$L^U_{\alpha\beta} = \begin{bmatrix} L^U_{ij} & L^U_{ip} & L^U_{i\theta} \\ L^U_{pj} & L^U_{pp} & L^U_{p\theta} \\ L^U_{\theta j} & L^U_{\theta p} & L^U_{\theta\theta} \end{bmatrix} \tag{4.86}$$

$$L^U_{ij} = -\delta_{ij}\rho_o \frac{D_o}{Dt} + (\lambda+\mu) \frac{\partial^2}{\partial x_i \partial x_j} + \delta_{ij}\mu \frac{\partial^2}{\partial x_m \partial x_m} \tag{4.87a}$$

$$L^U_{ip} = - \frac{\partial}{\partial x_i} \tag{4.87b}$$

$$L^U_{i\theta} = 0 \tag{4.87c}$$

$$L^U_{pj} = - p_o \frac{\partial}{\partial x_j} \tag{4.87d}$$

$$L^U_{pp} = - \frac{D_o}{Dt} \tag{4.87e}$$

$$L^U_{p\theta} = 0 \tag{4.87f}$$

$$L^U_{\theta j} = 0 \tag{4.87g}$$

$$L^U_{\theta p} = 0 \tag{4.87h}$$

$$L^U_{\theta\theta} = -\rho_o c_v \frac{D_o}{Dt} + k \frac{\partial^2}{\partial x_m \partial x_m} . \tag{4.87i}$$

Then, using $L^U_{\alpha\beta}$ to operate on the fundamental solution $g^U_{\alpha\beta}$ of (4.74) produces

$$L^U_{\alpha\beta} g^U_{\beta\gamma} + \delta_{\alpha\gamma}\delta(x-\xi)\delta(t-\tau) = 0 . \tag{4.88}$$

In (4.88), the subscript γ also varies from one to four and Kronecker's delta function has been generalized in an obvious manner.

The governing equations (4.84) must, of course, hold for all points of the flow region at every instant of time. Therefore, the lefthand side of (4.85) multiplied by an arbitrary function $\tilde{g}_{\alpha\gamma}$, and integrated over time and space must remain equal to zero. That is,

$$\langle \tilde{g}_{\alpha\gamma}, L^U_{\alpha\beta}u_\beta + \bar{f}_\alpha \rangle = \int_0^t\int_V \tilde{g}_{\alpha\gamma}(L^U_{\alpha\beta}u_\beta+\bar{f}_\alpha)dVd\tau = 0 , \tag{4.89}$$

where the standard notation for the inner product of two functions has been introduced. Returning to the explicit forms of the differential operators, this becomes

$$\begin{aligned}\int_0^t\int_V [&\tilde{g}_{i\gamma}\,[-\rho_o\dot{u}_i - \rho_o U_m u_{i,m} + (\lambda+\mu)u_{m,im} + \mu u_{i,mm} - u_{p,i} + \bar{f}_i] \\ &+ \tilde{g}_{p\gamma}\,[-p_o u_{m,m} - \dot{u}_p - U_m u_{p,m} + \bar{f}_p] \\ &+ \tilde{g}_{\theta\alpha}\,[-\rho_o c_v\dot{u}_\theta - \rho_o c_v U_m u_{\theta,m} + k u_{\theta,mm} + \bar{f}_\theta]dVd\tau = 0 ,\end{aligned} \tag{4.90}$$

in which commas represent spatial derivatives and superposed dots are partial derivatives with respect to time. Next, the divergence theorem can be applied, repeatedly, to the applicable terms in (4.90) to transfer spatial, as well as, temporal derivatives from u_β to $\tilde{g}_{\alpha\gamma}$. As a result, equations (4.90) are transformed into

$$\begin{aligned}&\int_0^t\int_S [\tilde{g}_{\alpha\gamma}t_\alpha - \tilde{f}_{\alpha\gamma}u_\alpha]dSd\tau + \int_0^t\int_V [\tilde{g}_{\alpha\gamma}\bar{f}_\alpha]dVd\tau - \int_V [\tilde{g}_{\alpha\gamma}u^\rho_\alpha]^t_0]dV \\ &+ \int_0^t\int_V \{[\rho_o\dot{\tilde{g}}_{i\gamma} + \rho_o U_m\tilde{g}_{i\gamma,m} + (\lambda+\mu)\tilde{g}_{m\gamma,mi} + \mu\tilde{g}_{i\gamma,mm} + p_o\tilde{g}_{p\gamma,i}]u_i \\ &+ [\tilde{g}_{m\gamma,m} + \dot{\tilde{g}}_{p\gamma} + U_m\tilde{g}_{p\gamma,m}]u_p\end{aligned}$$

$$+ [\rho_o c_v \dot{\tilde{g}}_{\theta\gamma} + \rho_o c_v U_m \tilde{g}_{\theta\gamma,m} + k\tilde{g}_{\theta\gamma,mm}] u_\theta \} dV d\tau = 0 \ , \tag{4.91}$$

where

$$t_i = \lambda u_{m,m} n_i + \mu(u_{m,i} + u_{i,m}) n_m - \rho_o U_m u_i n_m \tag{4.92a}$$

$$t_p = - U_m u_p n_m \tag{4.92b}$$

$$t_\theta = k u_{\theta,m} n_m - \rho_o c_v U_m u_\theta n_m \tag{4.92c}$$

$$\tilde{f}_{i\gamma} = \lambda \tilde{g}_{m\gamma,m} n_i + 2\mu \tilde{g}_{i\gamma,m} n_m + p_o \tilde{g}_{p\gamma} n_i \tag{4.93a}$$

$$\tilde{f}_{p\gamma} = \tilde{g}_{i\gamma} n_i \tag{4.93b}$$

$$\tilde{f}_{\theta\gamma} = k\tilde{g}_{\theta\gamma,m} n_m \tag{4.93c}$$

$$u_\alpha^\rho = \{\rho_o u_1 \quad \rho_o u_2 \quad u_p \quad \rho_o c_v u_\theta\}^T \tag{4.94}$$

with n_i defined as the unit normal to the surface S at X. To complete the derivation of the integral equation for any point ξ interior to S at time t, the last volume integral appearing in (4.91) must be reduced to $- u_\gamma(\xi,t)$. This is accomplished, if

$$\langle \tilde{L}^U_{\beta\alpha} \tilde{g}_{\alpha\gamma}, u_\beta \rangle = -u_\gamma(\xi,t) \tag{4.95}$$

or after making use of the properties of the delta function

$$\tilde{L}^U_{\beta\alpha} \tilde{g}_{\alpha\gamma} + \delta_{\beta\gamma} \delta(X-\xi)\delta(t-\tau) = 0 \ , \tag{4.96}$$

where the operator $\tilde{L}^U_{\beta\alpha}$ has components

$$\tilde{L}^U_{ji} = \delta_{ji}\rho_o \frac{D_o}{Dt} + (\lambda+\mu) \frac{\partial^2}{\partial x_j \partial x_i} + \delta_{ji}\mu \frac{\partial^2}{\partial x_m \partial x_m} \tag{4.97a}$$

$$\tilde{L}^U_{jp} = p_o \frac{\partial}{\partial x_j} \tag{4.97b}$$

$$\tilde{L}^U_{j\theta} = 0 \tag{4.97c}$$

$$\tilde{L}^U_{pi} = \frac{\partial}{\partial x_i} \tag{4.97d}$$

$$\tilde{L}^U_{pp} = \frac{D_o}{Dt} \tag{4.97e}$$

$$\tilde{L}^U_{p\theta} = 0 \tag{4.97f}$$

$$\tilde{L}^U_{\theta i} = 0 \tag{4.97g}$$

$$\tilde{L}^U_{\theta p} = 0 \tag{4.97h}$$

$$\tilde{L}^U_{\theta\theta} = \rho_o c_v \frac{D_o}{Dt} + k \frac{\partial^2}{\partial x_m \partial x_m} . \tag{4.97i}$$

Formally, $\tilde{L}^U_{\beta\alpha}$ is called the adjoint of the original compressible thermoviscous differential operator $L^U_{\alpha\beta}$, and $\tilde{g}_{\alpha\gamma}$ defined by (4.95) is the adjoint Green's function. This adjoint Green's function can be obtained simply by suitably transposing the fundamental solution presented in Section 4.3.1. That is,

$$\tilde{g}_{\alpha\gamma}(X,t;\xi,\tau) = g^U_{\gamma\alpha}(\xi,\tau;X,t) . \tag{4.98}$$

Substituting (4.98) into (4.91) produces the desired integral equation,

$$u_\gamma(\xi,t) = \int_S [g^U_{\gamma\alpha} * t_\alpha - f^U_{\gamma\alpha} * u_\alpha] dS + \int_V [g^U_{\gamma\alpha} * \bar{f}_\alpha] dV \tag{4.99}$$

in which, for simplicity, the initial conditions have been assumed zero. The * in (4.99) once again symbolizes a Riemann convolution integral.

Notice that this integral equation for compressible thermoviscous flow has a similar form to that for thermoelasticity as shown in equation (3.2). However, in (4.99), a volume integral is retained to include, in particular, the nonlinear body force terms.

4.4.2 Incompressible Viscous Flow

A derivation of the integral representation for the incompressible flow theories would follow the same lines as that just presented, and therefore, will not be repeated. In fact, a generalized integral equation identical to (4.99) would result. The only differences are in the explicit form of the fundamental solutions $g^U_{\gamma\alpha}$ and in the corresponding definitions of the functions $f^U_{\gamma\alpha}$ and t_α.

As may be recalled from (4.35), a portion of the convective effects are included in the body forces $\bar{f}_\alpha$. Assuming for the moment that this is the only non-zero component of $\bar{f}_\alpha$, then the volume integral in (4.99) can be rewritten as

$$\int_V \left[g^U_{\gamma\alpha} * \bar{f}_\alpha\right] dV = - \int_V \left[g^U_{\gamma\alpha} * \rho u_j \frac{\partial u_\alpha}{\partial x_j}\right] dV \ . \tag{4.100}$$

Applying the divergence theorem to the right-hand side of (4.100) produces

$$\int_V \left[g^U_{\gamma\alpha} * \rho u_j u_{\alpha,j}\right] dV = \int_S \left[g^U_{\gamma\alpha} * \rho u_\alpha u_j n_j\right] dS - \int_V \left[g^U_{\gamma\alpha,j} * \rho u_\alpha u_j\right] dV \ , \tag{4.101}$$

since, for the incompressible case, $u_{j,j}$ is identically zero. Finally, equation (4.99) becomes

$$u_\gamma(\xi,t) = \int_S \left[g^U_{\gamma\alpha} * t'_\alpha - f^U_{\gamma\alpha} * u_\alpha\right] dS + \int_V \left[g^U_{\gamma\alpha,j} * \rho u_\alpha u_j\right] dV \tag{4.102}$$

where

$$t'_\alpha = t_\alpha - \rho u_\alpha u_j n_j \ . \tag{4.103}$$

Notice, in particular, that (4.102) no longer involves velocity gradients. Consequently, from a computational standpoint, (4.102) is an attractive alternative to (4.99).

A similar integral formulation can also be developed by utilizing the stationary medium fundamental solutions $g_{\gamma\alpha}$. In this case, the reference

velocity U_i may still be used, but now the entire convective derivative must be included in the body forces. As a result, the integral equation is written

$$u_\gamma(\xi,t) = \int_S [g_{\gamma\alpha} * t'_\alpha{}' - f_{\gamma\alpha} * u_\alpha] dS + \int_V [g_{\gamma\alpha,j} * \rho u_\alpha v_j] dV \tag{4.104}$$

in which

$$t'_\alpha{}' = t_\alpha - \rho u_\alpha v_j n_j$$

and v_j is the total velocity.

4.4.3 Convective Heat Transfer

In this simplest case, equations (4.99) reduce to

$$\theta(\xi,t) = \int_S [-g^U * q + f^U * \theta] dS + \int_V [g^U * \dot{\phi}] dV \tag{4.106}$$

where g^U is defined by (4.78) and

$$f^U = -k g^U_{,m} n_m \tag{4.107}$$

$$q = k\theta_{,m} n_m + \rho_o c_v U_m \theta n_m \ . \tag{4.108}$$

Meanwhile, under steady conditions, equation (4.106) simplifies to

$$\theta(\xi,t) = \int_S [-G^U q + F^U \theta] dS + \int_V [G^U \dot{\phi}] dV \tag{4.109}$$

in which

$$F^U = -k G^U_{,m} n_m \tag{4.110}$$

with G^U given by (4.81).

4.5 Numerical Implementation

The numerical treatment of the equations in thermoviscous fluid dynamics follows very closely that described in Section 3 for transient

thermal stress analysis. However, now due to the volume integral appearing in (4.99), (4.102) or (4.104), the interior must be subdivided into cells. The geometry of each cell is defined by nodal points and quadratic shape functions. In two-dimensions, six and eight-noded cells are available. Meanwhile, either a linear or quadratic variation can be employed for the functional representation. Details of the techniques used for cell integration can be found in Mustoe (1984).

Just as for the thermoelastic case, a set of algebraic equations can be developed by writing the integral equation at each global node. However, now interior, as well as, boundary nodes must be included, and the resulting equations become highly nonlinear due to the convective terms. After the collocation process is complete, the final system of equations can be expressed in matrix form as

$$g^b(x,u) = A^b x + D^b \sigma^o - G^b t^o - B^b y = 0 \qquad (4.111a)$$

for boundary points, and as

$$g^u(x,u) = u + A^u x + D^u \sigma^o - G^u t^o - B^u y = 0 \qquad (4.111b)$$

for interior cell points, where the vectors σ^o and t^o have components defined by

$$\sigma^o_{i\beta} = \rho u_i u_\beta$$

$$t^o_\beta = \sigma^o_{i\beta} n_i$$

at each boundary and interior point. Once again x and y are the known and unknown boundary quantities, while u is the interior velocity vector, and the matrices A, B, D and G are developed from the integrals of the kernel functions appearing in (4.99), (4.102) or (4.104). At present, only

(4.104) has been implemented as a segment of the general purpose boundary element program, GP-BEST.

Initially, an iterative algorithm, along the lines of those used for BEM elastoplasticity, was employed to solve (4.111). However, convergence is usually achieved only at low Reynolds number. More generally, when employing the stationary fundamental solutions, the interior equations must be brought into the system matrix along with the boundary equations, and a full or modified Newton-Raphson algorithm must be utilized to obtain solutions at moderate or high Reynolds number. Symbolically, at each iteration m,

$$\begin{bmatrix} \frac{\partial q^b}{\partial x} & \frac{\partial q^b}{\partial u} \\ \frac{\partial q^u}{\partial x} & \frac{\partial q^u}{\partial u} \end{bmatrix} \begin{Bmatrix} (\Delta x)^m \\ (\Delta u)^m \end{Bmatrix} = - \begin{Bmatrix} g^b(x^m, u^m) \\ g^u(x^m, u^m) \end{Bmatrix} \tag{4.112}$$

where

$$x^{m+1} = x^m + (\Delta x)^m$$

$$u^{m+1} = u^m + (\Delta u)^m$$

and the derivatives on the lefthand side of (4.112) are evaluated at (x^m, u^m). In the numerical implementation, the above equations are arranged to form a block banded system matrix for efficient multi-region solutions.

It is anticipated that once the convective viscous kernels are implemented somewhat different solution strategies will be more appropriate. For example, at high velocities the system matrix will become sparse. In that case, bandwidth minimization is required and iterative equation solvers become quite attractive.

4.6 Coupling of Solid and Fluid

The coupling of the solid and fluid phases is most readily accommodated via the concept of the generic modeling region. Thus, the fluid-structure interface is nothing more than a boundary between two GMR's. In the simplest case, temperature, flux, and tractions are matched across the fluid-structure interface, while a temporal approximation is introduced to relate boundary displacements of the solid to the corresponding fluid velocities. However, additional sophistication is possible. For example, thermal resistance can be introduced to model the effects of coatings.

4.7 Examples

4.7.1 Parallel Flow

The two-dimensional parallel flow in a duct is a good verification problem for incompressible computational fluid dynamics codes. It has a simple analytical solution which can be used to test many aspects of programs. The convective terms disappear in the nonlinear solution, hence linear and nonlinear velocity profiles should be identical (Tadmor and Gogos, 1977).

As an example of a typical version of this problem, Figure 4.3 illustrates a 10 cell mesh with two regions. This simulates a plate sliding along the top of the fluid in pure shear. Pure shear tractions are applied at inlet and exit. Viscosity is unity and density is incremented to increase the effect of the convective terms in the equations. Newton iteration is used to converge to the nonlinear solution. It should be noted that this problem does not require this degree of refinement. This model merely tests many aspects of the computer program.

Figure 4.4 illustrates the linear velocity profile at the exit of the region. For density below 1000 the linear profile is reproduced exactly.

4.7.2 Driven Cavity

The two-dimensional driven cavity has become the standard test problem for incompressible computational fluid dynamics codes. In a way, this is unfortunate because of the ambiguities in the specification of the boundary conditions. However, numerous results are available for comparison purposes.

The incompressible fluid of uniform viscosity is confined within a unit square region. The fluid velocities on the left, right and bottom sides are fixed at zero, while a uniform non-zero velocity is specified in the x-direction along the top edge. Thus, in the top corners, the x-velocity is not clearly defined. To alleviate this difficulty in the present analysis, the magnitude of this velocity component is tapered to zero at the corners.

Results are presented for the 144 cell boundary element model shown in Figure 4.5. Notice that a higher level of refinement is used near the edges. Spatial plots of the resulting velocity vectors are displayed in Figures 4.6, 4.7, and 4.8 for Reynolds numbers (Re) of 100, 400 and 1000, respectively. Notice that, in particular, the shift of the vortical center follows that described by Burggraf (1966) in his classic paper. A more quantitative examination of the results can be found in Figure 4.9, where the horizontal velocities on the vertical centerline obtained from the present analysis (i.e., GP-BEST results) are compared to those of Ghia et al. (1982). It is assumed that the latter solutions are quite accurate since the authors employed a 129 by 129 finite difference grid. It is apparent, from the figure, that the present boundary element model has some difficulty in capturing the sharp knee of the curve at Re = 400. This becomes accentuated as the Reynolds number increases, and consequently, a finer mesh is required. It should be noted that the simple iterative

algorithm fails to converge much beyond Re = 100. Beyond that range the use of a Newton-Raphson type algorithm is imperative.

In order to obtain more accurate solutions at higher Reynolds number, the refined four region 324-cell boundary element model shown in Figure 4.10 was also analyzed. This provides a significant improvement in the results. For example, at Re = 1000, as seen from Figure 4.11, the secondary vortex in the lower right-hand corner is clearly visible. Additionally, the resulting horizontal velocities are compared to Ghia et al (1982) in Figure 4.12. Now, even the solution at Re=1000 is in excellent agreement.

4.7.3 Converging Channel

The two-dimensional incompressible flow through a converging channel also possesses a well known analytical solution which is purely radial (Millsaps and Pohlhausen, 1953). A comprehensive finite element study of this problem has been made by Gartling, et al (1977).

The boundary element model is shown in Figure 4.13. The mesh contains 96 cells and is divided into two regions. The boundary conditions were modeled using an exact specification of the boundary conditions appearing in the analytical solution (Fig. 4.13). Viscosity is unity and tractions and density are incremented to reach higher Reynolds numbers. The Reynolds number for this problem is defined as

$$R_e = \frac{\rho R_i V_2(R_i)}{\mu}$$

where $V_2(R_i)$ is the maximum velocity in the region, which is -24.0 for the problem solved here.

Figure 4.14 illustrates the results for two Reynolds numbers, indicating good accuracy along the entire width of the channel. Not only

are the velocities accurate, but the pressures and tractions are very accurate also.

It has been observed that finite element versions of this problem have several peculiarities which prevent the analytical solution from being reproduced. First of all, velocities are often specified at the inlet and at the wall and centerline, ambiguous boundary condition specification results. Also, typically a parabolic "fully developed" velocity profile is often specified at the inlet. However, the nonlinear solution has a flattened velocity distribution across the width of the channel (see Fig. 4.14). Hence, the analytical solution cannot be reproduced exactly if the "fully developed" profile is specified at the inlet. Also, the finite element modelers of this problem usually leave out the traction distribution at the exit and specify zero tractions there. This also gives rise to non-radial flow.

The reason for so much interest in the converging flow problem is that it is one of the few problems possessing an analytical solution. However, by specifying a model which does not correspond to this problem, as in the finite element case, one cannot accurately compare results to the analytical solution. Any such comparisons are merely qualitative. In this light, the boundary element model here has utilized an exact model of the boundary conditions appearing in the analytical solution. This way an accurate and meaningful comparison can be made.

4.7.4 Flow Over a Cylinder

Next, an example of unconfined flow around an obstacle is considered. In particular, the oft-studied case of a unit diameter circular cylinder is examined. The boundary element mesh is illustrated in Figure 4.15. Notice that three distinct regions are evident. The smallest region, labelled

GMR1, represents a thermoelastic thick-walled cylinder. Only the surface of the solid is discretized. The next region, GMR2, models a thermoviscous fluid in the vicinity of the cylinder. In GMR2 volume cells are required due to convective body forces. However, sufficiently remote from the cylinder, these body forces become negligible and once again a boundary-only region, in this case GMR3, is valid.

Steady-state velocity vector plots are displayed in Figures 4.16 and 4.17 for Re = 20 and 40, respectively. The recirculating zone, behind the cylinder, is clearly visible.

Additionally, the problem was extended to include thermal effects. The temperature of the fluid at inlet was specified as 1000°C, while that at the inner surface of the hollow cylinder was maintained at 0°C. The effective heat transfer coefficient between the fluid and solid can then be obtained from the resulting temperature and flux at the outer surface of the cylinder. The distribution of the nondimensional Nusselt number (Nu) around the circumference is plotted in Figure 4.18. These curves agree, at least, qualitatively with the experimental results of Eckert and Soehngen (1952). Of course, if the purpose of the analysis is to determine the temperature and stress in the solid, then there is really no need to compute the heat transfer coefficients. The desired solid temperatures and stresses come directly out of the analysis.

4.7.5 Flow Over an Airfoil

As a final example, the themoviscous flow over a NACA 0018 airfoil is considered. The boundary element model shown in Figure 4.19 once again utilizes symmetry and employs the multiregion concept with cells confined to the vicinity of the airfoil. The airfoil is heated externally by a hot gas, flowing from left to right, at unit temperature, and cooled to zero on the surface of an internal cooling hole. The conductivity of the airfoil

is set to one hundred times that of the hot gas, while unit values are assumed for the fluid density and viscosity.

The resulting steady-state velocity distribution at Re = 150 is displayed in Figure 4.20, while Figure 4.21 details the velocity profile just ahead of the leading edge of the blade. It should be noted that lift and drag can easily be calculated, since during the analysis, tractions are determined all along the blade surface. Next, shaded temperature contour plots of the region surrounding the airfoil are presented for Re = 10 and 150 in Figure 4.22. In the latter diagram, the hot regions are black, while lower temperature locations appear white. The effects of convection are visible downstream of the airfoil. Lastly, the surface temperature of the airfoil is plotted in Figure 4.23. Notice that the overall temperature increases with Reynolds number. In this particular case, the distribution is strongly influenced by the location of the single internal cooling hole.

When the Reynolds number is elevated further, the convective terms begin to dominate. In this flow regime, the physics of the problem demands that convective effects must be incorporated in the kernel functions. This is, in fact, true for all of the viscous flow examples presented thus far. As mentioned earlier, the inclusion of convection in the kernel functions is analogous to the upwinding techniques that are required in finite difference and finite element analyses.

The development and numerical verification of these convective thermoviscous flow kernels is now underway. However, the thermal portion of the new kernels, detailed in Section 4.3.4 and 4.4.3, has been implemented and provides some interesting results.

As an illustrative example, a convective heat transfer analysis was conducted for a pair of NACA 0018 airfoils in a uniform flow field. The boundary element model of the airfoils is shown in Figure 4.24. The hot

fluid once again flows from left to right, while the airfoils are cooled on their inner surfaces. It should be emphasized that with the assumption of a uniform fluid velocity, the problem permits a boundary-only analysis. Thus, the only mesh that is needed is that displayed in Figure 4.24. However, a number of interior points were added in the flow field for post-processing purposes.

Figure 4.25 depicts the temperature distribution in the fluid surrounding the airfoils at a Peclet (Pe) number of ten, where

$$Pe = \frac{Ul}{c} ,$$

with fluid velocity U, chord length l, and thermal diffusivity of the fluid c. Meanwhile, Figures 4.26 and 4.27 present the temperature field for Pe=100 and 1000, respectively. Strong convective effects are evident at the higher Peclet numbers. Finally, in Figures 4.28 and 4.29 the angle of attack is modified to 10^{o} and 20^{o} while maintaining Pe=1000.

It should be reiterated that the results shown in Figures 4.25-4.29 are based on a uniform flow field. Thus, the effects of viscosity have been ignored. However, the new convective thermoviscous kernels, when they are available, will have the same character as those for convective heat transfer, and hence, should provide a means for obtaining accurate high velocity solutions.

FIGURE 4.1

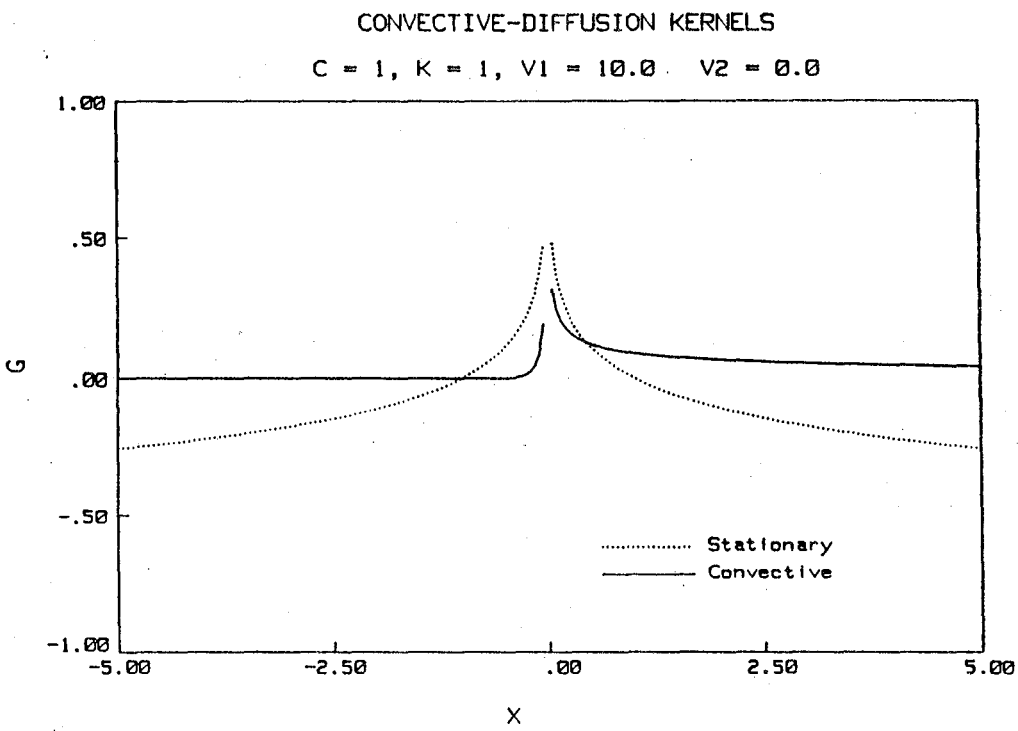

FIGURE 4.2

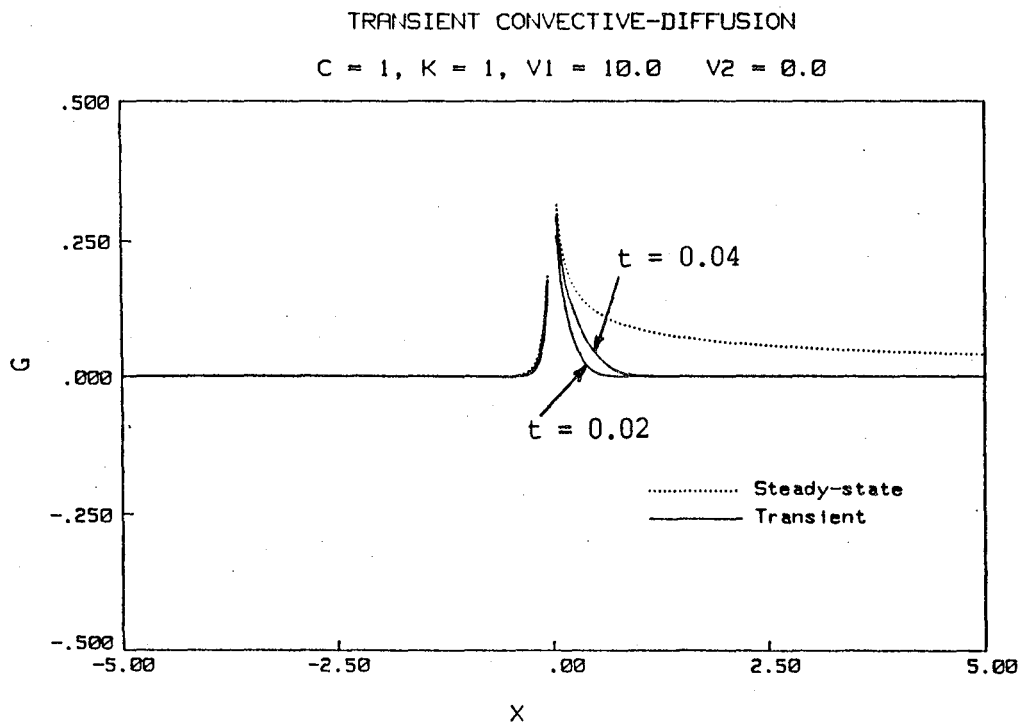

FIGURE 4.3

PARALLEL FLOW - BOUNDARY ELEMENT MODEL

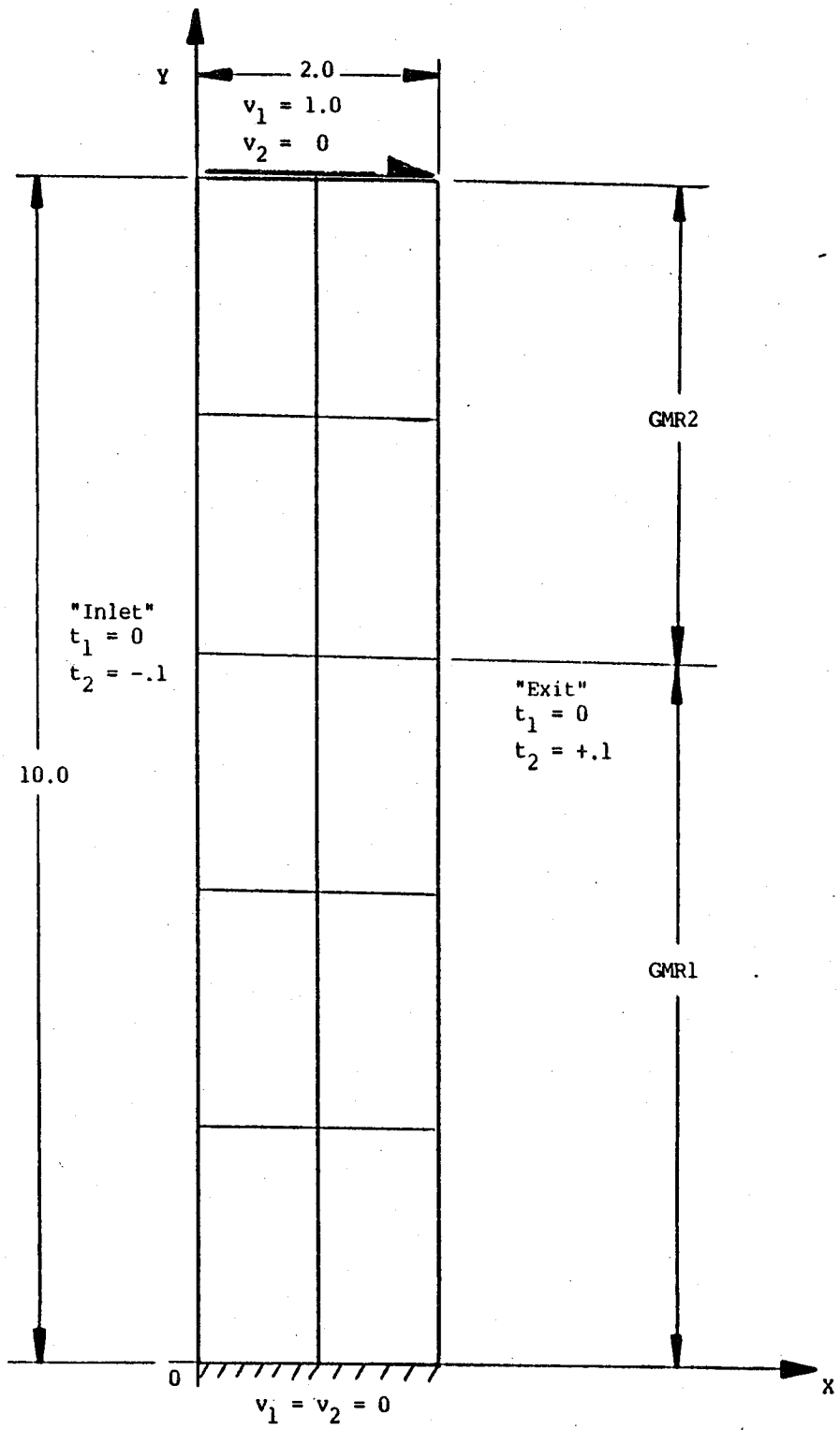

FIGURE 4.4

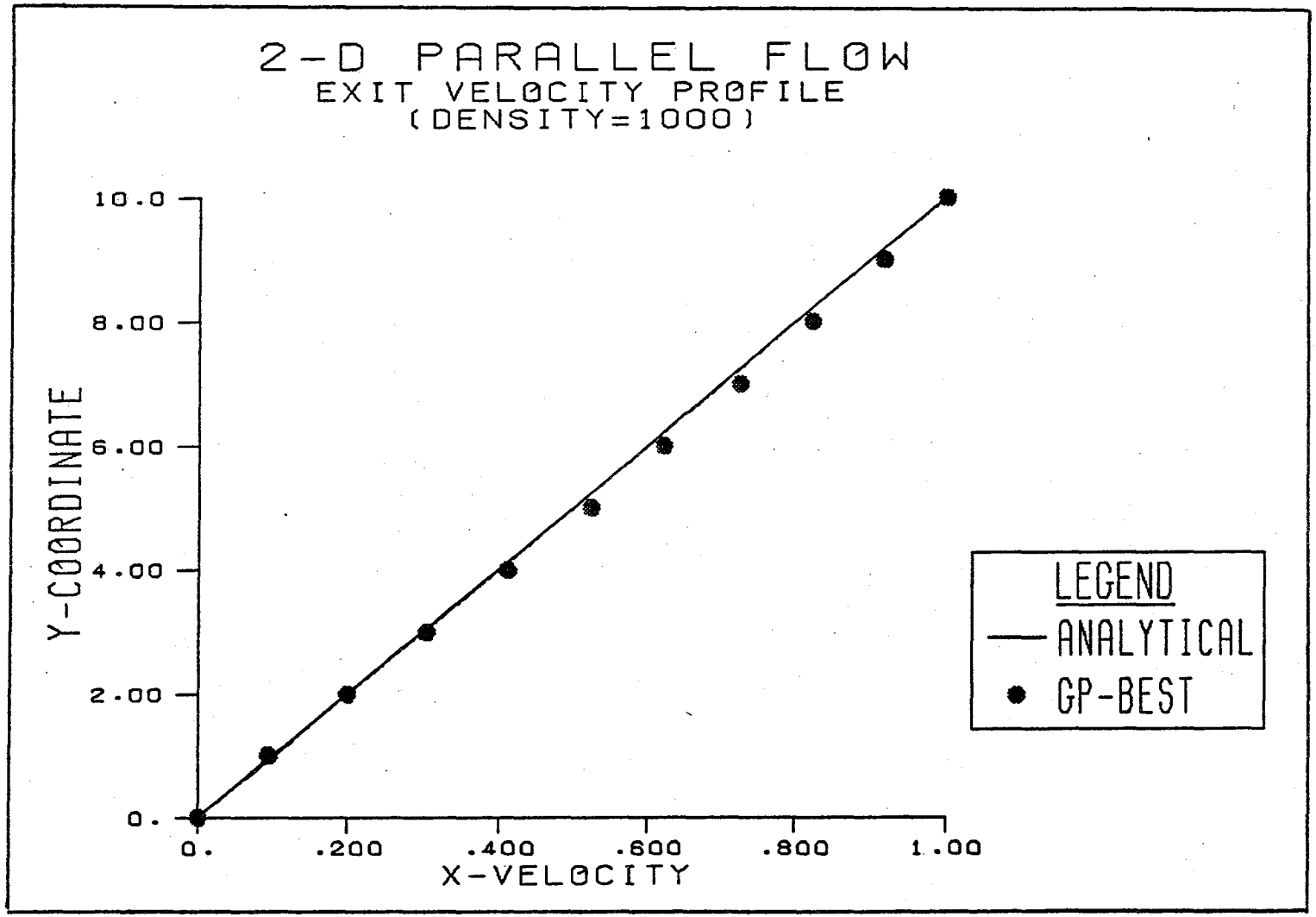
2-D PARALLEL FLOW
EXIT VELOCITY PROFILE
(DENSITY=1000)
Y-COORDINATE
10.0
8.00
6.00
4.00
2.00
0.
0.
.200
.400
.600
.800
1.00
X-VELOCITY
LEGEND
ANALYTICAL
GP-BEST

FIGURE 4.5

DRIVEN CAVITY

Boundary Element Model

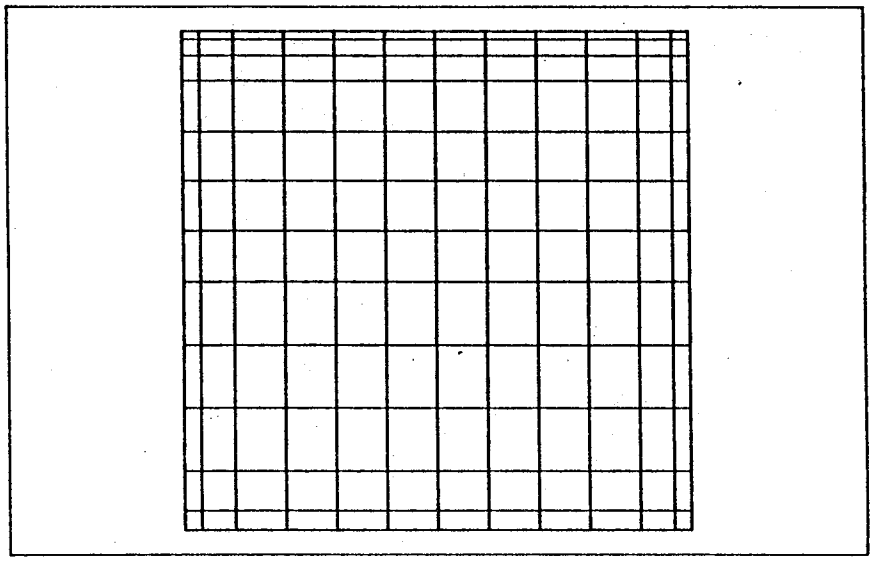

FIGURE 4.6

DRIVEN CAVITY

Steady-State Re = 100

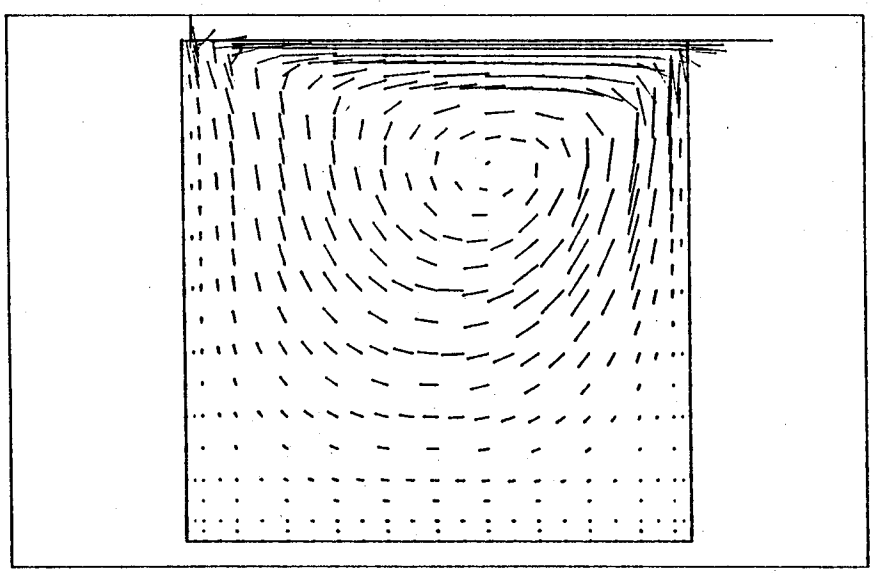

FIGURE 4.7

DRIVEN CAVITY

Steady-State Re = 400

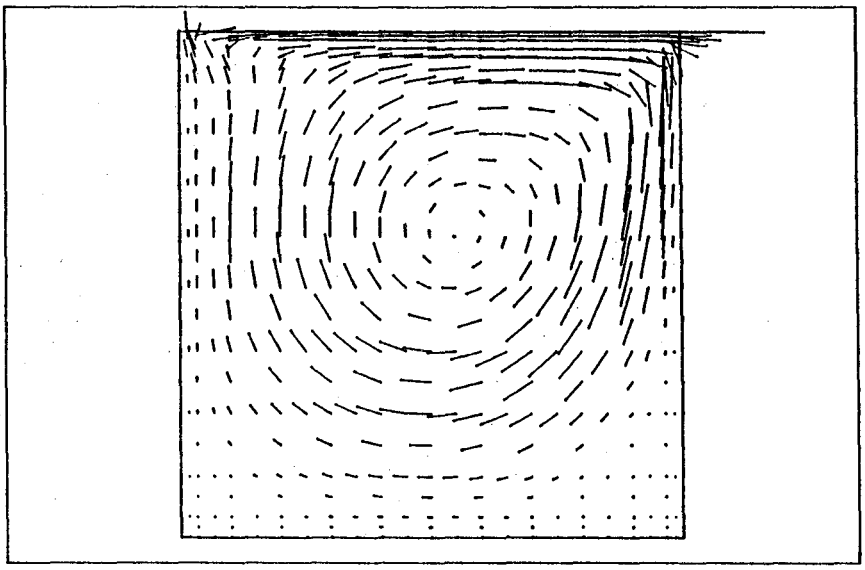

FIGURE 4.8

DRIVEN CAVITY

Steady-State Re = 1000

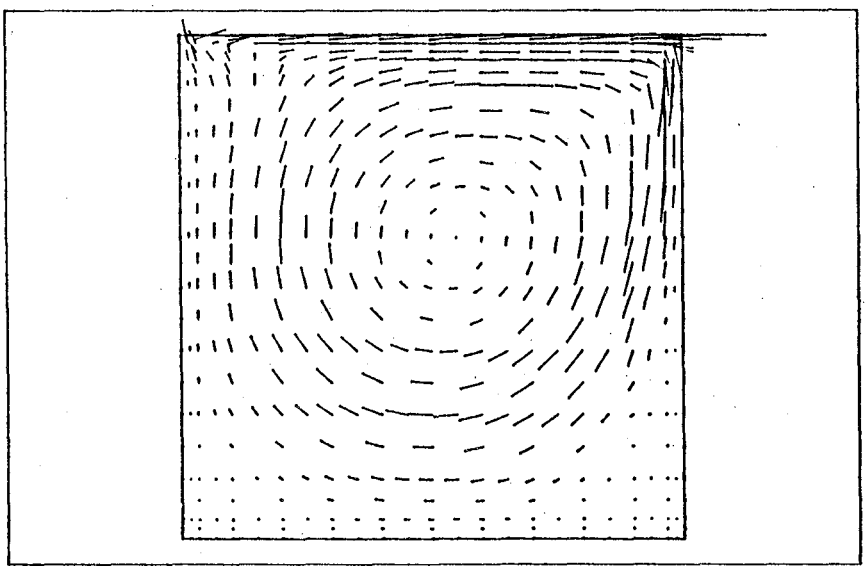

FIGURE 4.9

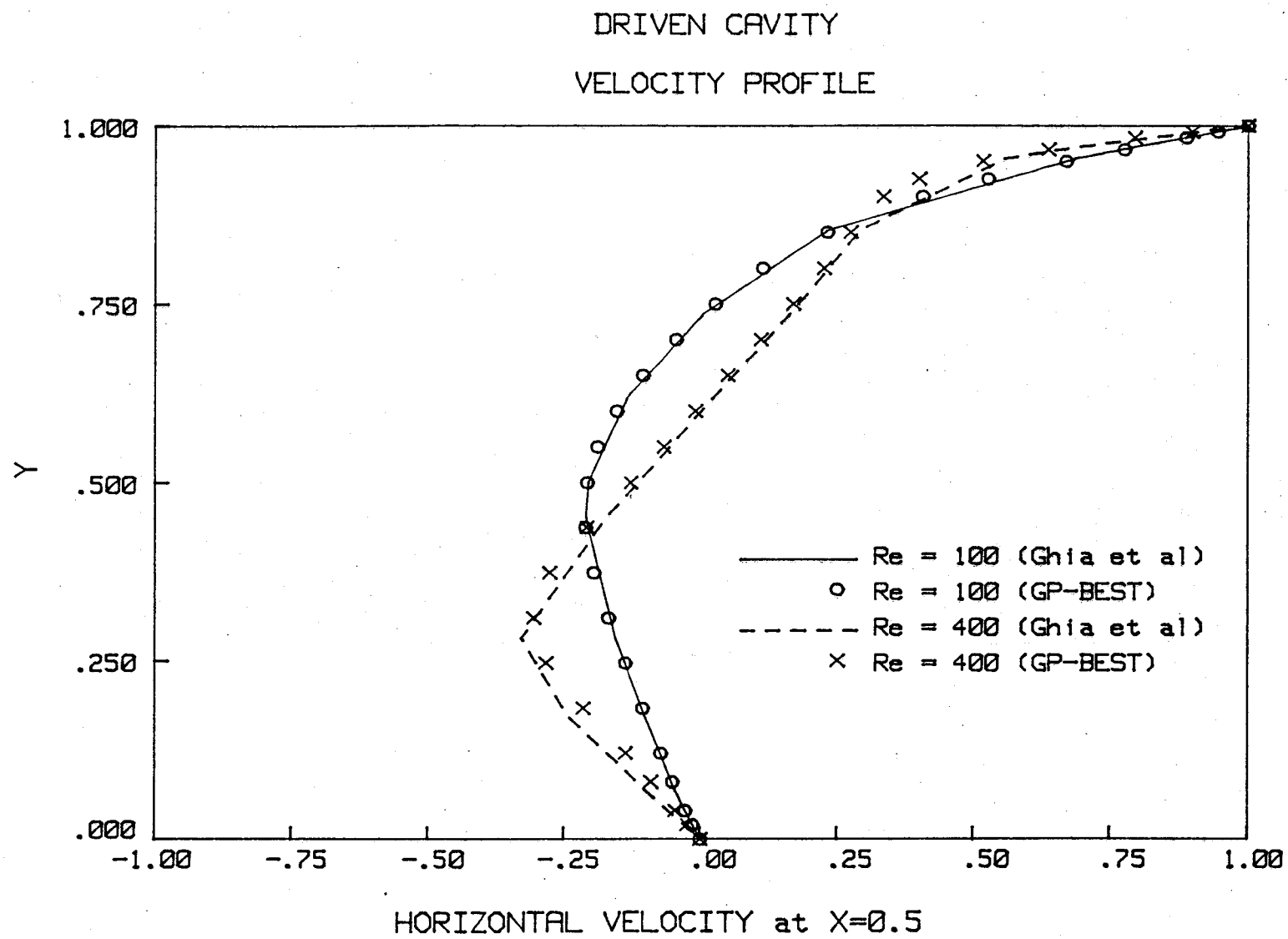
DRIVEN CAVITY
VELOCITY PROFILE
1.000
.750
.500
.250
.000
Y
-1.00
-.75
-.50
-.25
.00
.25
.50
.75
1.00
HORIZONTAL VELOCITY at X=0.5
Re = 100 (Ghia et al)
Re = 100 (GP-BEST)
Re = 400 (Ghia et al)
Re = 400 (GP-BEST)

FIGURE 4.10

DRIVEN CAVITY - FOUR REGION MODEL

Boundary Element Model

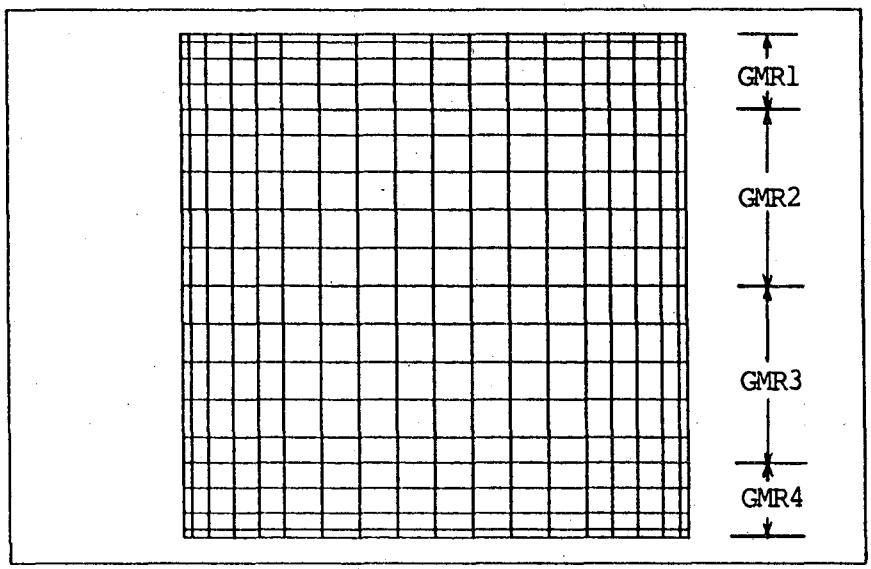

FIGURE 4.11

DRIVEN CAVITY - FOUR REGION MODEL

Lower Right Corner at Re = 1000

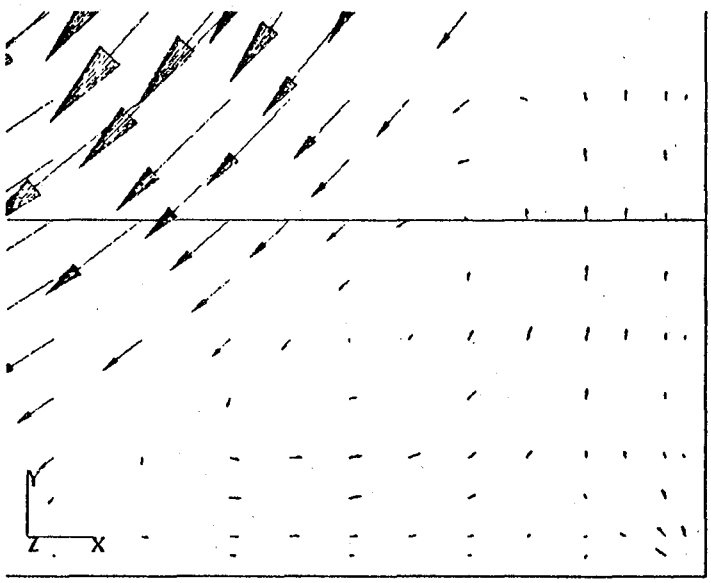

FIGURE 4.12

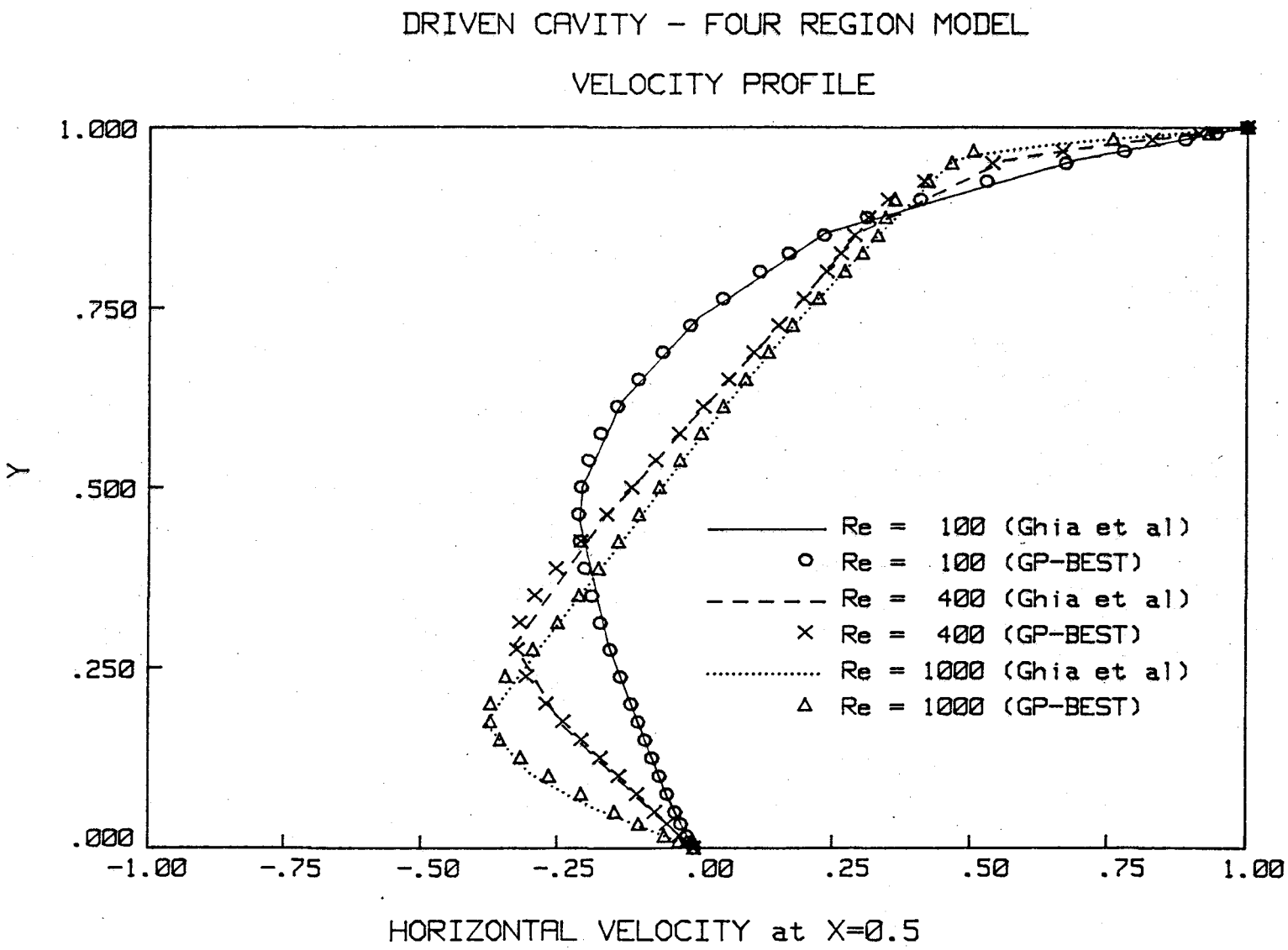
DRIVEN CAVITY - FOUR REGION MODEL
VELOCITY PROFILE
1.000
.750
.500
.250
.000
Y
-1.00
-.75
-.50
-.25
.00
.25
.50
.75
1.00
HORIZONTAL VELOCITY at X=0.5
Re = 100 (Ghia et al)
Re = 100 (GP-BEST)
Re = 400 (Ghia et al)
Re = 400 (GP-BEST)
Re = 1000 (Ghia et al)
Re = 1000 (GP-BEST)

FIGURE 4.13

CONVERGING CHANNEL - PROBLEM DEFINITION

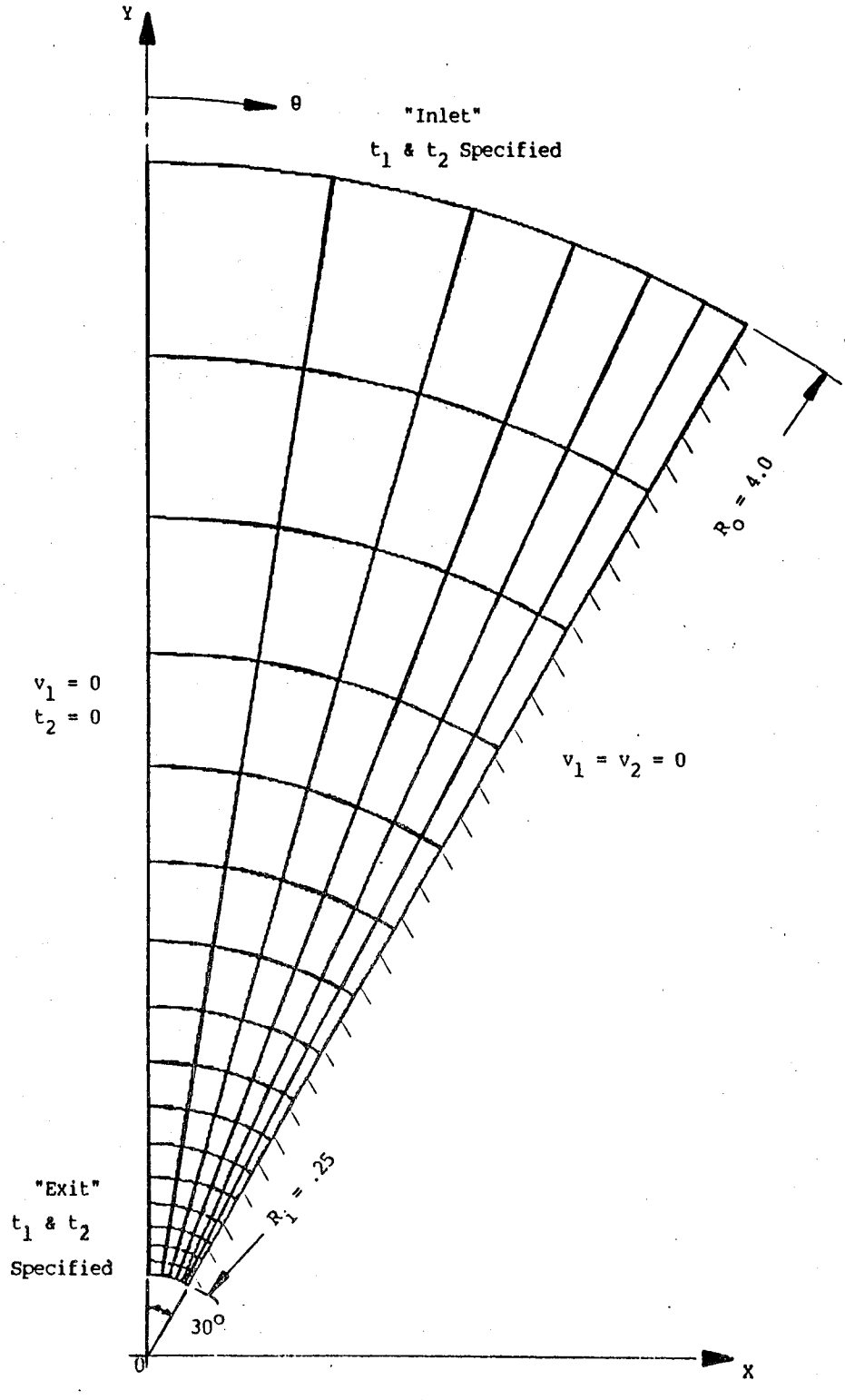

FIGURE 4.14

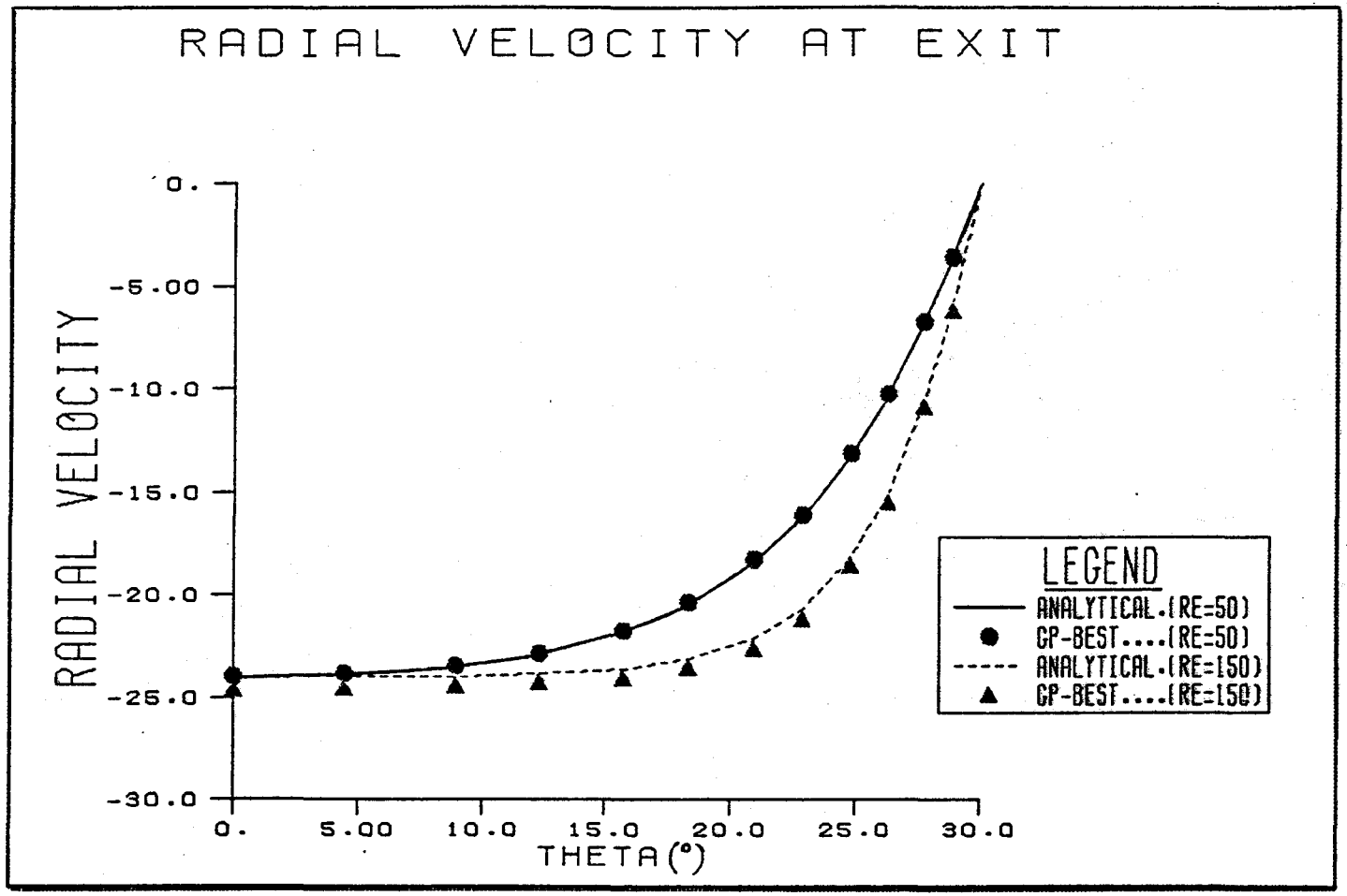
RADIAL VELOCITY AT EXIT
RADIAL VELOCITY
0.
-5.00
-10.0
-15.0
-20.0
-25.0
-30.0
0.
5.00
10.0
15.0
20.0
25.0
30.0
THETA(°)
LEGEND
ANALYTICAL.(RE=50)
GP-BEST....(RE=50)
ANALYTICAL.(RE=150)
GP-BEST....(RE=150)

FIGURE 4.15

FLOW AROUND A CYLINDER

Boundary Element Model

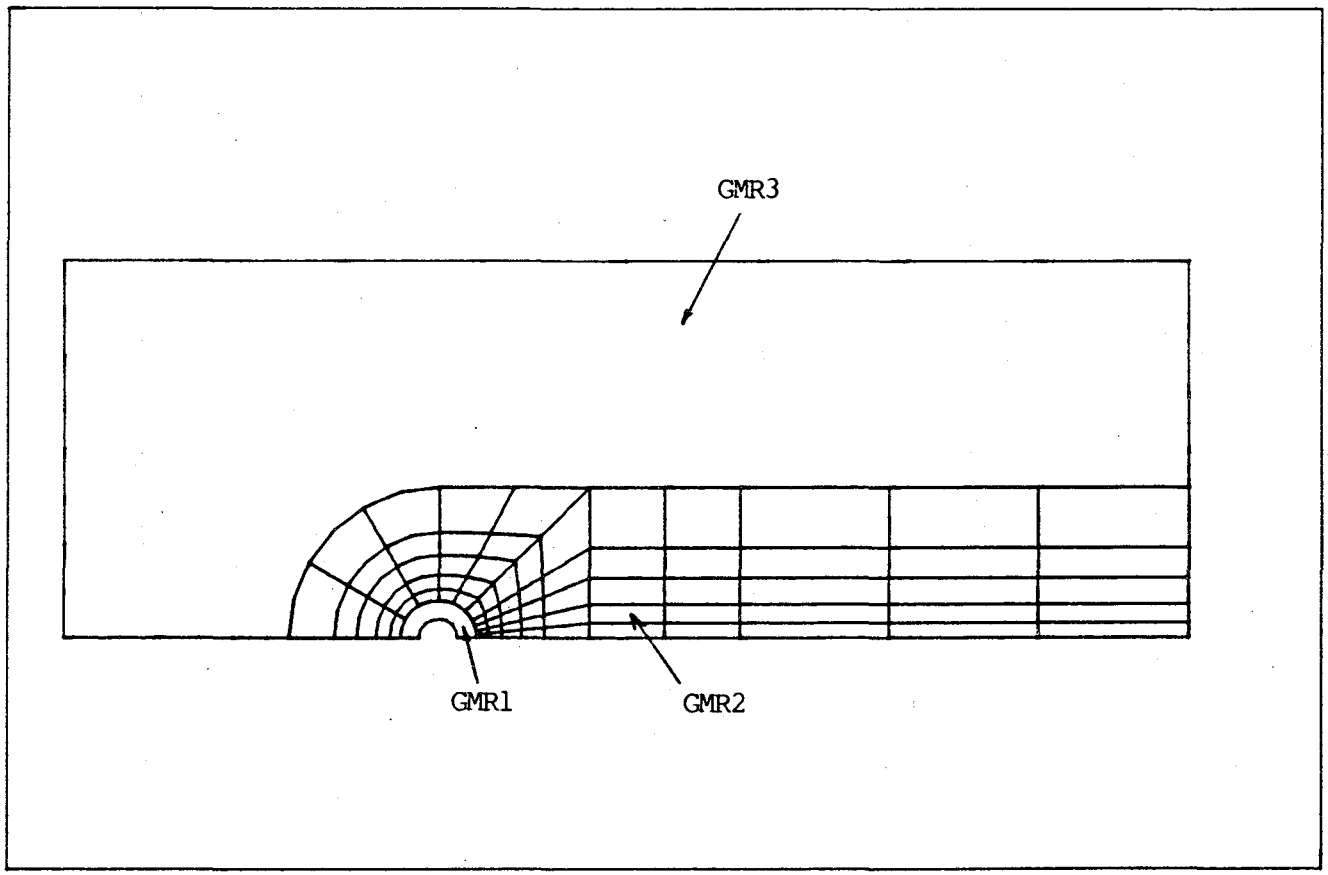

FIGURE 4.16

FLOW AROUND A CYLINDER

Re = 20

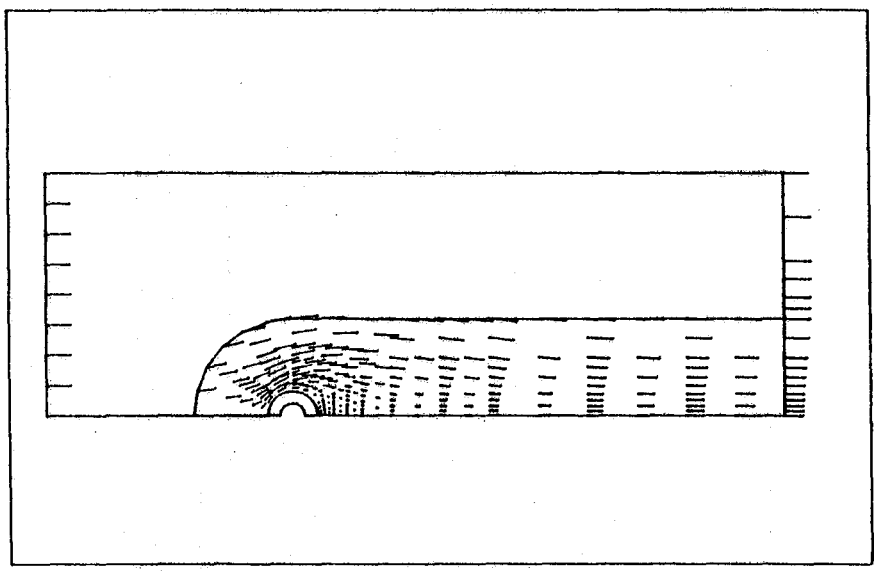

FLOW AROUND A CYLINDER

Re = 20

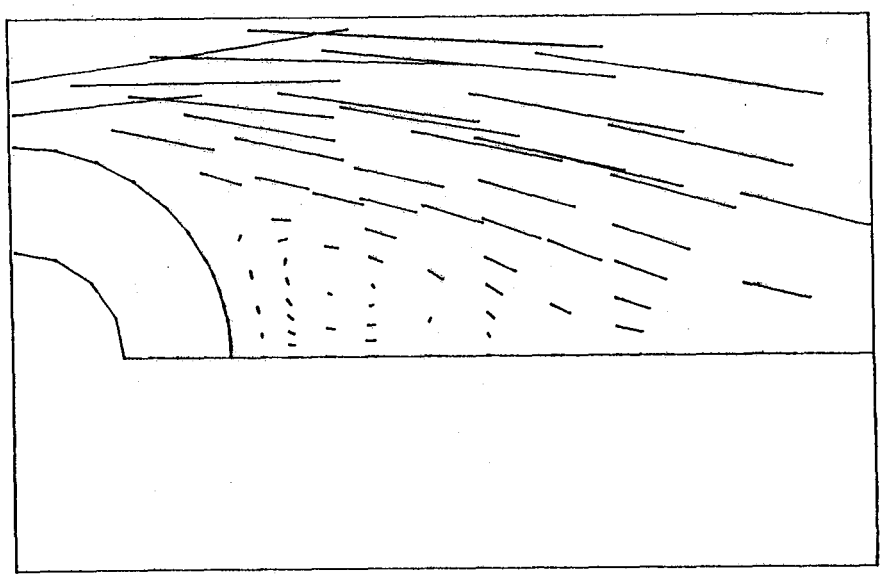

FIGURE 4.17

FLOW AROUND A CYLINDER

Re = 40

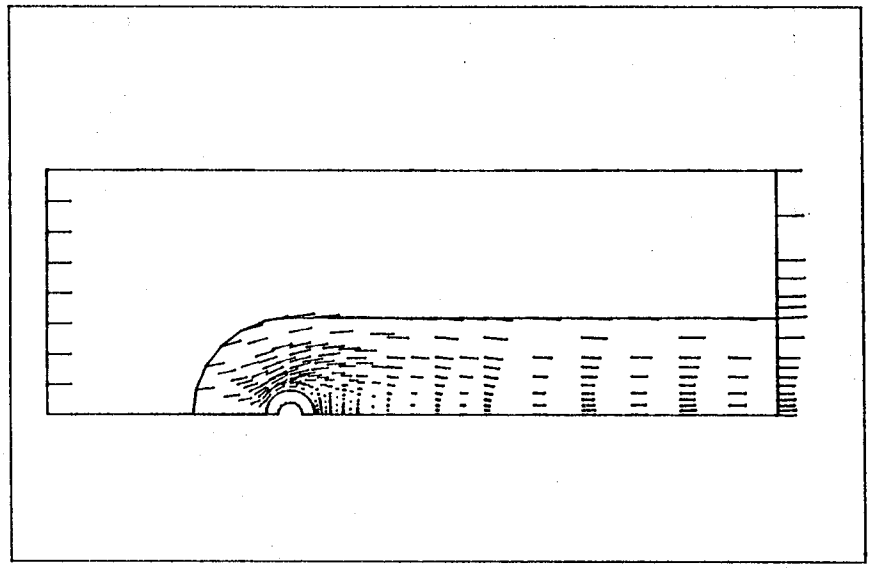

FLOW AROUND A CYLINDER

Re = 40

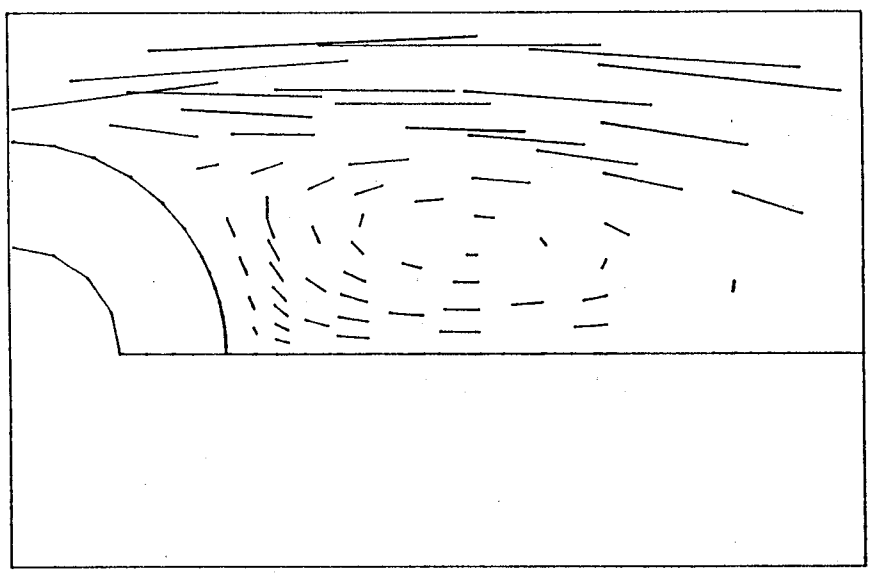

FIGURE 4.18

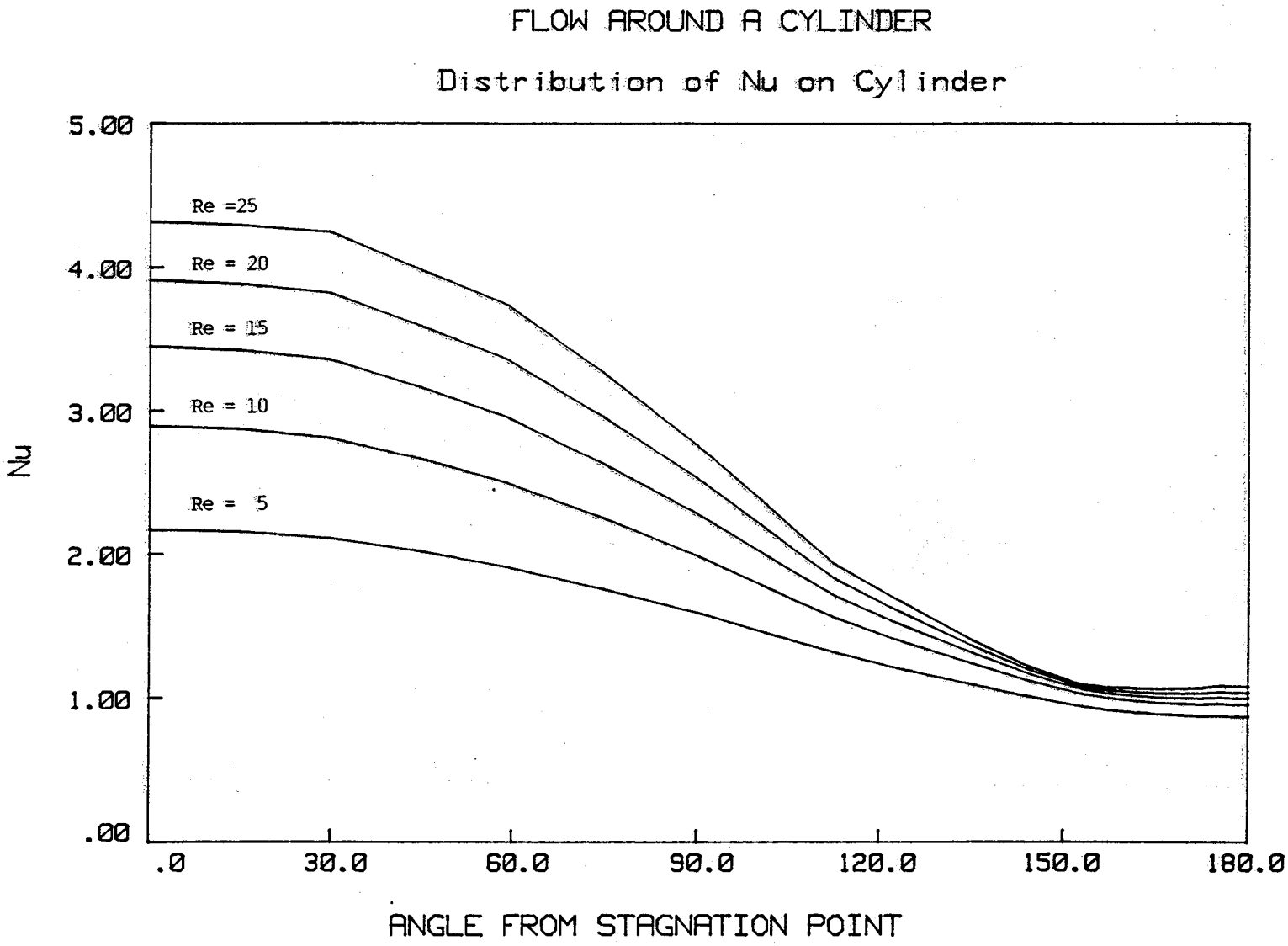
FLOW AROUND A CYLINDER
Distribution of Nu on Cylinder
5.00
4.00
3.00
2.00
1.00
.00
Nu
Re =25
Re = 20
Re = 15
Re = 10
Re = 5
.0
30.0
60.0
90.0
120.0
150.0
180.0
ANGLE FROM STAGNATION POINT

FIGURE 4.19

FLOW OVER AN AIRFOIL - BOUNDARY ELEMENT MODEL

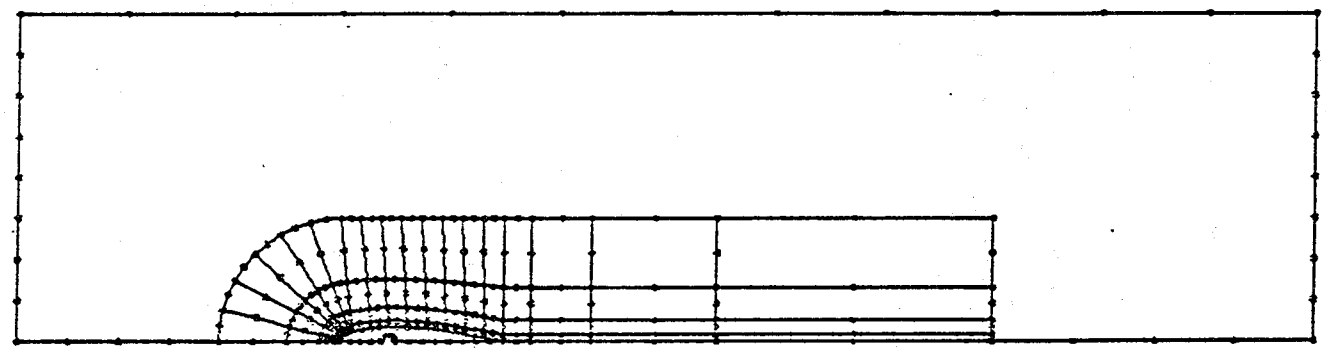

FIGURE 4.20

VELOCITY DISTRIBUTION AT RE = 150

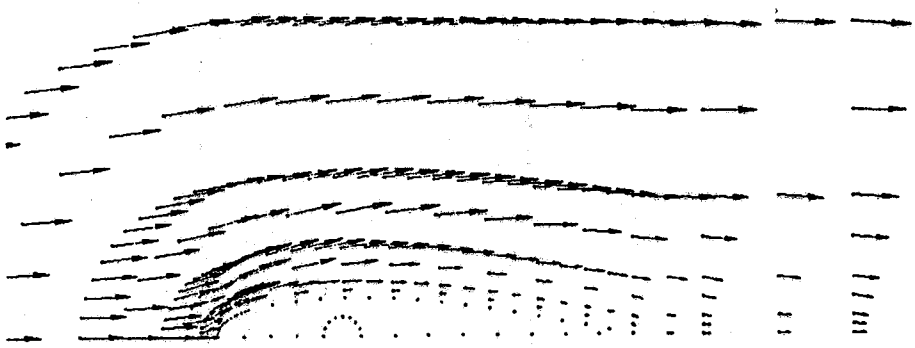

FIGURE 4.21

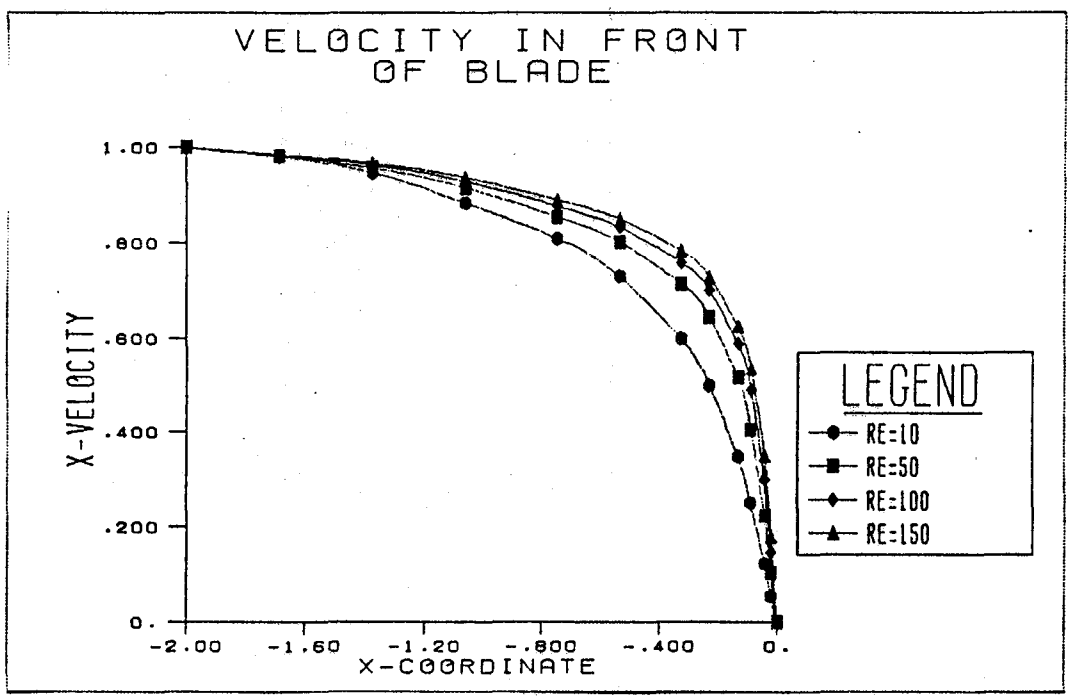

FIGURE 4.22

FLUID TEMPERATURE CONTOURS

Re = 10

Re = 150

FIGURE 4.23

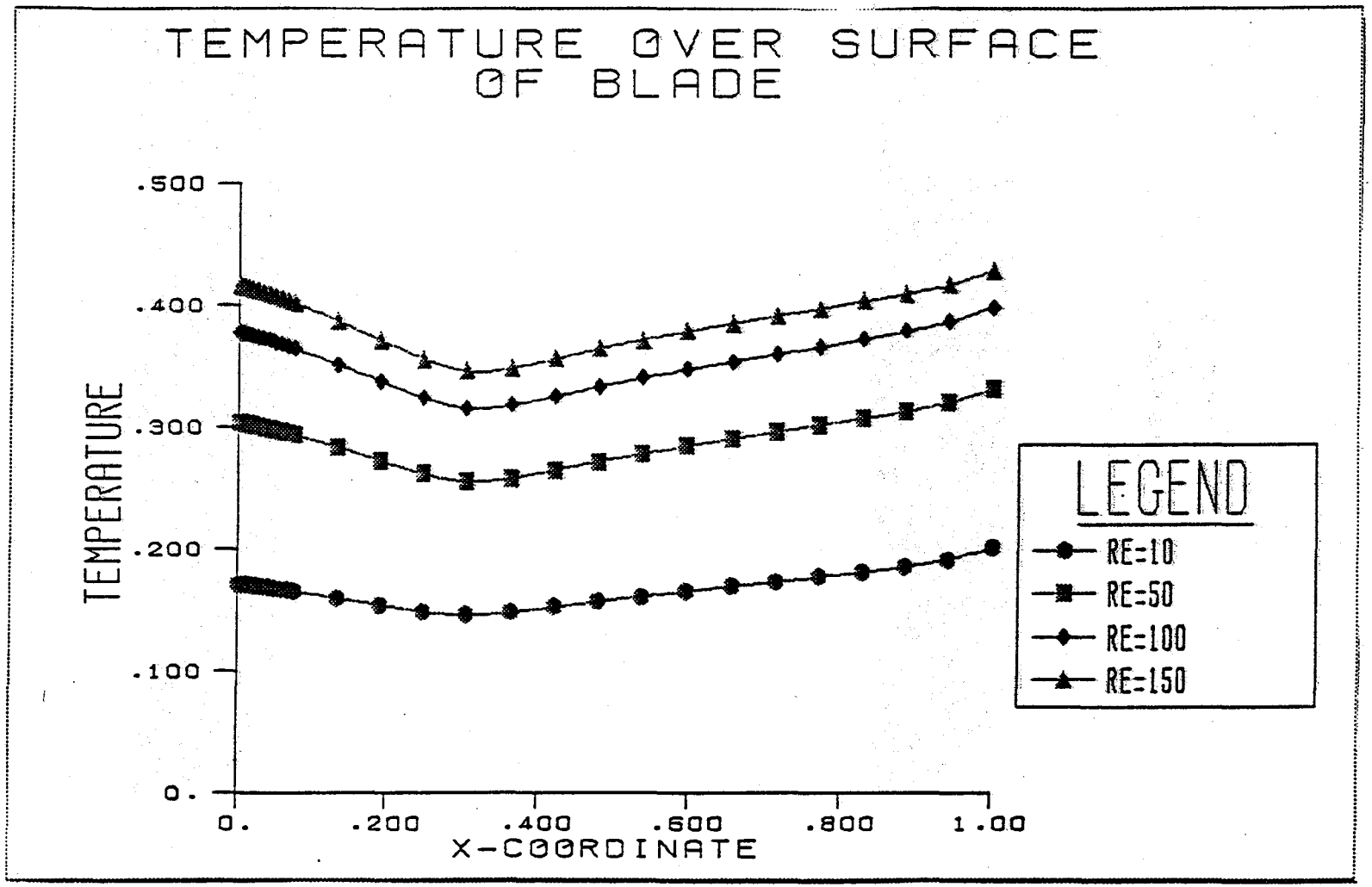
TEMPERATURE OVER SURFACE OF BLADE
.500
.400
.300
.200
.100
0.
TEMPERATURE
0.
.200
.400
.600
.800
1.00
X-COORDINATE
LEGEND
RE=10
RE=50
RE=100
RE=150

FIGURE 4.24

FLOW OVER NACA-0018 AIRFOILS

BOUNDARY ELEMENT MODEL

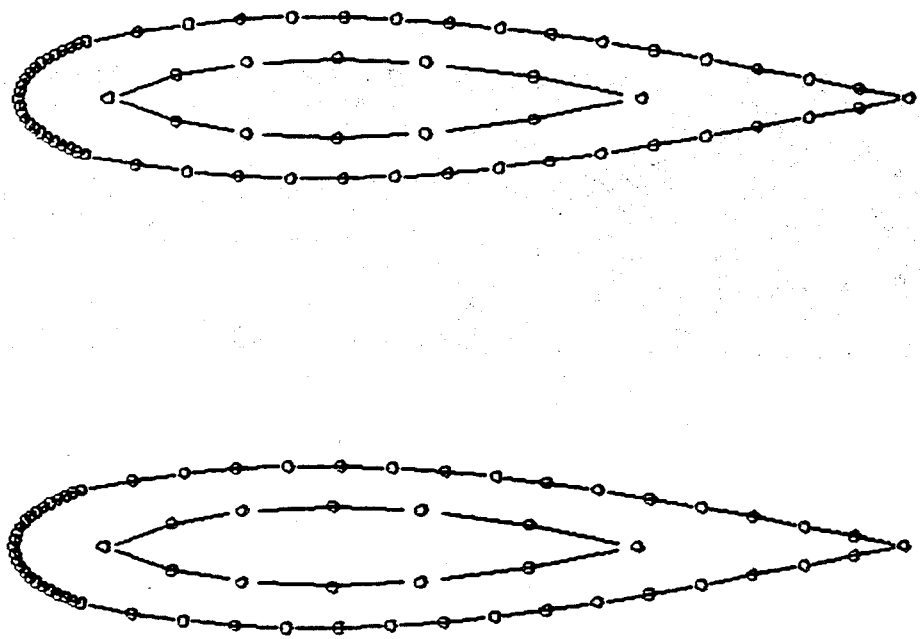

FIGURE 4.25

FLOW PAST A PAIR OF AIRFOILS

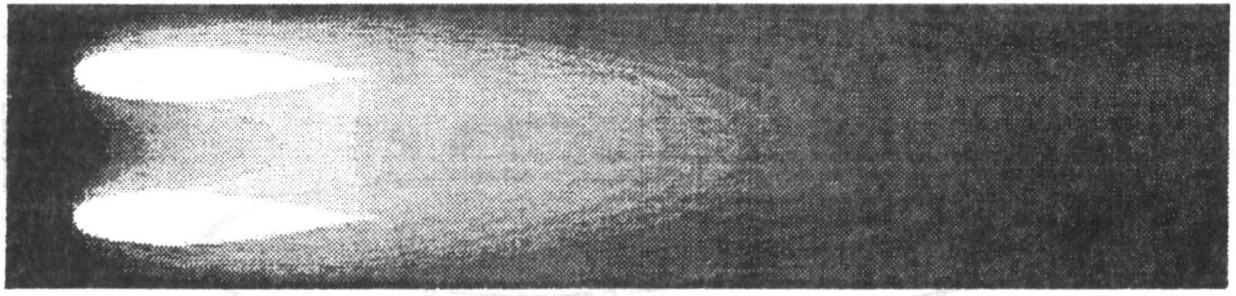

CONVECTIVE THERMAL FLOW (PE =10, ANGLE = 0)

FIGURE 4.26

FLOW PAST A PAIR OF AIRFOILS

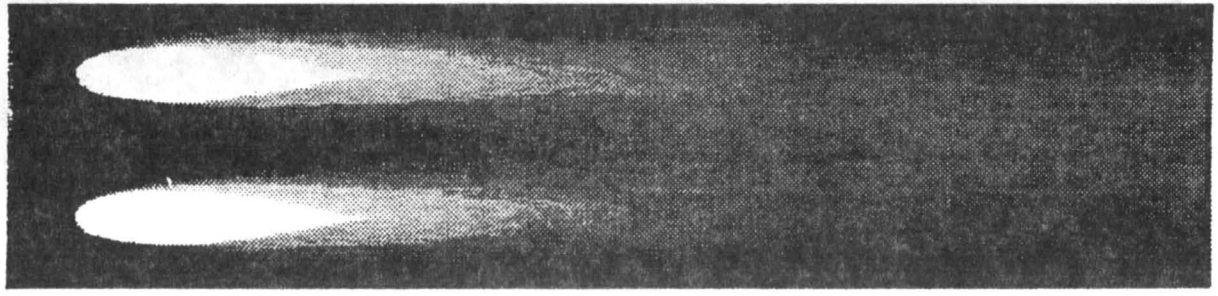

CONVECTIVE THERMAL FLOW (PE =100, ANGLE = 0)

FIGURE 4.27

FLOW PAST A PAIR OF AIRFOILS

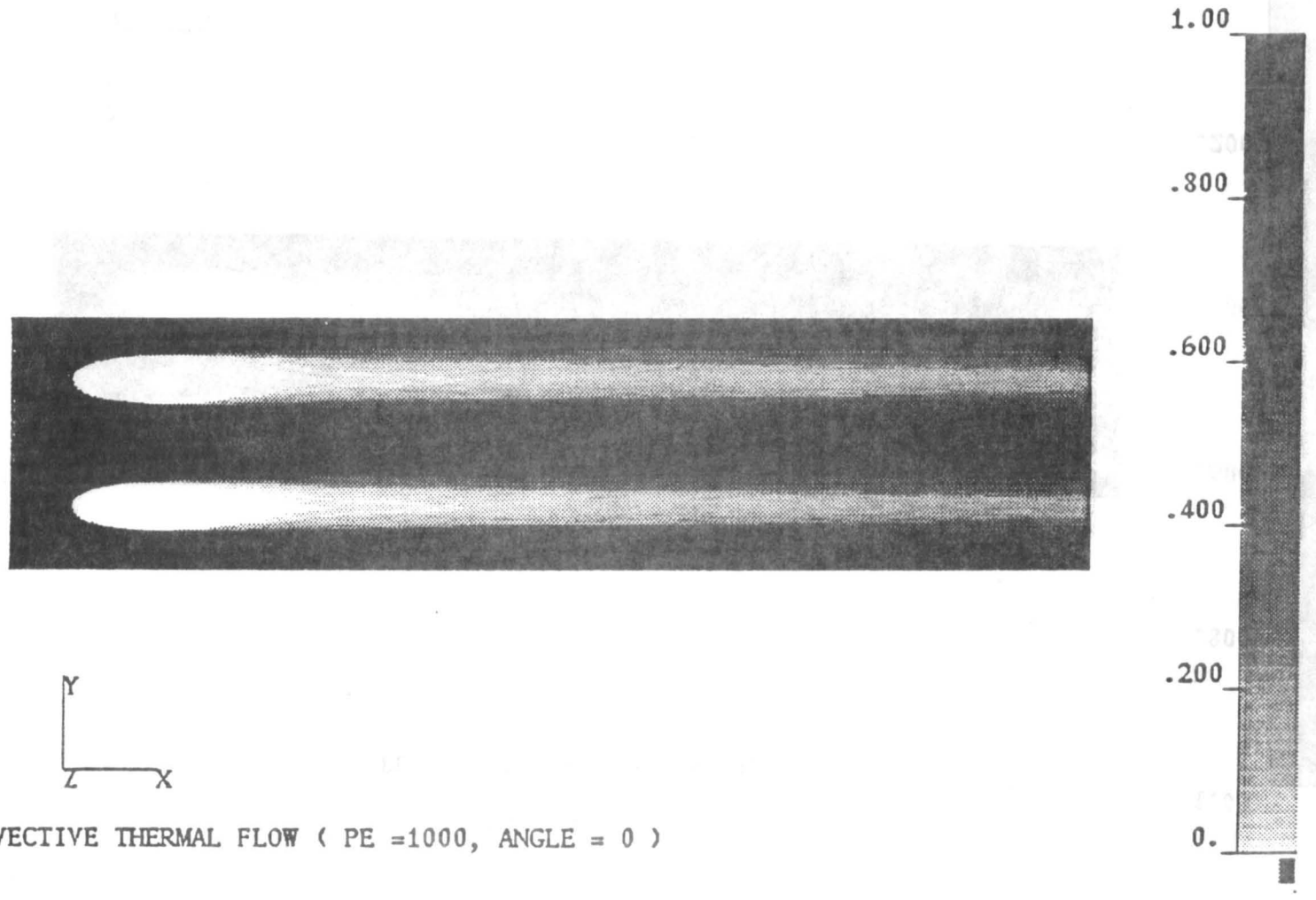

CONVECTIVE THERMAL FLOW (PE =1000, ANGLE = 0)

FIGURE 4.28

FLOW PAST A PAIR OF AIRFOILS

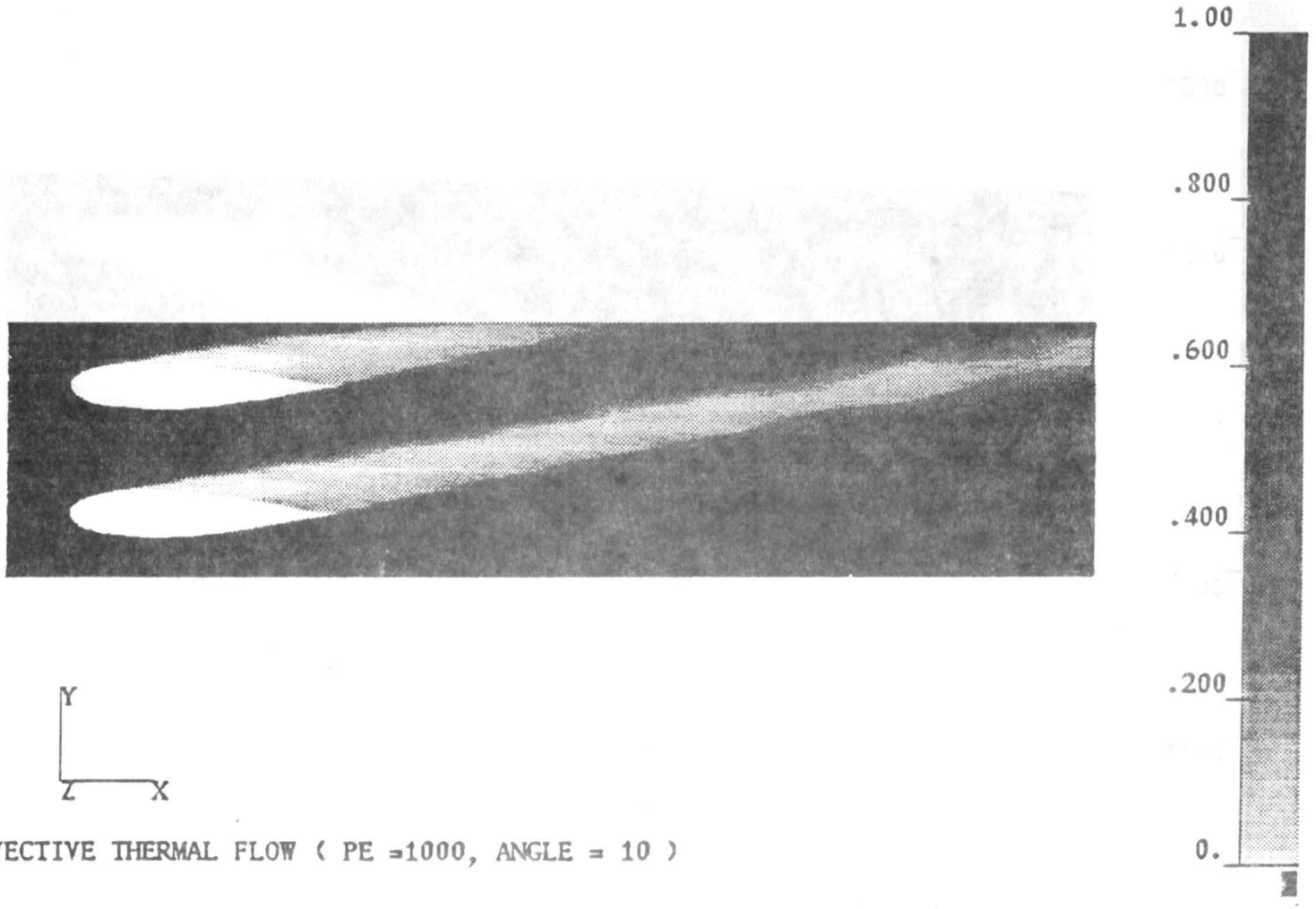

CONVECTIVE THERMAL FLOW (PE =1000, ANGLE = 10)

FIGURE 4.29

FLOW PAST A PAIR OF AIRFOILS

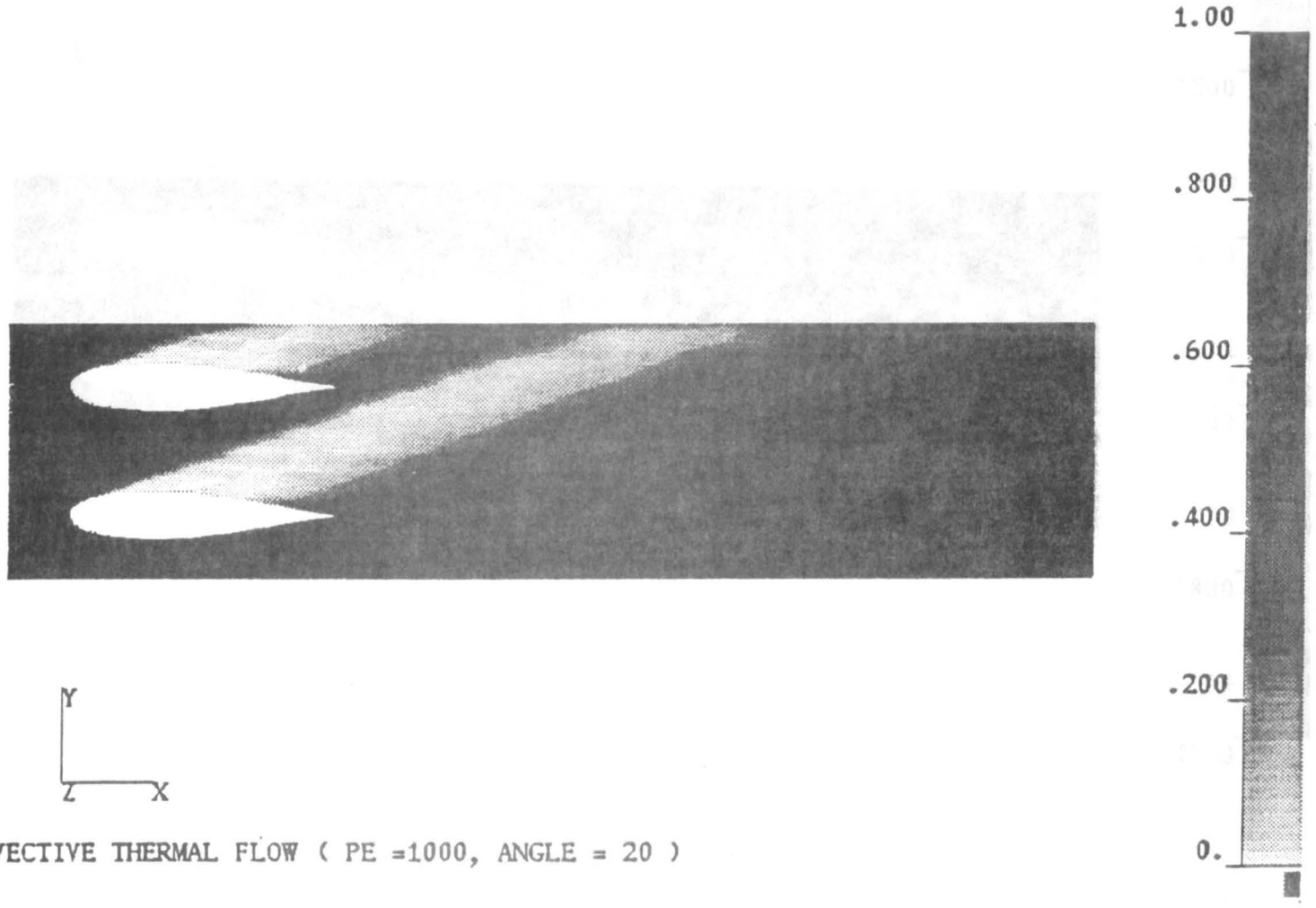

CONVECTIVE THERMAL FLOW (PE =1000, ANGLE = 20)

5. SUMMARY

Significant advancements have been made in the last twelve months toward the development of an integrated boundary element method for hot fluid-structure interaction. For the solids portion of the problem, the formulation is well developed. The boundary-only time domain thermoelastic formulation, detailed in Section 3 and Appendix B, was completed in the previous year. However, a number of enhancements have been incorporated to make the numerical implementation more efficient, more accurate, and to increase its applicability. For example, regarding computational aspects, full advantage is now taken of the uncoupled nature of the thermoelastic theory, so that convolution is only carried out on the temperature and flux related quantities. Additionally, for time steps beyond the first, a much reduced level of numerical integration is employed to evaluate the completely non-singular kernel functions. Meanwhile, extensions of the basic formulations have been made to include several practical facilities, such as time-dependent ambient temperatures, thermal resistance between regions to simulate coatings and air gaps, and the introduction of region-by-region reference temperatures. The resulting code has also gone through another round of verification testing, which has greatly improved its reliability.

The primary emphasis of the work performed under this grant has, of course, been directed toward the fluid, since boundary element applications to fluids are at a much less developed state. Considerable progress has been made on two fronts. The first major area involves improvements and extensions of the incompressible thermoviscous formulation originally developed last year. During the past twelve months, the accuracy and efficiency of the numerical integration has been significantly upgraded, the volume integrals have been rewritten to eliminate the need for

computation of velocity gradients, reference velocities and temperatures have been introduced on a region-by-region basis, and a Newton-Raphson algorithm has been developed to solve the highly nonlinear set of equations. The result, as is evident from the examples of Section 4, is an accurate general purpose boundary element approach to problems of thermoviscous flow in the low to medium Reynolds number range. As such, this development represents the first of its kind for this class of problems.

However, during the course of this work, it also became evident that the stationary media fundamental solutions of Appendix E do not contain enough of the physics of the problem at high Reynolds number. Moving media fundamental solutions and integral formulations are imperative for higher speed flows. Since these fundamental solutions do not exist in the literature, considerable effort has been expended toward their derivation. Approximate forms have been obtained for compressible thermoviscous flow, and are presented in Section 4.3. It should be emphasized that these convective solutions contain an analytical representation of upwinding and, for compressible flow, shock. The development of techniques for the numerical evaluation of the convective kernels is now underway. Meanwhile, the thermal portion pertaining to convective heat transfer, in a known flow field, has been completely implemented. This new formulation not only has produced some interesting results, but also provides considerable optimism for the success of the convective media approach to high speed thermoviscous flow.

6. WORKPLAN FOR THE NEXT YEAR

Based upon the experiences of this past year, future emphasis will naturally be placed upon the convective media approach, although some ongoing work on the transient stationary media algorithm will be completed. The following rather ambitious set of tasks are planned, in approximate chronological order, for the period November 1988 to November 1989:

1. Complete development of numerical techniques (e.g., rational approximations, series representations) for the evaluation of the convective compressible thermoviscous kernels.
2. Implement and validate the transient convective heat transfer formulation.
3. Complete the investigation of transient incompressible flow using the stationary media approach.
4. Implement and validate the new convective incompressible flow kernels.
5. Develop more efficient solution algorithms (e.g., iteration methods) and integration schemes for high Re flow.
6. Implement and validate convective compressible flow kernels.

APPENDIX A - REFERENCES

Ahmad, S. and Banerjee, P.K., (1988), 'Transient Elastodynamic Analysis of Three-dimensional Problems by BEM,' Int. Jour. Numerical Methods in Engineering, Vol. 26, No. 8, pp. 1560-1580.

Banerjee, P.K. and Butterfield, R. (1981), 'Boundary Element Methods in Engineering Science,' McGraw-Hill, London.

Banerjee, P.K., Ahmad, S. and Manolis, G.D. (1986), 'Transient Elastodynamic Analysis of Three-dimensional Problems by Boundary Element Method,' Earthquake Engineering and Structural Dynamics, Vol. 14, pp. 933-949.

Banerjee, P.K., Wilson, R.B. and Miller, N. (1985), 'Development of a Large BEM System for Three-dimensional Inelastic Analysis,' in Advanced Topics in Boundary Element Analysis, ed. T.A. Cruse, A.B. Pifko and H. Armen, AMD-V72, ASME, New York.

Banerjee, P.K., Wilson, R.B. and Miller, N. (1988), 'Advanced Elastic and Inelastic Three-dimensional Analysis of Gas Turbine Engine Structures by BEM,' Int. J. Num. Meth. Engrg., V26, pp. 393-411.

Boley, B.A. and Weiner, J.H. (1960), 'Theory of Thermal Stresses,' John Wiley and Sons, New York.

Burggraf, O.R. (1966), 'Analytical and Numerical Studies of the Structure of Steady Separated Flows,' J. Fluid Mech., V24, Part 1, pp. 113-151.

Carslaw, H.S. and Jaeger, J.C. (1947), Conduction of Heat in Solids, Clarendon Press, Oxford.

Chaudouet, A. (1987), 'Three-dimensional Transient Thermoelastic Analysis by the BIE Method,' Int. J. Num. Meth. Engrg., V24, pp. 25-45.

Cruse, T.A. (1974), 'An Improved Boundary Integral Equation Method for Three-Dimensional Elastic Stress Analysis,' Comp. and Struct., V4, pp. 741-754.

Cruse, T.A., and VanBuren, W. (1971), 'Three-dimensional Elastic Stress Analysis of a Fracture Specimen with an Edge Crack,' Int. J. Fract. Mech., V7, pp. 1-16.

Cruse, T.A., Snow, D.W. and Wilson, R.B. (1977), 'Numerical Solutions in Axisymmetric Elasticity,' Comp. and Struct., V7, pp. 445-451.

Dargush, G.F. (1987), BEM for the Analogous Problems of Thermoelasticity and Soil Consolidation, Ph.D. Dissertation, State University of New York at Buffalo.

Dargush, G.F. and Banerjee, P.K. (1988a), 'Development of a Boundary Element Method for Time-dependent Planar Thermoelasticity,' to appear in Int. J. Solids Struct.

Dargush, G.F. and Banerjee, P.K. (1988b), 'Boundary Element Methods in Three-dimensional Thermoelasticity,' submitted to Int. J. Solids Struct.

Dargush, G.F. and Banerjee, P.K. (1988c), 'Development of an Integrated BEM for Hot Fluid-Structure Interaction,' Advanced Earth-to-Orbit Propulsion Technology Conference, NASA CP-3012, Huntsville, May 1988.

Dargush, G.F. and Banerjee, P.K. (1989), 'Development of an Integrated BEM for Hot Fluid-Structure Interaction,' to appear International Gas Turbine and Aeroengine Congress and Exposition, ASME, Toronto.

Dargush, G., Banerjee, P.K. and Dunn, M.G (1987), Development of an Integrated BEM Approach for Hot Fluid Structure Interaction,NASA Annual Report, Grant NAG3-712.

Dargush, G.F., Manolis, G.D., Banerjee, P.K. and Dunn, M.G. (1986), Development of Integrated Boundary Element Approach to Fluid Structure Interaction for SSME, NASA Annual Report, Grant NAG3-712.

Dongarra, J.J. et al (1979), Linpak User's Guide, SIAM, Philadelphia.

Eckert, E.R.G. and Soehngen, E. (1952), 'Distribution of Heat-Transfer Coefficients Around Circular Cylinders in Crossflow at Reynolds Numbers From 20 to 500,' Transactions of the ASME, V74, pp. 343-347.

Gartling, D.K., Nickell, R.E., Tanner, R.E. (1977), 'A Finite Element Convergence Study for Accelerating Flow Problems,' Int. J. Num. Meth. Eng., V11, pp. 1155-1174.

Gel'fand, I.M. and Shilov, G.E. (1964), Generalized Functions, Vol. I - Properties and Operations, Academic Press, New York.

Ghia, U., Ghia, K.N. and Shin, C.T. (1982), 'High-Re Solutions for Incompressible Flow Using the Navier-Stokes Equations and a Multigrid Method,' J. Comp. Physics, V48, pp. 387-411.

Goldstein, M.E. (1976), Aeroacoustics, McGraw-Hill, New York.

Gunn, M.J. and Britto, A.M. (1984), CRISP User's and Programmer's Guide, Engineering Department, Cambridge University.

Latchat, J.C. and Watson, J.O. (1976), 'Effective Numerical Treatment of Boundary Integral Equations: A Formulation for Three-dimensional Elastostatics,' Int. J. Num. Meth. Engrg., V10, pp. 991-1005.

Ladyzhenskaya, O.A. (1969), The Mathematical Theory of Viscous Incompressible Flow, Gordon and Breach Science Publishers, New York.

Millsaps, K. and Pohlhausen, K. (1953), 'Thermal Distributions in Jeffery-Hamel Flows Between Nonparallel Plane Walls,' Journal of the Aeronautical Sciences, March, pp. 187-196.

Mustoe, G.G.W. (1984), 'Advanced Integration Schemes Over Boundary Elements and Volume Cells for Two- and Three-dimensional Nonlinear Analysis,' in Developments in Boundary Element Methods - III, ed. P.K. Banerjee and S. Mukherjee, Applied Science Publishers, England.

Piva, R. and Morino, L. (1987), 'Vector Green's Function Method for Unsteady Navier-Stokes Equations,' Meccanica, Vol. 22, pp. 76-85.

Piva, R., Graziani, G. and Morino, L. (1987) 'Boundary Integral Equation Method for Unsteady Viscous and Inviscid Flows,' IUTAM Symposium on Advanced Boundary Element Method, San Antonio, Texas.

Rizzo, F.J. and Shippy, D.J. (1977), 'An Advanced Boundary Integral Equation Method for Three-dimensional Thermoelasticity,' Int. J. Num. Meth. Eng., V11, pp. 1753-1768.

Sharp, S. and Crouch, S.L. (1986), 'Boundary Integral Methods for Thermoelasticity Problems,' J. Appl. Mech., V53, pp. 298-302.

Stroud, A.H. and Secrest, D. (1966), Gaussian Quadrature Formulas, Prentice Hall, New York.

Tadmor, Z. and Gogos, C.G. (1979), 'Principles of Polymer Processing,' John Wiley and Sons, New York.

Timoshenko, S.P. and Goodier, J.N. (1970), Theory of Elasticity, McGraw-Hill, New York.

Tosaka, N., and Kakuda, K. (1986), 'Numerical Solutions of Steady Incompressible Viscous Flow Problems by Integral Equation Method,' pp. 211-222 in R.P. Shaw et.al., Eds., Proc. 4th Intl. Symp. Innov. Num. Methods Engrg., Springer, Berlin.

Tosaka, N. and Kakuda, K. (1987) 'Numerical Simulations of Laminar and Turbulent Flows by Using an Integral Equation,' Boundary Elements IX, eds. Brebbia, Wendland and Kuhn, pp. 489-502.

Tosaka, N. and Onishi, K. (1986), 'Boundary Integral Equation Formulations for Unsteady Incompressible Viscous Fluid Flow by Time-differencing,' Engineering Analysis, V3, No. 2, pp. 101-104.

APPENDIX B - KERNELS FOR THERMOELASTICITY

This appendix contains the detailed presentations of all the kernel functions utilized in the formulations contained in Section 3. Two-dimensional (plane strain) kernels are provided, based upon continuous source and force fundamental solutions. For time-dependent uncoupled quasistatic thermoelasticity the following relationships must be used to determine the proper form of the functions required in the boundary element discretization. That is,

$$G^n_{\alpha\beta}(X-\xi) = G_{\alpha\beta}(X-\xi,n\Delta t) \qquad \text{for } n=1$$

$$G^n_{\alpha\beta}(X-\xi) = G_{\alpha\beta}(X-\xi,n\Delta t) - G_{\alpha\beta}(X-\xi,(n-1)\Delta t) \qquad \text{for } n>1 \ ,$$

with similar expressions holding for all the remaining kernels. In the specification of these kernels below, the arguments $(X-\xi,t)$ are assumed. The indices

i,j,k,l	vary from 1 to d
α,β	vary from 1 to (d+1)
θ	equals d+1

where d is the dimensionality of the problem. Additionally,

x_i	coordinates of integration point
ξ_i	coordinates of field point

$y_i = x_i - \xi_i \qquad r^2 = y_i y_i$.

For the displacement kernel,

$$G_{ij} = \frac{1}{8\pi} \frac{1}{\mu(1-\nu)} \left[\left(\frac{y_i y_j}{r^2}\right) - (\delta_{ij}) \ (3-4\nu) \ln r \right]$$

$$G_{i\theta} = 0$$

$$G_{\theta j} = \frac{r}{2\pi} \left(\frac{\beta}{k(\lambda+2\mu)}\right) \left[\left(\frac{y_j}{r}\right) \bar{g}_4(\eta) \right]$$

$$G_{\theta\theta} = \frac{1}{2\pi} \left(\frac{1}{k}\right) \left[\bar{g}_5(\eta) \right]$$

whereas, for the traction kernel,

$$F_{ij} = \frac{1}{4\pi r} \frac{1}{(1-\nu)} \left[-\left(\frac{2y_i y_j y_k n_k}{r^3}\right) - \left(\frac{\delta_{ij} y_k n_k + y_i n_j}{r}\right) (1-2\nu) \right.$$

$$\left. + \left(\frac{y_j n_i}{r}\right) (1-2\nu) \right]$$

$$F_{i\theta} = 0$$

$$F_{\theta j} = \frac{1}{4\pi} \left(\frac{\beta}{\lambda+2\mu}\right) \left[\left(\frac{y_j y_k n_k}{r^2}\right) \bar{f}_6(\eta) - (n_j) \bar{f}_7(\eta) \right]$$

$$F_{\theta\theta} = \frac{1}{2\pi r} \left[\left(\frac{y_k n_k}{r}\right) \bar{f}_8(\eta) \right] .$$

In the above,

$$\eta = \frac{r}{(ct)^{1/2}}$$

$$c = \frac{k}{\rho c_e}$$

$$E_1(z) = \int_z^\infty \frac{e^{-x}}{x} dx$$

$$\bar{h}_1(\eta) = \frac{4}{\eta^2} (1-e^{-\eta^2/4})$$

$$\bar{g}_4(\eta) = \frac{\bar{h}_1(\eta)}{2} + \frac{E_1(\frac{\eta^2}{4})}{2}$$

$$\bar{g}_5(\eta) = \frac{E_1(\frac{\eta^2}{4})}{2}$$

$$\bar{f}_6(\eta) = \bar{h}_1(\eta)$$

$$\bar{f}_7(\eta) = \frac{\bar{h}_1(\eta)}{2} + \frac{E_1(\frac{\eta^2}{4})}{2}$$

$$\bar{f}_8(\eta) = e^{-\eta^2/4} .$$

For the interior stress kernels,

$$E_{\beta ij} = \frac{2\mu\nu}{1-2\nu}\,\delta_{ij}\,\frac{\partial G_{\beta l}}{\partial \xi_l} + \mu\,\left(\frac{\partial G_{\beta i}}{\partial \xi_j} + \frac{\partial G_{\beta j}}{\partial \xi_i}\right) - \beta\delta_{ij}\,G_{\beta\theta}$$

$$D_{\beta ij} = \frac{2\mu\nu}{1-2\nu}\,\delta_{ij}\,\frac{\partial F_{\beta l}}{\partial \xi_l} + \mu\,\left(\frac{\partial F_{\beta i}}{\partial \xi_j} + \frac{\partial F_{\beta j}}{\partial \xi_i}\right) - \beta\delta_{ij}\,F_{\beta\theta}$$

where

$$\frac{\partial G_{ij}}{\partial \xi_k} = \frac{1}{8\pi r}\,\frac{1}{\mu(1-\nu)}\,\left[\left(\frac{2y_i y_j y_k}{r^3} - \frac{\delta_{jk}y_i}{r} - \frac{\delta_{ik}y_j}{r}\right)\right.$$

$$\left. + \left(\frac{\delta_{ij}y_k}{r}\right)\,\{(3-4\nu)\,\}\right]$$

$$\frac{\partial G_{\theta j}}{\partial \xi_k} = \frac{1}{4\pi}\,\left(\frac{\beta}{k(\lambda+2\mu)}\right)\,\left[\left(\frac{y_j y_k}{r^2}\right)\,\{\bar{h}_1\} - (\delta_{jk})\,\left\{\frac{\bar{h}_1}{2} + \frac{E_1}{2}\right\}\right]$$

$$\frac{\partial F_{ij}}{\partial \xi_k} = \frac{1}{4\pi r^2}\frac{1}{(1-\nu)}\left[-\left(\frac{4y_iy_jy_ky_ln_l}{r^4} - \frac{y_iy_jn_k}{r^2} - \frac{\delta_{jk}y_iy_ln_l}{r^2}\right.\right.$$

$$\left. - \frac{\delta_{ik}y_jy_ln_l}{r^2}\right)\bar{f}_1(\eta) - \left(\frac{2\delta_{ij}y_ky_ln_l}{r^2} - \delta_{ij}n_k + \frac{2y_iy_kn_j}{r^2} - \delta_{ik}n_j\right)\bar{f}_2(\eta)$$

$$\left. + \left(\frac{2y_jy_kn_i}{r^2} - \delta_{jk}n_i\right)\bar{f}_3(\eta)\right]$$

$$\frac{\partial F_{\theta j}}{\partial \xi_k} = \frac{1}{4\pi r}\left(\frac{\beta}{\lambda+2\mu}\right)\left[\left(\frac{2y_jy_ky_ln_l}{r^3}\right)\{2\bar{h}_1 - e^{-\eta^2/4}\}\right.$$

$$\left. - \left(\frac{y_kn_j}{r} + \frac{y_jn_k}{r} + \frac{\delta_{jk}y_ln_l}{r}\right)\{\bar{h}_1\}\right] .$$

$$\bar{f}_1(\eta) = 2$$

$$\bar{f}_2(\eta) = 1-2\nu$$

$$\bar{f}_3(\eta) = 1-2\nu$$

APPENDIX C - FUNDAMENTAL SOLUTION FOR CONVECTIVE COMPRESSIBLE THERMOVISCOUS FLOW

$$g^U_{ij} = \frac{\gamma(\lambda+2\mu)}{\rho_o^2 c_o^2} \frac{\partial^2 \beta_U}{\partial x_i \partial x_j} + \frac{1}{\rho_o} \int_0^t \left[\frac{\partial^2}{\partial x_i \partial x_j} (\beta_U - \alpha_U) \right.$$

$$\left. - e_{ikl} e_{lmj} \frac{\partial^2}{\partial x_k \partial x_m} (\mu \omega_U - \alpha_U) \right] d\tau$$

$$g^U_{pj} = - \frac{\partial \beta_U}{\partial x_j}$$

$$g^U_{\theta j} = 0$$

$$g^U_{ip} = \frac{\gamma}{c_o^2} \frac{\partial \beta_U}{\partial x_i}$$

$$g^U_{pp} = \frac{\gamma(\lambda+2\mu)}{\rho_o c_o^2} \frac{\partial^2 \beta_U}{\partial x_i \partial x_i} - \frac{\gamma}{c_o^2} \frac{D_o \beta_U}{Dt}$$

$$g^U_{\theta p} = 0$$

$$g^U_{i\theta} = 0$$

$$g^U_{p\theta} = 0$$

$$g^U_{\theta\theta} = \theta_U$$

where

$$\alpha_U = - \frac{\delta(t-\tau)}{2\pi} \ln r$$

$$\omega_U = \frac{1}{4\pi\mu} \frac{e^{-R_U/4c't'}}{t'}$$

$$\theta_U = \frac{1}{4\pi k} \frac{e^{-R_U/4ct'}}{t'}$$

$$\beta_U = \frac{c_o}{2\pi\bar{R}} \left[(1 + \frac{\eta t'}{\bar{R}^2} H(c_o t'-R_U) - \frac{\eta}{c_o^2} \delta(c_o t'-R_u) \right]$$

$$c' = \frac{\mu}{\rho_o} \qquad\qquad c = \frac{k}{\rho_o c_v}$$

$$\eta = \frac{\lambda+2\mu}{\rho_o}$$

$$t' = t-\tau$$

$$R_U^2 = (y_i-U_i t')(y_i - U_i t')$$

$$y_i = x_i-\xi_i$$

$$\bar{R}^2 = c_o^2 t'^2 - R_U^2$$

APPENDIX D - FUNDAMENTAL SOLUTION FOR CONVECTIVE INCOMPRESSIBLE THERMOVISCOUS FLOW

$$g^U_{ij} = - e_{ikl}e_{lmj} \int_0^t (\frac{\mu\omega_U}{\rho_o} - \frac{\alpha_U}{\rho_o})\, d\tau$$

$$g^U_{\theta j} = 0$$

$$g^U_{i\theta} = 0$$

$$g^U_{\theta\theta} = \theta_U$$

where

$$\alpha_U = - \frac{\delta(t-\tau)}{2\pi} \ln r$$

$$\omega_U = \frac{1}{4\pi\mu} \frac{e^{-R_U/4c't'}}{t'}$$

$$\theta_U = \frac{1}{4\pi k} \frac{e^{-R_U/4ct'}}{t'}$$

$$c' = \frac{\mu}{\rho_o} \qquad c = \frac{k}{\rho_o c_v}$$

$$t' = t-\tau$$

$$R_U^2 = (y_i - U_i t')(y_i - U_i t')$$

$$y_i = x_i - \xi_i$$

APPENDIX E - KERNELS FOR STATIONARY INCOMPRESSIBLE THERMOVISCOUS FLOW

This appendix contains details of the time-dependent incompressible kernels, based upon stationary media, necessary for the integral formulations of Section 4. Notation is consistent with that defined in Appendix B.

For the generalized velocity kernels,

$$G_{ij} = \frac{1}{4\pi\mu}\left[\left(\frac{y_i y_j}{r^2}\right) \{s_1(\varepsilon) - (\delta_{ij}) \left\{\frac{s_1(\varepsilon)}{2} - \frac{E_1(\frac{\varepsilon^2}{4})}{2}\right\} \right]$$

$$G_{i\theta} = 0$$

$$G_{\theta j} = 0$$

$$G_{\theta\theta} = \frac{1}{2\pi}\left(\frac{1}{k}\right)\left[\frac{E_1(\frac{\eta^2}{4})}{2} \right]$$

whereas, for the generalized traction kernel,

$$F_{ij} = \frac{1}{2\pi r}\left[\left(\frac{y_i n_j}{r}\right) \{s_1 - e^{-\varepsilon^2/4}\} + \left(\frac{\delta_{ij} y_k n_k}{r}\right) \{s_1 - e^{-\varepsilon^2/4}\} \right.$$

$$\left. - \left(\frac{y_j n_i}{r}\right) \{H(t) - s_1\} - \left(\frac{2 y_i y_j y_k n_k}{r^3}\right) \{2s_1 - e^{-\varepsilon^2/4}\} \right]$$

$$F_{i\theta} = 0$$

$$F_{\theta j} = 0$$

$$F_{\theta\theta} = \frac{1}{2\pi r}\left[\left(\frac{y_k n_k}{r}\right) e^{-\eta^2/4} \right].$$

In the above,

$$\varepsilon = \frac{r}{(c't)^{1/2}}$$

$$c' = \frac{\mu}{\rho}$$

$$s_1(\varepsilon) = \frac{4}{\varepsilon^2}\,(1-e^{-\varepsilon^2/4})$$

$$\eta = \frac{r}{(ct)^{1/2}}$$

$$c = \frac{k}{\rho c_\varepsilon}$$

$$E_1(z) = \int_z^\infty \frac{e^{-u}}{u}\,du$$

Meanwhile, for the interior strain rates,

$$E_{ijk} = \frac{1}{4\pi r}\left(\frac{1}{\mu}\right)\left[-\left(\frac{\delta_{jk}y_i}{r}\right)\{s_1\} - \left(\frac{\delta_{ik}y_j}{r}\right)\{s_1\} + \left(\frac{2y_iy_jy_k}{r^3}\right)\{2s_1-e^{-\varepsilon^2/4}\} + \left(\frac{\delta_{ij}y_k}{r}\right)\{2e^{-\varepsilon^2/4}-s_1\}\right]$$

$$D_{ijk} = \frac{1}{2\pi r^2}\left[-\left(\frac{y_iy_jy_ky_mn_m}{r^4}\right)\bar{g}_1 - \left(\frac{\delta_{ij}y_ky_mn_m}{r^2} + \frac{y_iy_kn_j}{r^2}\right)\bar{g}_2 + \left(\frac{y_jy_kn_i}{r^2}\right)\bar{g}_3 + \left(\frac{y_iy_jn_k}{r^2} + \frac{\delta_{jk}y_iy_mn_m}{r^2} + \frac{\delta_{ik}y_jy_mn_m}{r^2}\right)g_1 + (\delta_{ij}n_k + \delta_{ik}n_j)g_2 - (\delta_{jk}n_i)g_3\right]$$

where

$$g_1 = 4s_1 - 2e^{-\varepsilon^2/4}$$

$$g_2 = -s_1 + e^{-\varepsilon^2/4}$$

$$g_3 = H(t) - s_1$$

$$\bar{g}_1 = 24s_1 - 16e^{-\eta^2/4} - \varepsilon^2 e^{-\varepsilon^2/4}$$

$$\bar{g}_2 = -4s_1 + re^{-\varepsilon^2/4} + \frac{\varepsilon^2}{2} e^{-\varepsilon^2/4}$$

$$\bar{g}_3 = 4s_1 - 2e^{-\varepsilon^2/4} - 2H(t).$$

REPORT DOCUMENTATION PAGE

Form Approved
OMB No. 0704-0188

1. AGENCY USE ONLY (*Leave blank*)	2. REPORT DATE	3. REPORT TYPE AND DATES COVERED
	November 1991	Annual Report Nov. 87–Nov. 88

4. TITLE AND SUBTITLE

Development of an Integrated BEM Approach for Hot Fluid Structure Interaction

5. FUNDING NUMBERS

WU–553–13–00
G–NAG3–712

6. AUTHOR(S)

Gary F. Dargush, Prasanta K. Banerjee, and Keith A. Honkala

7. PERFORMING ORGANIZATION NAME(S) AND ADDRESS(ES)

State University of New York at Buffalo
Department of Civil Engineering
Buffalo, New York 14225

8. PERFORMING ORGANIZATION REPORT NUMBER

None

9. SPONSORING/MONITORING AGENCY NAMES(S) AND ADDRESS(ES)

National Aeronautics and Space Administration
Lewis Research Center
Cleveland, Ohio 44135–3191

10. SPONSORING/MONITORING AGENCY REPORT NUMBER

NASA CR–189052

11. SUPPLEMENTARY NOTES

Project Manager, C.C. Chamis, Structures Division, NASA Lewis Research Center, (216) 433–3252.

12a. DISTRIBUTION/AVAILABILITY STATEMENT

Unclassified - Unlimited
Subject Category 39

12b. DISTRIBUTION CODE

13. ABSTRACT ***(Maximum 200 words)***

The development of a boundary element formulation for the study of hot fluid-structure interaction in Earth-to-Orbit engine hot section components is described. The initial primary thrust of the program to date has been directed quite naturally toward the examination of fluid flow, since boundary element methods for fluids are at a much less developed state. This required the development of integral formulations for both the solid and fluid, and some preliminary infrastructural enhancements to a boundary element code to permit coupling of the fluid-structure problem. Boundary element formulations are implemented in two-dimensions for both the solid and the fluid. The solid is modeled as an uncoupled thermoelastic medium under plane strain conditions, while several formulations are investigated for the fluid. For example, both vorticity and primitive variable approaches are implemented for viscous, incompressible flow, and a compressible version is developed. All of the above boundary element implementations are incorporated in a general purpose two-dimensional code. Thus, problems involving intricate geometry, multiple generic modeling regions, and arbitrary boundary conditions are all supported.

14. SUBJECT TERMS

Fluids; Viscous incompressible; Flow; Compressible two-dimensional; Computer code; Vorticity; Thermoelastic medium; Plain strain

15. NUMBER OF PAGES
114

16. PRICE CODE
A06

17. SECURITY CLASSIFICATION OF REPORT	18. SECURITY CLASSIFICATION OF THIS PAGE	19. SECURITY CLASSIFICATION OF ABSTRACT	20. LIMITATION OF ABSTRACT
Unclassified	Unclassified	Unclassified	

NSN 7540-01-280-5500

☆U.S. GOVERNMENT PRINTING OFFICE: 1992 - 648-034/40036

Standard Form 298 (Rev. 2-89)
Prescribed by ANSI Std. Z39-18
298-102